Effect of extended neurotransmitter stimulation on neuronal stability

by

Katherine M Pearce

A Dissertation

Submitted to the Faculty of

WORCESTER POLYTECHNIC INTITUTE

In partial fulfillment of the requirements for the degree of

Doctor of Philosophy

in

Biochemistry

August 2021

Approved by

Dr. Suzanne Scarlata – Dissertation Advisor. Professor, Chemistry and Biochemistry. WPI

Dr. Carissa Olsen – Chairperson of Defense. Assistant Professor, Chemistry and Biochemistry. WPI

Dr. Padmini Rangamani - Professor, Mechanical and Aerospace Engineering, University of California San Diego.

Dr. Jagan Srinivasan - Associate Professor, Biological Science

Table of Contents

ABSTRACT OF DISSERTATION

Neuronal plasticity is an important mechanism for growth, learning and memory however many diseases arise from its dysfunction leading to degradation. Calcium is known to be a contributing factor to the formation and breaking of neural networks the effect of extended neurotransmitter induced calcium release is not fully understood. Here we outline how extended Gαq stimulation mediated by changes in membrane tension lead to retraction of neurites in PC12 cells and disruption of axons in C. *elegans*. To understand retraction, we systematically broke down and mathematically modeled the components of the Gαq/PLCβ /PI(4,5)P_2 and found that the driving force of retraction was led by calcium mediate changes in membrane tension followed by cytoskeletal dynamics. Our model of calcium mediated tension driven retraction translated into C. *elegans* where retraction that we saw in cultured cell surfaced as morphological changes in neuronal processes. We found under extended stress two hallmark

aging morphologies, beading and waving, occurred in higher concentrations compared to normal aging and show a connection between beading and mitochondrial stress with age.

ACKNOWLEDMENTS

List of Figures and Figures

CHAPTER I - GENERAL INTRODUCTION

Overview. Neuronal cell structure is highly complex and can deform when subjected to environmental stress or in diseased states. Neurons consist of a cell body and two or more thin extensions, dendrites, emanating from the body that connect with neighboring neurons at points called synapses. Neurons must have the ability to break and reform synapses as an organism learns and grows (I-1). This plasticity is essential for cell function, but under stressed conditions, the ability to properly break and repair connections can be hindered and even stopped completely (I-2,I-3).

Calcium plays a key role in many neuronal functions such as neurite outgrowth and axon regeneration (I-4). However, despite the fact that calcium has been studied in neurons for many years (I-5,I-6) the full extent of its function within the cell is not yet fully understood. The balance between healthy and abnormal calcium homeostasis can easily be disrupted and diseases such as autism and amyotrophic lateral sclerosis (ALS) are associated with excitotoxic levels of calcium in cells (I-7). The goal of this thesis is to better understand a simulated diseased state, (i.e. extended stimulation due to elevated calcium) on neuronal function. These studies employed two model systems: PC12 cells that differentiate into a neuronal line with the addition of nerve growth factor (NGF) and serum starvation. as well as the neuronal circuit of a small organism, *Caenorhabditis elegans.* When a cell is stimulated with neurotransmitters such as acetylcholine (or its stable derivative carbachol) G-protein coupled receptors (GPCRs) are activated followed by the Gαq/calcium pathway leading to downstream increases in cellular calcium from the endoplasmic reticulum (ER) (I-8,I-9). We followed the behavior of PC12 cells

with extended stimulation by acetylcholine. Surprisingly, we see retraction of the neurites into the soma of the cell. This prompted further exploration into the underlying mechanical responsible for retraction which led to studies of actin and actin modifying proteins, changes in the plasma membrane and changes in membrane tension that occurs under stimulation and retraction. Our results showed that the changes in tension initiated with the hydrolysis of PIP_2 and subsequent GPCR internalization, were key factors driving retraction.

To better understand the role of plasma membrane tension, two methods were used. In the first, an exogenous membrane tension modifying protein caveolin was utilized. Caveolin proteins and their domains caveolae are not normally found in high concentrations in neurons (I-10). Additionally, membrane tension was varied by hyper-osmotic stress where salt was added to change the osmolarity from 300mOsm to ~550mOsm. These studies enabled us to better define the impact of membrane tension in neurite retraction.

In this dissertation, fluorescent microscopy was used in several forms such as calcium imaging, fluorescent lifetime imaging microscopy (FLIM) to measure changes in tension using the probe Laurdan, and number and brightness (N&B) to see how caveolin localizes in the membrane. These techniques allowed us to study the effect of extended stimulation of the Gaq/calcium pathway as well as changes in tension seen under hyper-osmotic stress. To further look at membrane tension atomic force microscopy (AFM) was also used to see how overall membrane tension changed after stimulation and retraction by acetylcholine and salt addition.

G-PROTIEN COUPLED RECEPTOR (GPCRS) AND CALCIUM DYNAMICS

This section is an excerpt from "Regulation of bifunctional proteins in cells: Lessons from the phospholipase Cβ/G protein pathway" done in collaboration with Lela Jackson and Androniqi

*Qifti. (*Jackson, L*,* Qifti, A*,* Pearce, KM*,* Scarlata, S. *Regulation of bifunctional proteins in cells: Lessons from the phospholipase Cβ/G protein pathway. Protein Science. 2020; 29: 1258– 1268. https://doi.org/10.1002/pro.3809)*

Most sensory information is received and processed by the G protein signaling system (I-11). This pathway allows external hormones and neurotransmitters to elicit different cell responses, such as movement or morphology changes. G protein pathways are initiated when an extracellular agent binds to its specific G protein coupled receptor (GPCR). GPCRs are a large family of seven transmembrane proteins that interact and respond to a diverse array of ligands that include hormones, neurotransmitters, vasodilators, many pharmaceutical agents, and light. Ligand binding allows GPCRs to activate their associated G proteins by catalyzing the exchange of GDP for GTP on the Gα subunits peripherally bound to the plasma membrane (I-12, I-13). Heterotrimeric G proteins are composed of three subunits (α, β, and γ). In the GTP-bound state, Gα has a ~50-fold weaker affinity to Gβγ subunits, (I-14) which destabilizes the heterotrimer leaving the Gα and Gβγ to separately bind to and activate specific proteins. Once the complex is destabilized, the Gα and the Gβγ subunits each act as effectors on specific targets. Depending on the Gα subunit family, Gα will act to stimulate or inhibit adenylyl cyclase (AC), activate phosphoinositide-specific phospholipase C (PI-PLC), or regulate RhoA proteins. Alternatively, Gβγ subunits are thought to play a role in calcium channel activity, and regulate protein kinases and small G-proteins, such as ERK1/2, JNK, phosphoinositide-3 kinase (PI3K), and mitogen-activated protein kinases (MAPKs)(I-15).

In contrast to the ~800 different GPCRs, there are only four families of heterotrimeric G proteins that are classified by their Gα subunits (I-16). PLCβ is the main effector of Gαq (I-17), and

activation of Gαq increases the binding affinity of PLCβ ~20–40-fold (Figure 1, I-18). Gαq is coupled to receptors for neurotransmitters such as dopamine and acetylcholine, as well as hormones that mediate vasoconstriction and inflammation, such as bradykinin and angiotensin II. PLCβ is soluble but binds to membranes, where it catalyzes the hydrolysis of phosphatidylinositol 4,5 bisphosphate (PIP2), which is found at low levels in the plasma membrane (I-19). PIP2 hydrolysis catalyzed by PLCβ leads to two products: the lipid portion, diacylglycerol, which activates protein kinase C, and the soluble head group, 1,4,5 inositol trisphosphate (IP3). IP3 diffuses to the endoplasmic reticulum (ER) where it binds to IP3 receptors. These receptors are Ca^{2+} channels and when IP3 binds, they open, releasing Ca^{2+} from intracellular stores into the cytoplasm. This increased level of calcium changes the activity of a wide range of enzymes that carry out key cellular events such as generating action potentials and neurotransmission in neurons, or initiating muscle contraction (I-20-I-22). Besides being activated by Gαq, two of the four known isoforms of PLCβ can be activated by Gβγ subunits (I-23). Although Gβγ subunits have the potential to be released by any G protein family, release is generally associated with Gαi subunits thus connecting PLCβ and calcium signals to large and diverse array of GPCRs.

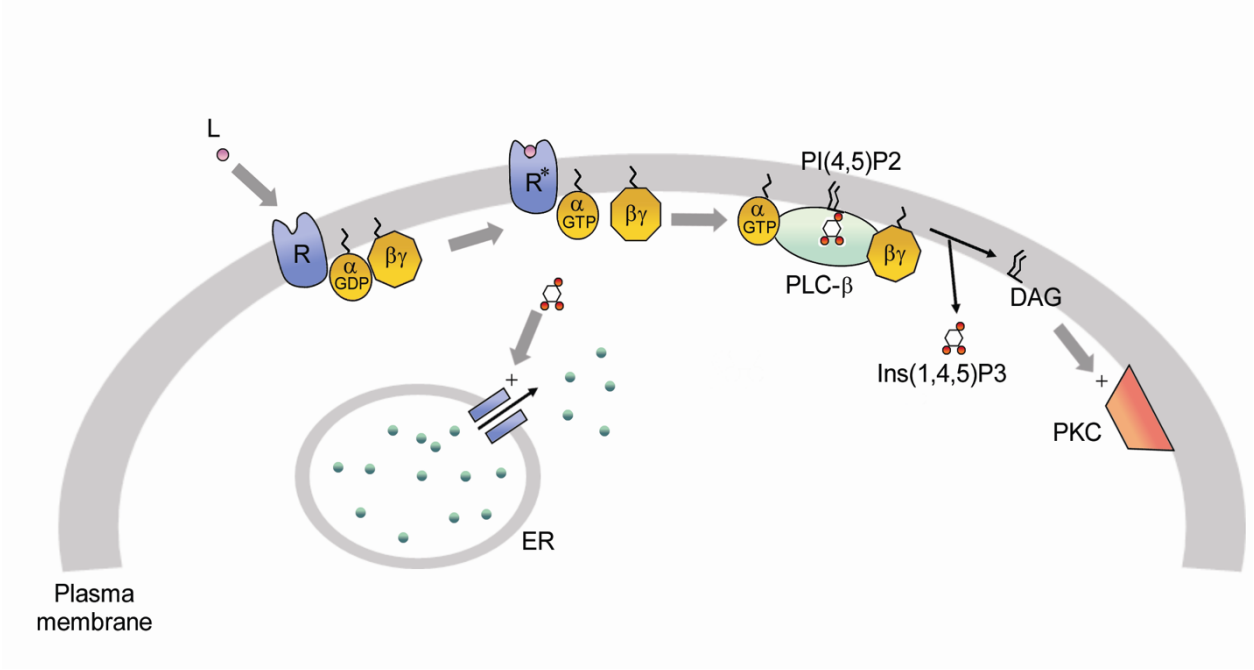

Figure I-1. *From Reference 8. Cartoon of the Gαq/PLCβ signaling system showing simultaneous activation of PLCβ by both Gβγ and Gα subunits (see References I-31, I-32)*

In order to access its substrate, PLCβ must bind to the plasma membrane. Binding of PLCβ to model membranes is strong and fairly nonspecific with partition coefficients ranging from 10 to 100 μM (I-24). This range of affinities suggests a transient membrane association in the range of 0.1 to 1 s (see References I-25, I-26). Studies using purified proteins and model membranes suggest that PLCβ initially binds to membranes where it diffuses and hops along the membrane until it encounters Gαq (I-24). It is unclear whether a similar scenario occurs in cells since the amount of membrane available for binding may be lower, and if this is the case, PLCβ will bind directly to Gαq. Once activated, the affinity between Gαq and PLCβ1 increases 20-fold (I-14). The high affinity between Gαq and PLCβ (Kd ~1 nM) is attributed to the tucking of Gαq into a nook between the C2 domain and C-terminal tail (Figure 2) of PLCβ1 (I-27).

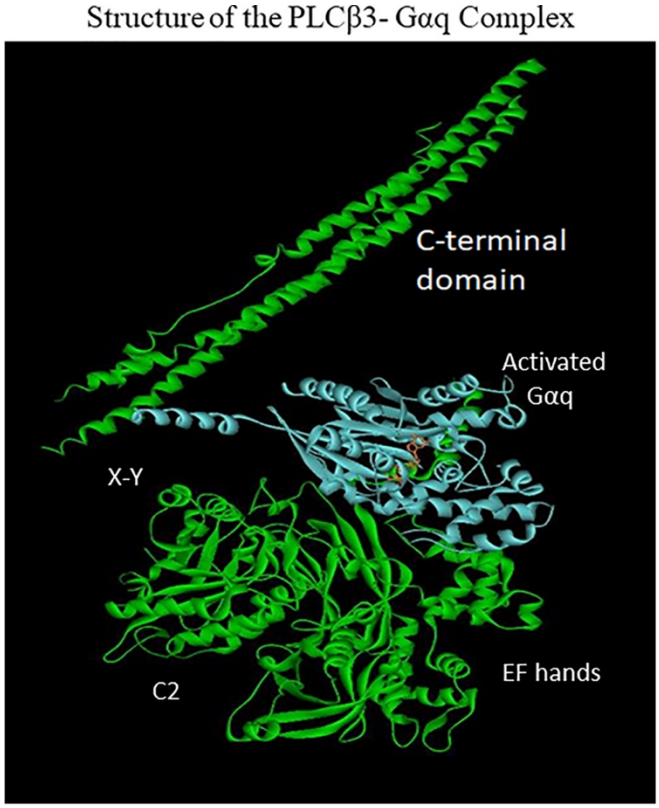

Figure I-5. *Crystal structure (PDB Id: 4GNK) of the PLCβ2 (green) -Gαq (blue) complex showing the extended C-terminal domain and where the various domains are indicated. Missing is an unstructured 52aa connector between the C2 and C-terminal domains.*

The initial activation of PLCβ and subsequent calcium release results in a series of coordinated events involving changes in protein associations, modifications, and localization (I-28). Calcium release is enhanced by two major effects (I-21). One is the activation of PLCδ. PLCδ has a similar structure as PLCβ but is not activated by G proteins. Instead, PLCδ becomes highly active when calcium levels in the cell rise, synergizing PLCβ activity (see Reference I-29). Additionally, increased calcium opens calcium-activated calcium channels on the plasma membrane, allowing external calcium to enter the cell (I-30).

CALCIUM DYNAMICS

The importance of calcium in all cell types and specifically neuronal cells has been a topic of study for decades. However, due to the diversity of calcium responses within the cell we still not fully understand the wide array of roles calcium plays. In neuronal cells, calcium has been shown to play key roles in determining subtype, proliferation, differentiation and cytoskeletal rearrangements (I-21). Calcium activity can be both spontaneous and experience driven. In the earliest stages of neuronal development cells show spontaneous calcium activity that plays a significant role in their eventual differentiation. This early activity can come in one of two forms, calcium spikes or waves. Calcium spikes are a characteristic rapid increase in cellular calcium from internal and/or external stores of calcium mediated through ion channels. This increase is then followed by a slow decay (~3 minutes) to basal calcium levels. Calcium spikes have been shown to be necessary for regulation of neurotransmitters such as GABAergic neurons (I-33). Removal calcium spikes either by addition of calcium chelators or blocking calcium channels show a significant loss of GABAergic neurons during development. However,

this phenotype can be rescued by external addition of salts such as KCl showing that calcium spikes are essential for proper development. (I-34).

Calcium can be regulated by multiple mechanisms in both developing and developed neurons. Voltage gated ion channels are used to signal neurotransmitter release and synaptic vesicles can regulate dendritic action potentials. Transient calcium levels are also regulated by neurotransmitters via receptor gated channels. This type of regulation by proteins such as GPCRs lead to the efflux of calcium from internal stores in the ER that extends throughout the cell. The ER stands as the most important store of internal calcium and ER receptors such as IP3 receptors mediate the release and uptake of calcium from the ER. Under certain circumstances calcium is also released and re-taken into the mitochondria. This regulation by the mitochondria is used as a back-up if the ER is incapable of quick re-uptake of calcium and the cell is reaching cytotoxic levels (I-36) This uptake of calcium to the mitochondria can also induce Ca^{2+} dependent reactive oxygen species (ROS) pathway. Increased levels of calcium lead to an increase in ROS which then leads to a responsive release in calcium leading a negative feedback loop of increasing cellular calcium (I-35). Finally, calcium can regulated by a calcium feedback loop creating calcium-induced calcium release (CICR). CICR can occur in multiple forms but generally is regarded to relay a signal across a cell or extend the life of increased calcium levels needs for transcription which can last minutes.

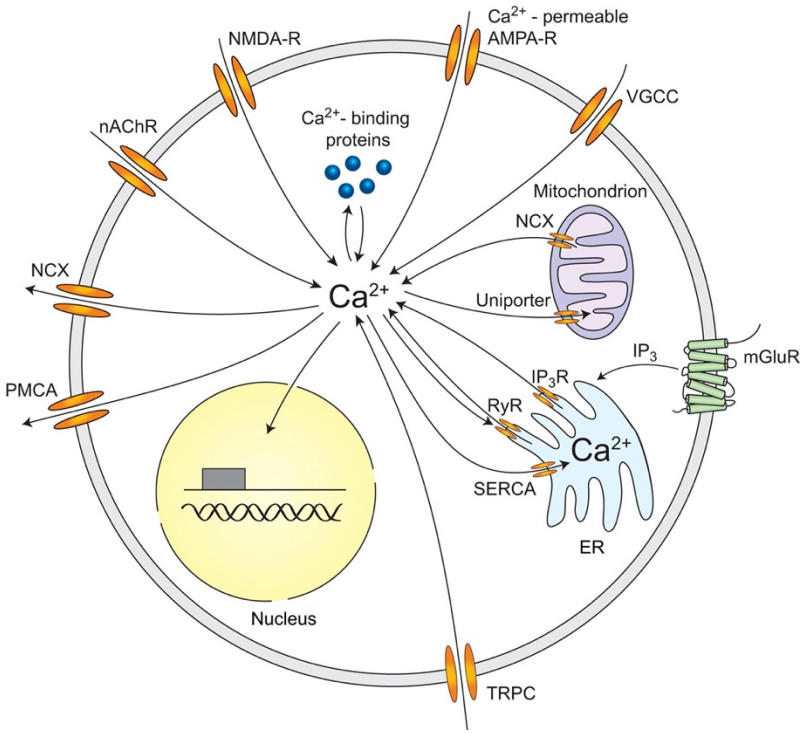

Figure I-9. Calcium signaling and methods of regulation in neuronal cells. (37) Christine Grienberger, Arthur Konnerth, "Imaging Calcium in Neurons", Neuron, *Volume 73, Issue 5,2012,Pages 862-885,ISSN 0896-6273*

CAVEOLAE DOMAINS AND CAVEOLIN PROTEINS

Caveolae domains were first discovered in the 1950s with the introduction of electron microscopy. A large quantity of what we know now as caveolae were described in several cell types throughout the late 1900s. However, it was not until the 1990s that caveolin-1 was discovered and found to be a major component in caveolae (I-38). Caveolae domains are described as flask shaped invaginations of the membrane that are ~70nm in width (I-39). They occur in many cells types and can be found singularly or in clusters (I-39). Caveolins are a family of proteins that are found in caveolae. They are integral membrane proteins that are

approximately 22kDA in size. There are three types of caveolins, however, in this dissertation we have focused on caveolin-1 (Cav1) and caveolin-3 (Cav3). Both of these Cav isoforms form hairpin loops in the inner leaflet of the plasma membrane and have both C and N termini exposed (I-39-I-40). Cav1 is present in almost all cell types while Cav3 is muscle specific. Cav1 and Cav3 are both integral to the formation of complete caveolae structure. When Cav1 and Cav3 knockout mice were examined, there was either a complete or partial loss of caveolae respectively (I-38).

CAENORHABDITIS ELEGANS AS A NEUONAL MODEL

Caenorhabditis elegans are a small transparent nematode that are found worldwide (I-41). They have a rapid life cycle to adulthood of 3 days with four developmental stages (L1-L4) and are naturally hermaphroditic with males occurring approximately 0.2% of the time. Being a self-fertilizing hermaphrodite, they can reproduce frequently making then a strong genetic model. The complete connectome of the hermaphrodite consisting of 302 neurons have allowed a "wiring diagram" to be made making C. *elegans* an excellent neuronal model as we know how each neuron interacts with others (I-42). C. *elegans* have also given rise to multiple different fluorescence studies with the addition of fluorescent tags to the entire nervous system all the way down to single cells. These fluorescent strains allow for live single cell studies to be conducted on the organism level.

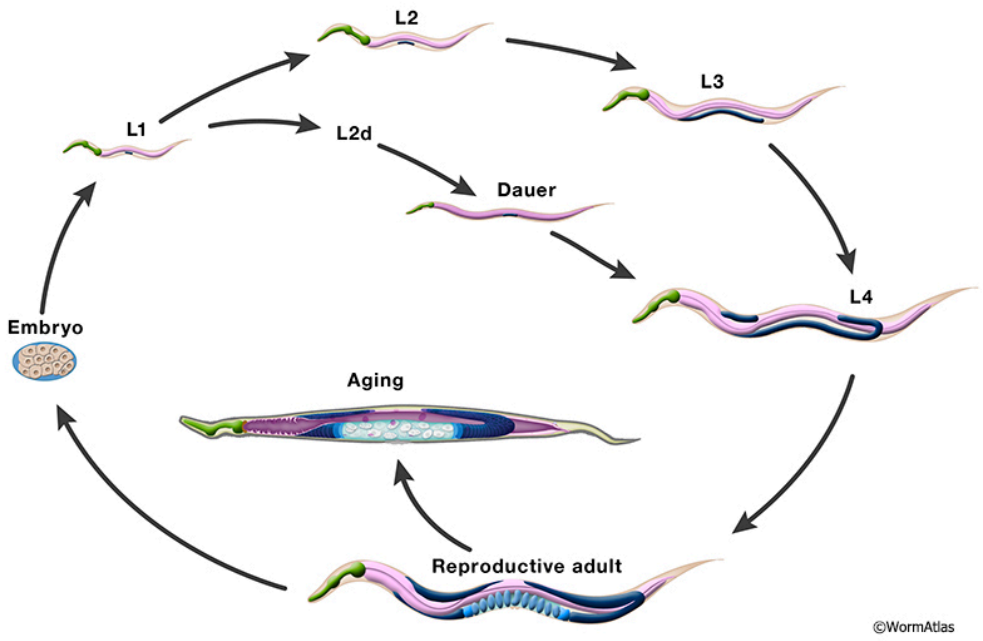

Figure I-10. *Life cycle of C. elegans. This process takes ~3 days form egg to adulthood. They can then live for ~15 days into adulthood. (WormAtlas.com).*

Fluorescently tagged strains used in this dissertation.

QW1166. zfIs42 [rig-3p::GCaMP3::SL2::mCherry + lin-15(+)] Fluorescently tagged GCaMP intrinsically found in all neurons. ***ZB154*** zdIs5[pmec-4::gfp] graciously given to the lab by the Driscoll Lab (Rutgers) tags the membrane protein mec-4 found in the six soft touch neurons (I-43). These neurons have long extended axons allowing for single cell axon morphology analysis under different conditions and ages. **CLP215** twnEx8 (mec-7p::tomm20::mCherry + myo-2p::GFP) which tags mec-7 found in the outer layer of mitochondria in the six soft touch neurons. CLP215 was obtained directly from C. elegans Genetics Center.

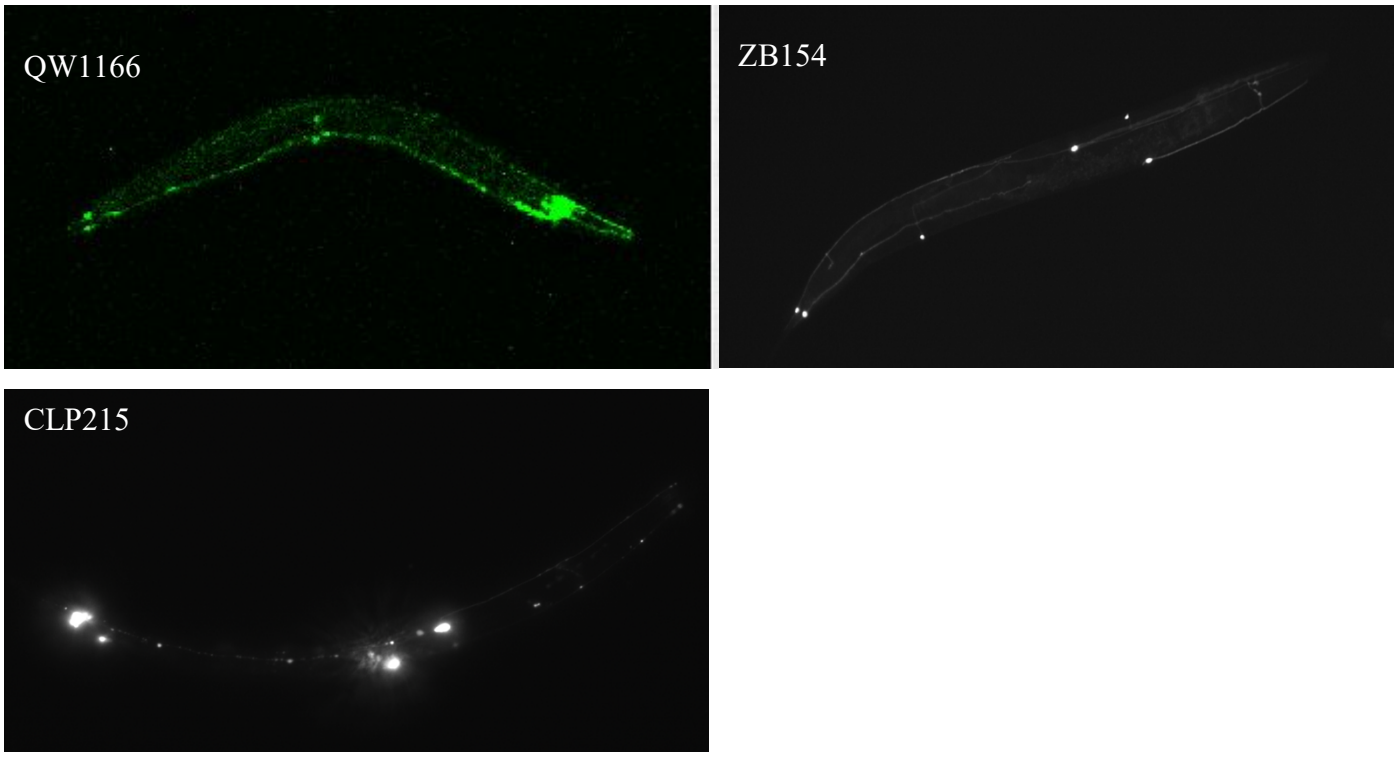

***Figure I 12**. . Images of the three worm strains used in this dissertation.*

RESEARCH AIMS IN THIS DISSERTATION

This dissertation began with a phenomenon seen in differentiated PC12 cells, i.e. retraction caused by neurotransmitter activation. Retraction is characterized by the pulling back a neurite toward the soma of the cell. Once we realized this behavior was reproducible, we began to answer this question by systematically breaking town the components of retraction; calcium efflux, actin dynamics and membrane tension.

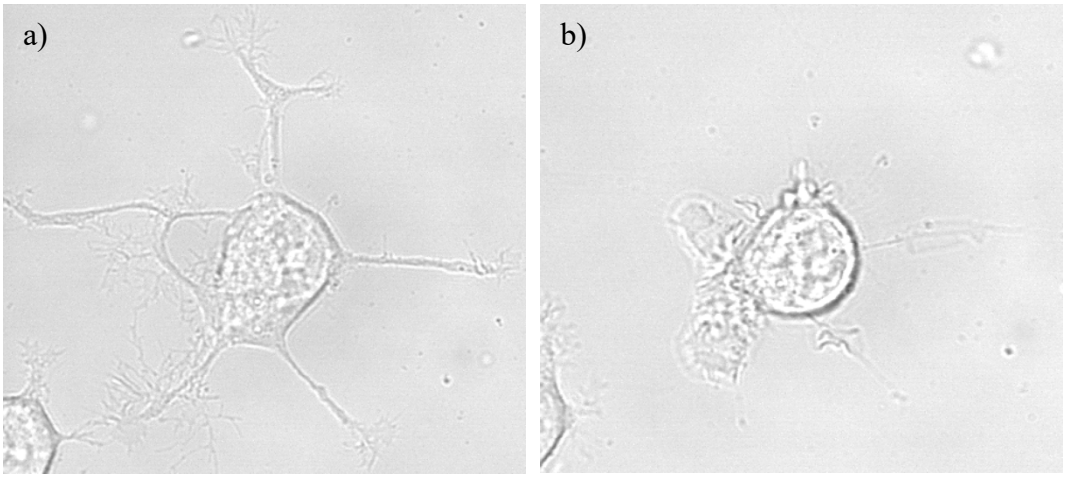

Figure I-14. *Retraction in differentiated PC12 cells. a) differentiated PC12 cell before stimulation. b) cell after stimulation with carbachol and neurites have retracted*

From this model, we tested whether the same effect could be seen in the small organism, C. *elegans.* While retraction occurs in a different manner than cells, we did see breaking in the nerve ring and beading and waving along the ventral nerve and other neurons. To understand this phenomenon in both cells and C.*elegans* with age, we devised a series of questions to answer the over-arching question of how Gαq stimulation and membrane tension effect structure and stability of neuronal cells.

The first question we asked is whether retraction caused by extended stimulation of the Gαq pathway. This question, along with the mechanism behind retraction in PC12 cells is answered and subsequently computationally modeled using fluorescent microscopy techniques to look at changes in calcium behavior, actin dynamics as well as actin modifying proteins and finally by externally changing the membrane tension with the addition of salt. These studies will be discussed in Chapter 2. How does this model derived from individual cells translate to the

neural network in C. *elegans*? This question will be addressed in Chapter 3. How the addition of exogenous caveolin change neuronal membrane tension and subsequent retraction. This question will be discussed in Chapter 4. The future directions and general discussion will be in Chapter 5.

CHAPTER II - Gαq-mediated calcium dynamics and membrane tension modulate neurite plasticity

Authors and manuscript breakdown: This manuscript was completely equally by co first authors Katherine Pearce (KP) and Miriam Bell (MB). The experimental work and analysis were done by KP. The modeling work was done by MB. Introduction, results and discussion were done in collaboration of KP and MB. Atomic force microscopy work was completed and analyzed by Will Linthicum in collaboration with KP.

ABSTRACT

The formation and disruption of synaptic connections during development is a fundamental step in neural circuit formation. Subneuronal structures such as neurites are known to be sensitive to the level of spontaneous neuronal activity but the specifics of how neurotransmitter-induced calcium activity regulates neurite homeostasis are not yet fully understood. In response to stimulation by neurotransmitters such as acetylcholine, calcium responses in cells are mediated the Gαq/phospholipase Cβ (PLCβ)/ phosphatidylinositol 4,5 bisphosphate ($PI(4,5)P_2$) signaling pathway. Here, we show that prolonged Gαq stimulation results in the retraction of neurites in PC12 cells and rupture of neuronal synapses by modulating membrane tension. To understand the underlying cause, we dissected the behavior of individual components of the Gαq/PLCβ /$PI(4,5)P_2$ pathway during retraction, and correlated these to the retraction of the membrane and cytoskeletal elements impacted by calcium signaling. We developed a mathematical model that combines biochemical signaling with membrane tension and cytoskeletal mechanics, to show how signaling events are coupled to retraction velocity, membrane tension and actin

dynamics. The coupling between calcium and neurite retraction is shown to be operative in the *C. elegans* nervous system. This study uncovers a novel mechanochemical connection between Gαq/PLCβ /PI(4,5)P_2 that couples calcium responses with neural plasticity.

INTRODUCTION:

Throughout the course of an organism's life, different neuronal connections break and reform to generate new electrical patterns that allow for optimal function during development and through adulthood. This plasticity of neuronal connections allows the rewiring of circuitry necessary for memory and learning (II-1, II-3). Understanding the factors that permit appropriate and efficient rewiring is essential for understanding both developmental and neurodegenerative diseases.

Calcium is a key mediator of neuronal functions such as axonal growth, neurite protrusion, and spinogenesis (II-4, II-5). Previous studies have shown that spontaneous activity in neurons can results in a frequency dependent rate of axon elongation such that the rate of axon elongation is inversely proportional to the frequency of calcium transients (II-6, II-7). The role of calcium in neurite growth and protrusions associated with development has been studied in different contexts (II-8). This outgrowth process is stimulated by neurotrophic factors that carefully regulate the spatiotemporal aspects of intracellular calcium. Neurite growth can also be triggered by stress, pharmacological agents, or starvation (II-9, II-10) These factors may occur during disease states and contribute to inappropriate neurite growth, which can result in an increased number of smaller and non-productive neurites, as seen in autism (II-10).

Neurodegenerative diseases are associated with the disruption of normal calcium signaling. Specifically, diseases such as autism and amyotrophic lateral sclerosis (ALS) have

been linked to over-excitation of neurons or excitotoxicity caused by abnormal calcium homeostasis (II-11). However, the link between calcium homeostasis and the mechanical processes underlying neurite retraction remain poorly understood. Understanding the link between dysfunction of cellular calcium, especially prolonged signaling, and neuronal function is critical to understand the mechanisms that underlie diseases typified by inappropriate neuronal excitation. While previous research has focused on the short-term effects of elevated cellular calcium after stimulation and its effects on neurite growth or on spontaneous spiking activity (II-6, II-7, II-12). Little is known about the effect of extended elevated calcium on these same neurites over time, i.e. cases that mimic an extended overstimulated state. In this study, we investigate the effects of prolonged stimulation of Gαq/PLCβ/PIP_2 /calcium signaling pathway by the neurotransmitter acetylcholine, in a model neuronal cell line, PC12, and in the neuronal network in a small organism, *Caenorhabditis elegans*.

Calcium signals in neurites can be generated by several mechanisms. In synapses, postsynaptic cells receive an influx of calcium directly through the opening of transmembrane channels in response to neurotransmitter release (II-13). Neurotransmitters, such as acetylcholine, activate G protein coupled receptors (GPCRs) on the plasma membrane to generate the release of calcium from intracellular stores (II-9). Furthermore, neurotropic factors activate receptor tyrosine kinases to increase intracellular calcium through another phospholipase C family, PLCγ. Downstream from these events are the opening of calcium-activated calcium channels on the endoplasmic reticulum (ER) membrane. Many of these channels are thought to respond to the increase in cytosolic calcium and to changes to the physical properties of the plasma membrane. These increases in cellular calcium regulate specific transcription factors and post-transcriptional processes

that lead to appropriate downstream responses (II-14).

In this study, we show that neurites will completely retract to the soma by extended stimulation of the GPCR/Gαq/PLCβ pathway. This pathway mediates signals from many hormones and neurotransmitters such as acetylcholine, dopamine, histamine, and melatonin (II-15). Signaling begins with ligand binding to its specific G protein coupled receptor to activate the Gαq family of G proteins by exchange of GTP for GDP. The GTP-bound Gαq subunits then actives phospholipase Cβ (PLCβ). PLCβ catalyzes the hydrolysis of phosphatidylinositol 4,5-biphosphate (PIP_2) to inositol 1,4,5-triphosphate (IP_3) and diacylglycerol (DAG). IP_3 binds to receptors on the endoplasmic reticulum allowing the release of calcium from intracellular stores into the cytoplasm. The elevated calcium can then change the activity of a variety of intracellular proteins to generate a specific cell response.

Incorporated in this pathway are a number of positive and negative feedback loops. The initial calcium release generated by PLCβ in turn stimulates the highly active PLCδ that synergizes the calcium response (II-16). Increased calcium also opens calcium-induced calcium channels, further strengthening calcium responses (II-17). Negative feedback comes from the internalization of ligand-bound receptors into endosomes over a few minutes that typically return unbound receptors to the plasma membrane over a period of 20-30 min (II-18). Additionally, Gαq has a GTPase activity that returns it to the basal state and this activity is stimulated by the GTPase activating (GAP) activity of PLCβ (II-19), along with RGS proteins that quickly turn-off the signal (II-20). It is notable that these feedback loops are highly sensitive to the concentration of the pathway components, the concentrations of competing species as well as the physical state of the plasma membrane which drives

aggregation of the ligand-bound receptor and internalization, the accessibility of $PI(4,5)P_2$ substrates to PLCβ and PLCδ, and the opening of calcium channels.

Components of the Gαq/PLCβ/$PI(4,5)P_2$ pathway are also involved in the regulation of membrane tension and cytoskeletal remodeling. The coupling between membrane tension and cytoskeletal adhesion through $PI(4,5)P_2$ was established nearly two decades ago by Sheetz and coworkers (II-21, II-22) In a series of elegant experiments, they showed that PIP_2 regulates cytoskeleton-plasma membrane adhesion (II-21) and that membrane tension plays a critical role in actin remodeling, membrane trafficking, and cell motility (II-23-25). Subsequently, researchers have continued to establish and identify increasing roles played by the plasma membrane tension and cortical tension in different cellular reorganization processes (II-26-28). Specifically, in neurons, dynamics of growth cone formation, neurite protrusion, and axonal contractility have been shown to be mechanochemically coupled processes (II-29, II-30).

Despite these advances in neuronal biophysics, our understanding of synaptic rupture and neurite retraction remains incomplete especially in terms of the mechanisms that underlie overexcitatory responses. In this study, we set out to investigate the effects of prolonged (i.e. several minutes) agonist stimulation of the Gαq signaling pathway in a model neuronal cell line (PC12). We find that prolonged stimulation results in tension-driven neurite retraction unlike the behavior seen in shorter exposures to neurotransmitters. To understand the factors that underlie the observed neurite retraction, we followed the individual components during the process and developed a mathematical model to predict the effects of calcium stimulation by acetylcholine (ACh) and its extended response on retraction through mobilization of the pathways that impact neurite retraction.

Our predictive models showing that membrane tension and actin reorganization are coupled to calcium dynamics through Gαq/PLCβ/$PI(4,5)P_2$ were verified in cultured PC12

cells as well as in the neuronal network of the nematode *Caenorhabditis elegans.* The 302 neurons that (II-31) comprise the nervous system of *C. elegans* have been well characterized and these organisms have been used as models to understand neurite formation and retraction (II-31). Because of their optical clarity, *C. elegans* allows us to monitor the effects of acetylcholine stimulation on synapses in real time by microscopy. We find that the *C. elegans* neural architecture exhibits the same retraction behavior when exposed to Gαq agonists showing rupture along the spine in the nerve ring, suggesting that the coupling between membrane tension and calcium dynamics occur on the organism level. Taken together, our studies connect signaling processes with mechanical effects that allow us to predict the signaling conditions that shift from outgrowth and maintenance to retraction.

RESULTS

Prolonged exposure to carbachol causes neurite retraction

Cultured PC12 cells differentiate to a neuronal phenotype upon treatment with nerve growth factor (NGF) which initiates activation through TrkA receptors (II-32). This treatment results in growth of neurites from the cell body that extend to roughly 3 times the length of the body over a 36-hr period. These neurites can then connect with neurites from other cells resulting in long tubular structures (II-33).

Addition of a Gαq agonist to the cells activates PLCβ to catalyze the hydrolysis of $PI(4,5)P_2$. This hydrolysis releases $Ins(1,4,5)P_3$ into the cytosol that then binds to $Ins(1,4,5)P_3$ receptors on the ER to release calcium from intracellular stores. In addition to eliciting calcium signals, $PI(4,5)P_2$ hydrolysis can exert mechanical effects on cells by altering membrane tension and actin-membrane adhesion (II-22) (II-21, II-27). We sought to

understand the interactions between the Gαq/PLCβ pathway and mechanical features of membrane-actin interaction **(Fig. lA, B).**

We found that when we add a Gαq agonist, such as carbachol or bradykinin, to PC12 cells, the well-formed neurites become thinner, their connections rupture (compare **Fig lC to Fig. lE, S1)** and they retract toward the soma after a period of 5-10 minutes **(Fig. lE, F).** After retraction, the excess membrane appears as blebs around the sides of the cell **(Fig. lG).** This behavior was seen in every cell viewed in over 100 experiments but was not seen when a PLCβ inhibitor was added, or a Gαi agonist, such as isoproterenol was used. The initiation and rate of retraction depended on the particular treatment and condition of the experiment, as described below. The extent of retraction in a specific time period was robust to the length and thickness of the neurite.

Neurite retraction is coupled with Gαq/PLCβ/calcium pathway

We followed the activation of the Gαq/PLCβ/calcium signaling pathway upon stimulation in single PC12 cells using the fluorescent calcium indicator, Calcium Green, to

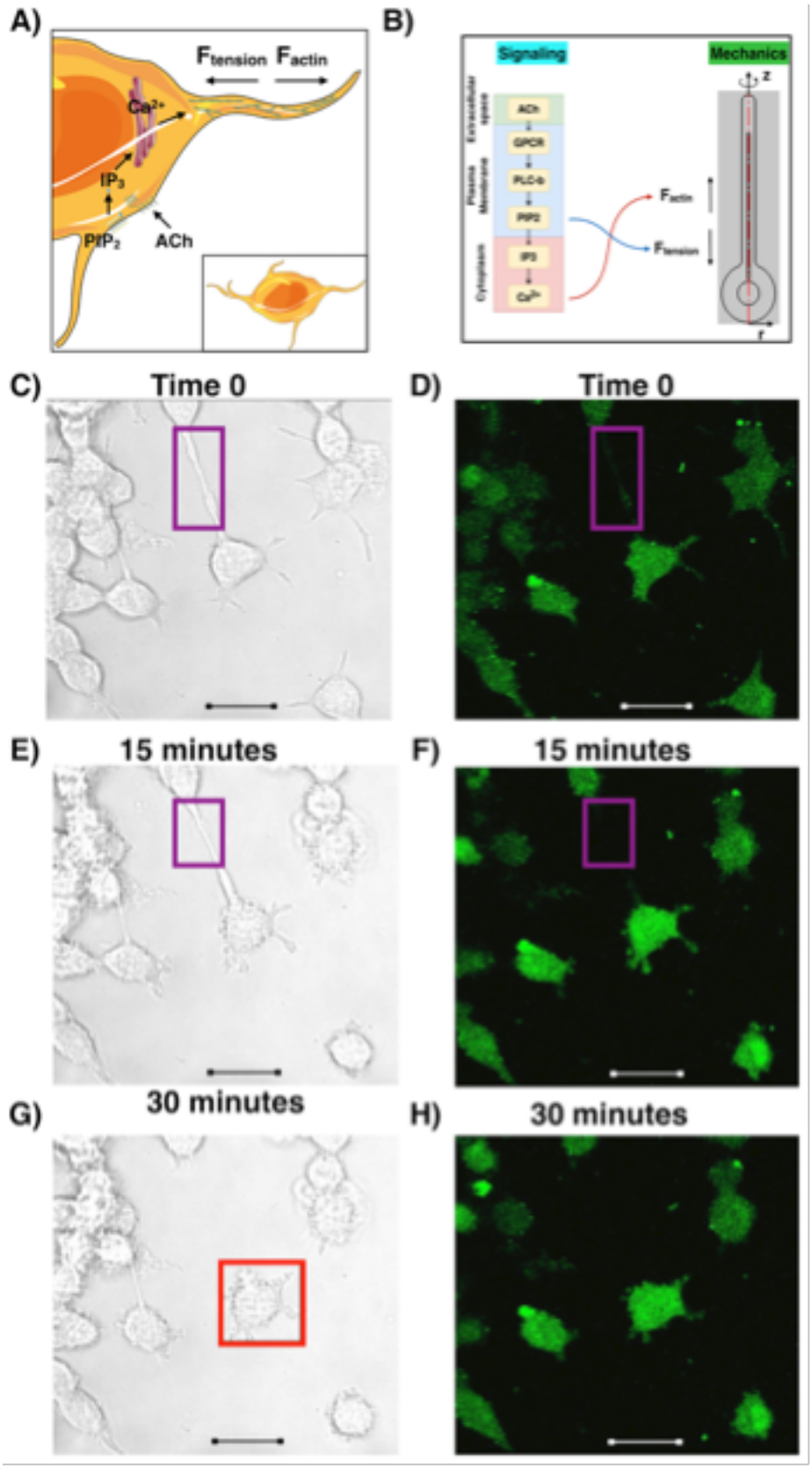
A)
$F_{tension}$ F_{actin}
Ca^{2+}
IP_3
PIP_2
ACh
B)
Signaling
Mechanics
Extracellular space
Plasma Membrane
Cytoplasm
ACh
GPCR
PLC-b
PIP2
IP3
Ca^{2+}
F_{actin}
$F_{tension}$
z
r
C)
Time 0
D)
Time 0
E)
15 minutes
F)
15 minutes
G)
30 minutes
H)
30 minutes

Figure II- 1*. Neurite retraction in PC12 cells is induced by calcium stimulation.*

A) *Cartoon of the mechanochemical events underlying neurite retraction in a PC12 cell. The figure depicts the interconnection between calcium signaling and force regulation due to membrane cortical tension and actin remodeling.* ***B)*** *Schematic showing the coupling between signaling and mechanical changes within the PC12 cell. We identify membrane cortical tension and actin dynamics as key players controlling neurite retraction rates, and link calcium dynamics to actin reorganization and force generation, and* $PI(4,5)P_2$ *hydrolysis to membrane tension change and tension force generation. Using this coupled model, we are able to reproduce the neurite retraction behavior observed experimentally.* ***C-D)*** *Sample images of differentiated PC12 cells before stimulation. Confocal phase contrast* ***(C)*** *and fluorescence images of cells loaded with a fluorescent calcium sensor, Calcium Green, are shown* ***(D)****.* ***(E-G)*** *Stimulation of cells with carbachol results in neurite thinning, retraction and synaptic rupture. 15 minutes after the addition of carbachol, we observe membrane retraction (e.g. purple box), and thinning of the neurite (****E-F****). 30 minutes after carbachol addition, we see a complete retraction of the neurites into the soma and membrane blebbing at the retraction sties (e.g. red box) (****G-H****). In all images, the scale bar is 20μm. Identical behavior was seen in 20 cells.*

determine whether neurite retraction is concurrent with activation. Our approach was to follow some of the molecular constituents of the Gαq pathway and determine the temporal correlation between activation of the individual signal components and neurite retraction. The retraction velocities of a generic Gαq-coupled receptor (i.e. the bradykinin receptor type 2 or B2R) were measured by transfecting cells with a fluorescent-tagged construct and stimulating the cells with agonist (i.e. bradykinin). We note that B2R is not endogenous to PC12 cells, thus allowing us to compare Gαq-associated retraction with those that result from stimulation of endogenous muscarinic receptors. We find identical retraction behavior for neurite retraction after stimulating the B2R transfected cells with bradykinin as those that result from carbachol stimulation **(Fig. 2).** These results support a connection between neurite retraction and Gαq/PLCβ activation.

We calculated the velocity of neurite retraction by analyzing the decrease in length of each neurite at each time point during the experiment (see *Methods*). These velocities were analyzed for PC12 cells transfected with eCFP-B2R *(blue)* and for the plasma membrane *(orange)* as monitored by the phase contrast imaging (**Fig. 2A**). We find that the velocity of retraction of the plasma membrane is more gradual than that of the receptor suggesting that movement of the receptor towards the soma precedes the membrane.

Activation of the PLCβ pathway through Gαq-GPCRs results in hydrolysis of the signaling lipid $PI(4,5)P_2$. We followed the change in the level and distribution of $PI(4,5)P_2$ of the plasma membrane surrounding the soma and neurite during retraction using a fluorescent $PI(4,5)P_2$ sensor (i.e. eGFP-PH-PLCδ1). Our data show that $PI(4,5)P_2$ moves from the neurite into the soma with a similar retraction velocity as the GPCR **(Fig. 2E).** However, this movement is oscillatory showing three precipitous drops and recovery during the retraction event. These are three distinct movements of $PI(4,5)P_2$ during the observed

retraction occur at similar times (~3, 10 and 15 min) for all cells tested, and are interpreted as being due to $PI(4,5)P_2$ replenishment during the course of the retraction.

In general, Gαq activation produces an increase in the calcium typified by an initial spike in the first few minutes followed by a slow recovery. We followed the calcium behavior upon stimulation in single cells using a fluorescent calcium indicator, Calcium Green **(Fig 1D, F, H** and **2J).** Correlating calcium responses with neurite retraction shows that retraction occurs even in this initial phase and continues through the duration of the recovery phase.

We constructed a spatial model of the Gαq/PLCβ/$PI(4,5)P_2$ signaling pathway using reaction-diffusion equations. The reactions, kinetic parameters, and diffusion constants are given in **Tables S1-4** in the Supplementary Material (*SOM*). The soma of the PC12 cell was modeled as a sphere with a radius of 5 μm, and the neurite was modeled as a cylinder with a radius of 1.25 μm and length of 30 μm. The endoplasmic reticulum was modeled as a cylinder with a radius of 0.25 μm and length of 25 μm, and the nucleus as a sphere with a radius of 2 μm. Geometric details are given in **Table S5**. The nucleus was treated as an excluded volume, while the ER was treated as a calcium source. Computational modeling of this pathway in a three-dimensional spatial model using finite elements captured the calcium transients with the same time scale as the experiments (compare **Fig. 2J** and **Fig. 2K).** This framework sets the stage for the mechanical coupling of calcium dynamics to neurite retraction.

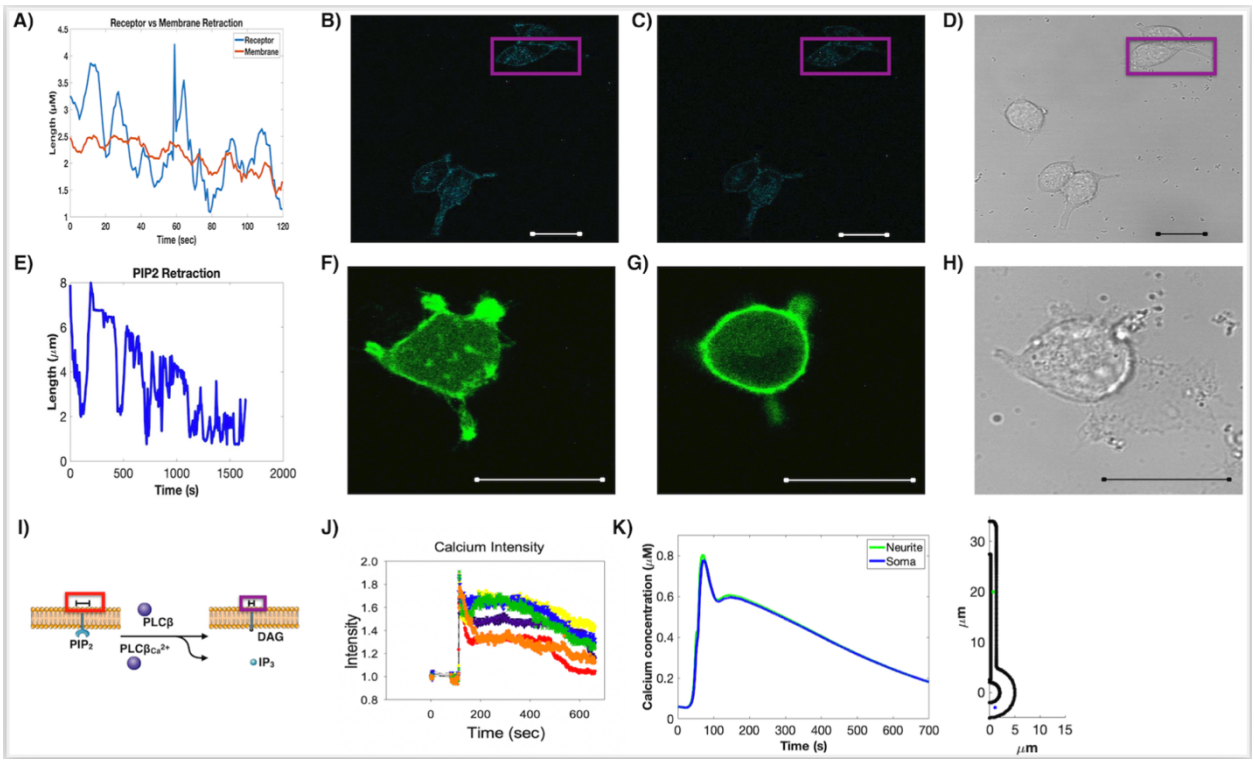

Figure II- 2. *Neurite retraction of PC12 cells upon Gαq stimulation*

A) *Decrease in neurite length of the B2R receptor in PC12 cells (blue) as compared to slow reduction in length of the membrane as followed by phase contrast (orange).* ***B)*** *Images of differentiated PC12 cells expressing eCFP-B2R prior to stimulation with bradykinin and* ***(C)*** *30 minutes after stimulation where purple box shows the retraction data of* ***(A)****, and the corresponding phase contrast image is shown in* ***(D)****.* ***E)*** *Decrease in neurite length as followed using a fluorescent PI(4,5)P_2 sensor, PH-PLCδ1 (Garcia et al., 1995) where distinct oscillations are seen.* ***F)*** *Images of a differentiated PC12 cells expressing PH-PLCδ1, prior to stimulation,* ***(G)*** *30 minutes after stimulation with carbachol, and* ***(H)*** *the corresponding phase contrast image are shown.* ***I)*** *Cartoon showing the hydrolysis of PI(4,5)P_2 to Ins(1,4,5)P_3 and DAG depicting the larger head group of PIP_2, denoted by the scale bar (red box), as compared to the smaller DAG that remains in the membrane after hydrolysis, (purple box). This decrease in the size of the membrane bound molecule*

(PI(4,5)P_2 to DAG) leads to a local change in tension (denoted by the scale bars). IP_3 moves into the cytosol and to the ER, causing a release of calcium. ***J)*** *Graph of calcium intensity in neurites of six different cells. This graph shows the lag time after the addition of carbachol, the initial spike in calcium and the slow recovery.* ***K)*** *Model replicating the intensity of calcium over time at two spatial locations (in the neurite and in the soma) after stimulation by carbachol. Inset: location of traces within the model geometry (in the neurite and in the soma). In all images, the scale bar is 20μm, and n>15 cells.*

Actin remodeling proteins affect the dynamics of neurite retraction

Actin filaments are the major cytoskeletal components of synapses and are the key modulators of neurite plasticity. An actin filament is a dynamic structure in which monomers disassemble from one end and reassemble on the other; a behavior knows as molecular treadmilling. Retraction involves inward movement of the actin structure that defines the neurite shape and so any model of retraction must incorporate actin disassembly. In neurites, actin filament remodeling is known to be associated with the drag forces related to protrusion (II-26). Additionally, $PI(4,5)P_2$ hydrolysis is closely connected to membrane-actin adhesion and membrane tension regulation (II-26).

Based on our experimental observations **(Fig. 2),** we coupled $PI(4,5)P_2$ hydrolysis and calcium release following carbachol-stimulation with a mechanical model that balances the forces due to actin depolymerization and membrane cortical tension change. Due to the timescale separation between the biochemical signaling dynamics and neurite retraction, we coupled the 3D spatial model of the Gαq/PLCβ/calcium signaling pathway **(Fig. lA-B)** to an ordinary differential equation model of neurite mechanics, assuming uniform signaling dynamics at extended timescales (Section **S1-2** in *SOM*). Briefly, the mechanical model proposes a force balance acting on the tip of the neurite (II-34). The force due to the actin cytoskeleton is acting outward, away from the soma and the force exerted by the membrane cortical tension is acting towards the soma. In this case, we assume that the cortical tension is a function of the change in the area of the membrane. This change in membrane area can result from $PI(4,5)P_2$ hydrolysis (II-22, II-21) from endocytosis of GPCRs (II-35) and from changes in tension (II-36). The force exerted by the actin cytoskeleton is modeled phenomenologically as a function of calcium-mediated cofilin and retrograde flow (II-37). Thus, the net force balance can be written as:

$$\underbrace{-F_{tension}}_{\text{Force due to cortical membrane tension}} + \underbrace{F_{actin}}_{\text{Force due to actin dynamics}} = \underbrace{\frac{\eta}{k_L L}\frac{dL}{dt}}_{\text{Drag forces}} \quad (1),$$

where

$$\eta = \underbrace{\mu_e}_{\text{drag coefficient for external fluid}} + \underbrace{\frac{\mu_m}{\delta}}_{\text{drag coefficient for membrane}} \quad (2).$$

Modeling the neurite as a cylinder with a hemispherical end cap, we obtain the governing equation for the length of the neurite as

$$\underbrace{\frac{dL}{dt}}_{\text{rate of change of neurite length}} = \underbrace{\frac{k_L L}{\eta}}_{\text{drag coefficients and length effects}} \underbrace{(-F_{tension} + F_{actin})}_{\text{Forces}} \quad (3).$$

This governing equation combines the force balance above with experimental observations that retraction velocity is proportional to neurite length. The force due to membrane cortical tension and actin dynamics depend on equations for τ and F_{actin}, respectively, given as

$$\frac{d\tau}{dt} = \underbrace{\frac{dArea}{dt}(f(PIP_2))}_{\substack{\text{area change} \\ \text{with PIP2 dependence}}} \underbrace{F_{perPIP_2}}_{\substack{\text{tension change} \\ \text{per PIP2}}} \underbrace{\frac{k_{tension}}{A_0}}_{\text{unit correction}} \quad (4),$$

and

$$\frac{dF_{actin}}{dt} = \underbrace{\frac{F_{perActin}k_{actin}}{L_0}}_{\substack{\text{Force and length} \\ \text{effects}}} \underbrace{(k_{const} + k_{cofilin} + k_{actin} + k_{drebrin})}_{\text{k contributions}} \frac{dL}{dt} \quad (5).$$

This is a phenomenological model with a combination of parameters from literature and constants fit to the experimental results, *(see SOM)*. In particular, Eqs. (4) and (5) have dependence on f(PIP2) and g(CofilinAct), which are sigmoidal functions that trigger in

response to PI(4,5)P2 and activated cofilin, respectively(Zmurchok et al., 2018).

Using this model, we simulated calcium-mediated neurite retraction in control cells. We found that the model is able to capture the dynamics of neurite retractions events **(Fig. 3C).** These models utilized experimental retraction data collected using differentiated PC12 cells transfected with low amounts of mCherry-actin to fit the phenomenological constants **(Fig. 3)**. Effectively, the model predicts that when the force exerted by actin is matched by the force due to tension, there is no change in the length of the neurite. Upon increase in PI(4,5)P_2 hydrolysis and calcium release into the cytosol, the forces due to membrane cortical tension increase while the forces exerted by the actin decrease and the neurite pulls back.

If this prediction is true, then we should be able to alter neurite retraction behavior by altering the expression of actin-related proteins or by membrane tension separately. We next probed neurite retraction dynamics by varying the concentration of select actin-related proteins such as cofilin, drebrin, and actin itself both in experiments and modeling.

Actin modulators regulate neurite retraction velocity

We followed actin disassembly in real time during carbachol-stimulated retraction using mCherry-actin in control cells and cells over-expressing cofilin or drebrin **(Fig. 4).** Cofilin increases severing of actin filaments increasing actin filament breakdown while drebrin stabilizes actin filament inhibiting disassembly (II-38-41). **Fig. 4 D-L** are screen shots of the time lapse video made during retraction where **Fig 4. D-F** are representative cells prior to stimulation with carbachol, **Fig. 4G-I** show the same cells at the beginning of retraction, and **Fig. 4J-L** show the cells at longer times. Movies of retraction *(SOM2)* were analyzed to obtain the retraction velocities during the three different conditions **(Fig. 4M-P).** This quantification enables the comparison of neurite retraction dynamics of actin in our control

versus actin when cofilin and drebrin are overexpressed. As expected, overexpression of cofilin enhances the rate of neurite retraction **(Fig. 4M** versus **Fig. 4N),** and complete retraction results in cells with a trapezoidal morphology rather than the circular one typified of undifferentiated PC12 cells. This altered morphology likely stems from the lower number of actin filaments throughout the cell due to cofilin overexpression (II-42).

We expected that transfection of the cells with drebrin would strongly impede neurite retraction in the presence of carbachol because drebrin is known to bind assembled actin filaments (F-actin) and stabilize them (II-43-II-45). Low amounts of actin allowed a sustained linear decrease (Fig. 4O) whose compiled average is within error of mCherry-actin along (Fig. 4P). These data support the idea that disruption of the intact actin network and its dynamic modeling when impeded by cofilin overexpression (increased severing) or by drebrin overexpression (inhibition of disassembly and remodeling) are key driving forces in governing retraction dynamics.

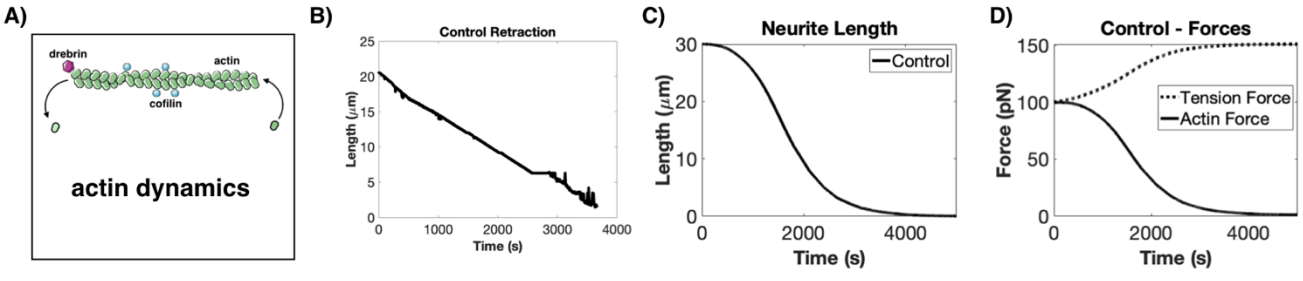

E)

Retraction Start Times of Control Cells	
Neurite 1	2.2 minutes
Neurite 2	2.4 minutes
Neurite 3	8.0 minutes
Neurite 4	7.8 minutes
Neurite 5	2.6 minutes
Neurite 6	4.0 minutes
Neurite 7	4.2 minutes
Neurite 8	2.5 minutes

Figure II- 3. *Modeling of neurite retraction.*

A) *Simplified schematic of actin dynamics depicting assembly/disassembly as a combination of effects due to actin, cofilin, and drebrin concentration.* ***B)*** *Example of the retraction in response to carbachol stimulation of differentiated PC12 cells transfected with mCherry-actin. Identical behavior was seen over an average of 8 neurites shown in the table* ***E). C)*** *Computational results for neurite retraction determined from the described model.* ***D)*** *Calculation of force plots due to increased tension in response to PI(4,5)P_2 hydrolysis, internalization of ligand-bound GPCRs, and tension effects. The force due to actin decreases and switches direction in response to actin breakdown and retrograde flow.* ***E)*** *Table showing the variation of retraction times within the same condition.*

We modeled overexpression of cofilin, drebrin, and actin in the mechanical framework by altering the F_{actin} terms *(Eq.* 5) to represent the known effects of these proteins through the 'k' contributions for each protein. We modeled actin force overall as a stress-strain relationship, where the 'k' terms captured the contribution of each protein to overall actin force dynamics. For example, cofilin expression was incorporated in our constitutive equation as an increase in the total cofilin available for calcium activation, which therefore causes a faster decrease in F_{actin} by increasing the magnitude of the rate of change of F_{actin} through the $k_{cofilin}$ term. As a result, our model predicts that neurite retraction velocity is faster for cofilin overexpression compared to control **(Fig. 4R,V).** Similarly, we modeled drebrin overexpression by increasing drebrin concentration within the $k_{drebrin}$ term, consistent with experimental observations that a higher drebrin concentration slows actin depolymerization and thus slows the decrease in F_{actin} (II-39, II-43). Therefore, our model predicts that drebrin overexpression slows neurite retraction velocity compared to control **(Fig. 4S,W).** Actin overexpression can be modeled in a similar fashion as drebrin and is captured through the k_{actin} term. Thus, increasing actin concentration is essentially increasing the actin-to-cofilin ratio and therefore slowing the decrease in F_{actin}. Our model predicts that actin overexpression will slow neurite retraction velocities compared to control **(Fig. 4Q,U).**

The results in **Fig. 4** show that by varying cofilin, drebrin, and actin concentrations, we predict different actin force dynamics that translate to different neurite retraction rates. Specifically, we predict that cofilin, actin, and drebrin overexpression leads to more rapid, slower, and slightly slower neurite retraction velocities compared to control, respectively. Our modeling results agree with the experimental observations and suggest that actin disassembly and inhibition of reassembly are necessary for retraction. To support these studies, we quantified experiments that measured retraction of control cells and cells that overexpress

actin, cofilin and drebrin. The experimental velocities of the retractions are plotted in **Fig. 4P** and validate our model predictions in **Fig. 4X**.

Neurite retraction can be driven by membrane tension.

Given that there are two contributions to the force acting on the neurite, one from actin and the other from membrane cortical tension, we next asked whether neurite retraction could be driven by changes to the membrane cortical tension alone. We directly tested this idea using hyper-osmotic stress to increase membrane tension. Increasing the hyperosmotic stress from 300 to 600 mOsm on cultured PC12 cells resulted in the same retraction behavior and timescale as seen with carbachol stimulation **(Fig. 5A).** To determine the change in membrane tension induced by this change in osmolarity, we measured tension by atomic force microscopy (AFM). This method allows us to assess the stiffness of cells by measuring the amount of deflection experienced by a cantilever with known spring constant as it indents the surface of the cell. For undifferentiated, differentiated, and retracted PC12 cells, AFM measurements were taken at the base of the neurites or retracted neurites. The stiffness of each cell was determined by averaging the stiffness values at three separate locations on each cell in order to combat the inherent heterogeneity in cell structure while ensuring no localized damage from a previous measurement. Undifferentiated cells were the stiffest condition tested, followed by retracted and then differentiated **(Fig. 5B).**

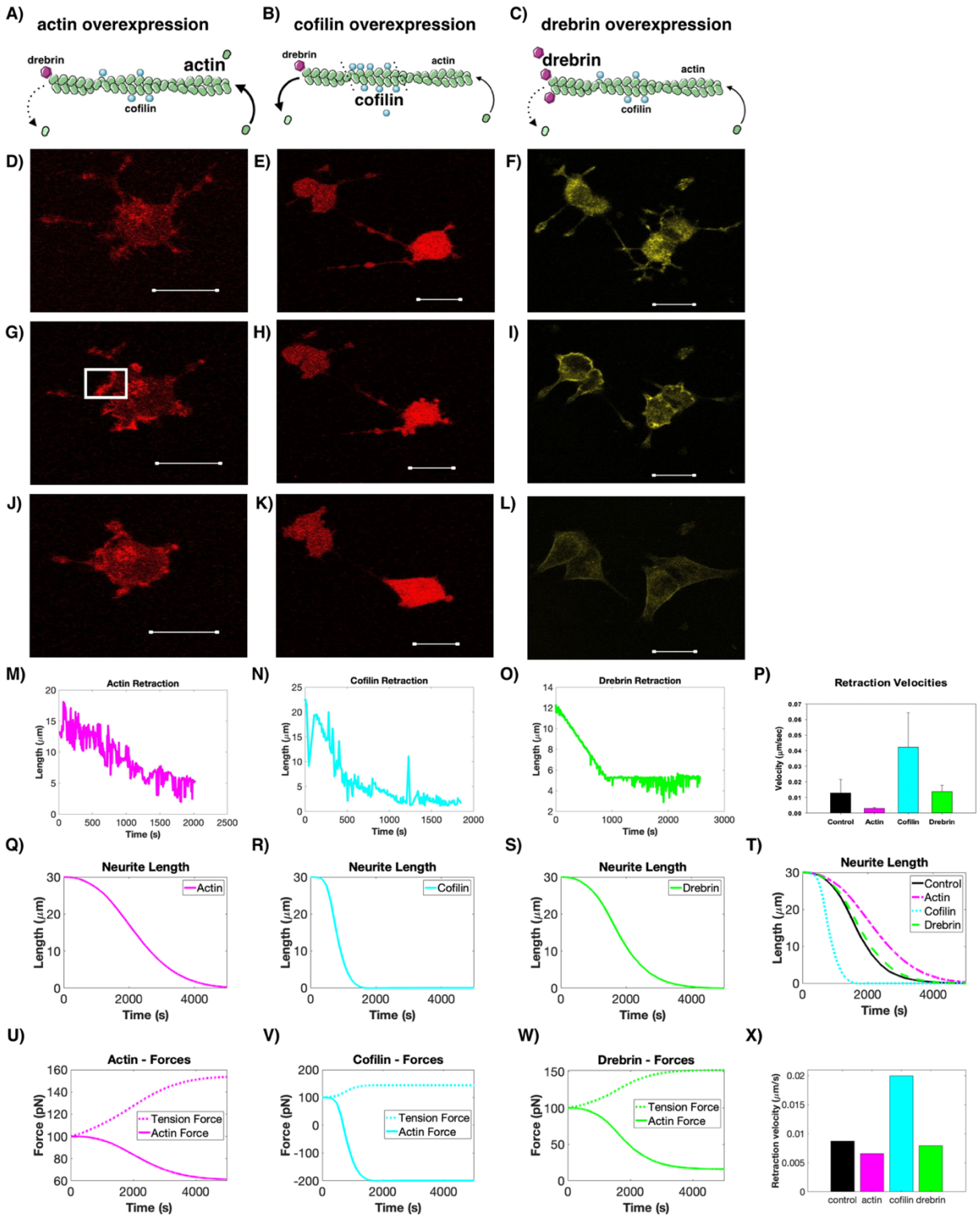

Figure II- 4. *Experimental validation of model predictions*

***Figure 4**: **A-C)** Schematic of the experimental study to test the actin force model where mCherry-actin, mCherry-cofilin or eYFP-Drebrin was expressed at varying levels in PC12 cells using increasing amounts of DNA in the transfections. The corresponding images shown directly below. While cofilin activity is mediated by calcium, actin and drebrin dynamics depend on local concentrations.*

*Column 1 (panels **A, D, G, J, M, Q, U**) are results from studies following mCherry-actin expressed in PC12 cells. The increase in actin, as estimated by western blotting, reduces the change in the actin force. Panel **D** is an example image of cells before carbachol stimulation. **G** is 15 minutes post-stimulation showing the beginning stage of actin breakdown indicated by the white box, and **J** is 30 minutes post-stimulation. A representative retraction velocity curve is shown in **M**. Panels **Q** and **U** are the results of modeling the retraction velocity **(Q)**, due to a tension force and actin force (**U**). We note that the overexpression of actin leads to less of a decrease in actin force since the increased actin concentration slows overall actin breakdown.*

*Column 2 (panels **B, E, H, K, N, R, V**) shows how cofilin overexpression creates a large negative actin force to increase the rate of disassembly as shown in the schematic **(B)**. Panel **E** is an example image of cells expressing cofilin-RFP before carbachol stimulation, **H** is 7 minutes post-stimulation, and **K** is 16 minutes post-stimulation. A representative retraction velocity curve is shown in **N**. Panel **R** and **V** are the results of modeling the retraction velocity **(R)**, due to the tension force and a larger negative actin force (**V**), since increased cofilin concentration increases actin breakdown.*

*Column 3 (panels **C, F, I, L, O, S, W**) shows how drebrin overexpression slows the change in actin force as shown in the schematic **(C)**. Panel **F** is an example image of cells expressing drebrin-eYFP before carbachol stimulation. **I** is 15 minutes post-stimulation, and*

***L** is 30 minutes post-stimulation. A representative retraction velocity curve is shown in **O**. A representative retraction velocity curve is shown in **O**. Panels **S** and **W** are the results of modeling the retraction velocity **(S)**, due to the tension force and actin force (**W**). We note that increased drebrin concentration resists actin breakdown.*

*Panels **P**, **T** and **X** are compiled retraction velocities obtained experimentally **(P)**, control (n=4), actin(n=4), cofilin(n=3), drebrin(n=4) showing standard error, and computationally (**T** and **X**), showing the very close correlation between experimental and theoretical results. All scale bars = 20 μm.*

We also used AFM to determine the stiffness of cells subjected to hypo-osmotic and hyper- osmotic stress for undifferenced and differentiated PC12 cells. Hypo-osmotic and hyper-osmotic stress, which leads to cell swelling and cell dehydration respectively, results in an increase and decrease in cell stiffness, respectively **(Fig. 5B).** Force curves that are representative of the average stiffness value for each condition show a smooth Hertz model relationship between indentation depth and applied force as expected **(Fig. 5C-D).** Taken together, these studies show a direct correlation between cell stiffness and osmotic stress, which is also correlated to retraction.

Within our model, we can also probe neurite retraction dynamics by varying the contribution of tension, the τ component, of the mechanical model. Membrane cortical tension is altered under hyperosmotic conditions when water expulsion from the cell leads to a reduction in volume-to-surface area ratio. Therefore, to model hyperosmotic conditions instead of a carbachol stimulus, we predict that this volume-to-surface area ratio change causes an increase in membrane cortical tension**.** Therefore, we model a slightly elevated membrane cortical tension initial condition that triggers a related force (**Fig. 5E**) and neurite retraction (**Fig 5F).** We also see a change in actin force, triggered due to the coupling between actin and tension in the model, which is also predicted experimentally due to the necessary actin reorganization during retraction caused by hyperosmotic conditions. Therefore, our model predicts neurite retraction in the absence of a ligand stimulus with hyperosmotic conditions **(Fig. 5F),** indicating that membrane cortical tension is a key component governing neurite retraction dynamics.

We tested whether the retraction that results from osmotic stress is convergent with the Gαq/PLCβ pathway. Keeping in mind that membrane compression regulates calcium flux to drive actin dynamics in model systems (II-46 – II-48) we determined whether hyper-osmotic stress will open calcium channels to allow divalent cation influx to relieve the osmotic stress. Using a fluorescence

calcium indicator, we found that increasing the osmotic strength from 300 to 600 mOsm results in a small increase in intracellular calcium that is ~10% of the increase seen for ACh stimulation. To verify that calcium is mediating retraction, we removed extracellular calcium from the media and found that even though increasing the osmotic strength through the addition of KCl caused membrane folds and puckering, consistent with a loss in cell volume, neurite length remained constant (**Fig. 5G**). This result indicates that the two types of retraction pathways converge on calcium levels, those initiated by Gαq/PLCβ stimulation and those initiated by extracellular calcium influx by tension sensitive calcium channels.

Prolonged exposure to Gαq agonists leads to nerve ring disruption in *C. elegans*

To determine whether we could disrupt neuronal connections and retract neurites in a neuronal network, we used the optically clear model system, C. *elegans*. We first used a strain of *C. elegans* (QW1166) that expresses an integrated fluorescent calcium sensor G-CaMP throughout the nervous system. This system allows us to visualize by fluorescence, the neurons that show increased calcium levels in response to acetylcholine stimulation. This specific strain has fluorescence in every neuron in the nerve ring allowing us to look at the ring as a whole, as well as fluorescence in the entire ventral nerve of the worm that extends the entire length of the worm. We focused on acetylcholine signals emanating from neurons within the nerve ring located in the head of the worm and along the ventral nerve cord **(Fig 6A)**

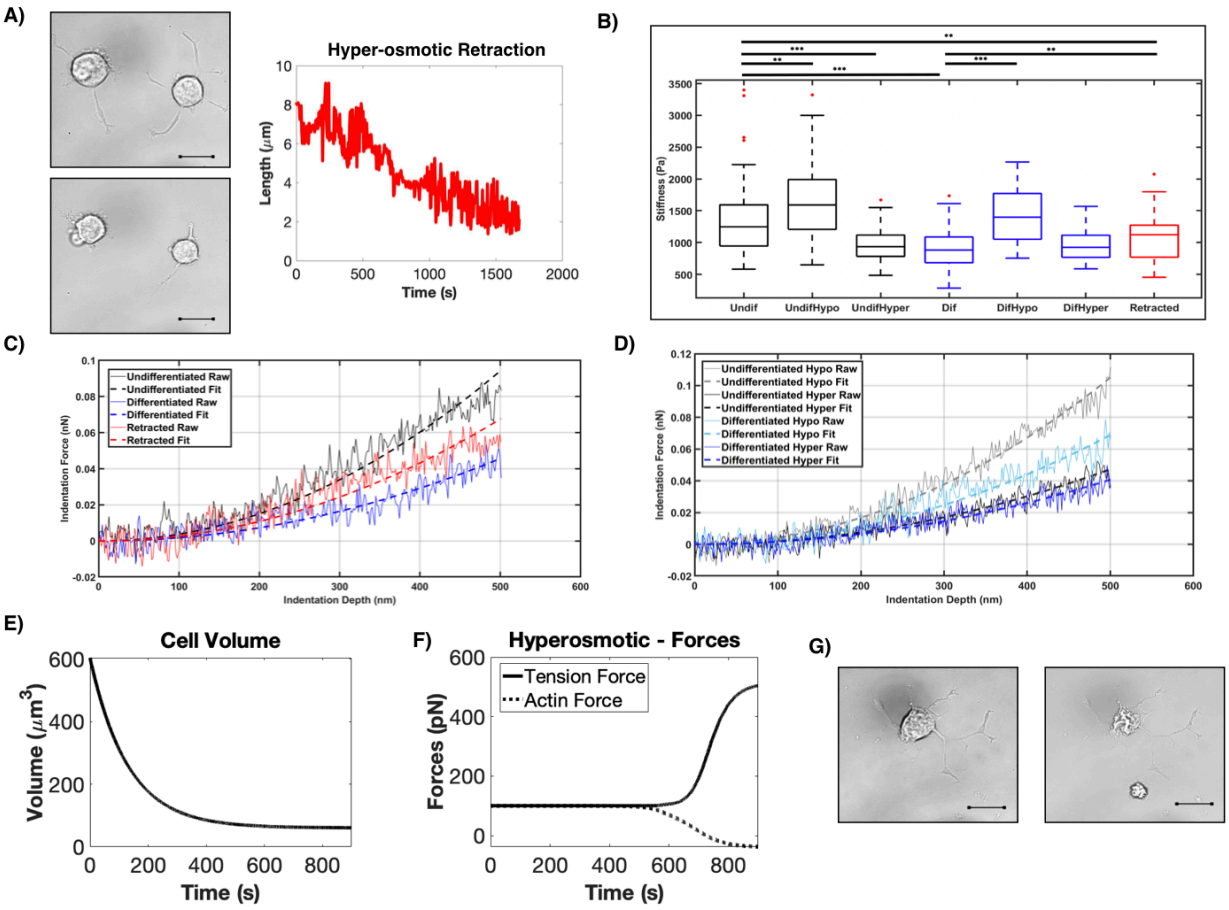

Figure II- 5. *Neurite retraction can be induced by membrane tension in response to hyper-osmotic stress.*

*A) Phase contrast images of PC12 cells under isotonic conditions (300 mOsm, top left) and hyper-osmotic conditions (450 mOsm, bottom left) after 10 minutes). The corresponding neurite retraction curve for the cell on the left is shown to the right. B) Cell stiffness as measured by atomic force microscopy of undifferentiated and differentiated PC12 cells under isotonic conditions and cells subjected to hypo-osmotic (150 mOsm) or hyper-osmotic (450 mOsm) stress where the number of cells n =14 – 46, and were * = $p < 0.05$, ** = $p < 0.01$, ***= $p < 0.001$. C-D) Force curves representative of the average stiffness values in B with automated Hertz model fitting (see methods) over 500nm indentation for untreated cells (left) and hypo-osmotic /hyper-osmotic treated cells (right). E-F) Hyperosmotic stress is modeled as an*

instantaneous increase in membrane tension due to the reduction in volume-to-surface area ratio, which causes a membrane tension increase and a smaller cytoskeletal force (E), and triggers neurite retraction (F) in the absence of ligand input. G) Phase contrast images of a differentiated PC12 cells before the application of osmotic stress (left) and after increasing the osmolarity from 300 to 600 mOsm in calcium-free media. Note the loss in cell volume seen by membrane puckering but without retraction (right)

Normal signal transmission can be seen in the images in **Fig 6B.** For these studies, we only wished to determine whether there is broad neuronal rupture and retraction within the nerve ring and along the ventral nerve which would be indicated by the lack of fluorescence in the center in the ring and dark spots along the ventral nerve. In every worm tested (n=10), we find neuronal rupture with acetylcholine stimulation that occurs in the nerve ring close to the organism's mouth **(Fig. 6C).** Additionally, we see a distinct pilling of the ventral nerve that displays thinning and clustering, and portions that are no longer fluorescent indicting large-scale neuronal damage.

We confirmed the connection between neuronal network disruption produced by extended acetylcholine stimulation to membrane tension by subjecting the worms hyper-osmotic stress (increasing the salt solution concentration by 50%). After osmotic stress, these organisms showed a lack of fluorescence in the nerve ring indicating rupture and retraction of neurons. Also, we see much larger segments of the ventral nerve that have been disrupted with less pilling than that seen for acetylcholine stimulation **(Fig. 6D).** The somewhat different morphological effects on the ventral nerve seen in osmotic stress is most likely due to the ability of the stress to be distributed uniformly along the length of organism as opposed to carbachol whose receptors are concentrated mostly in the mouth.

To support neuronal disruption of the worms by acetylcholine, we followed changes in movement of the whole organisms using a chemotaxis assay with and without acetylcholine stimulation. These studies were also done using the *C.elegans* QW1166 strain. We see that after treatment with acetylcholine 83% of the worms moved towards the attractant while the remaining 17% did not move at all **(Fig. 6F).**

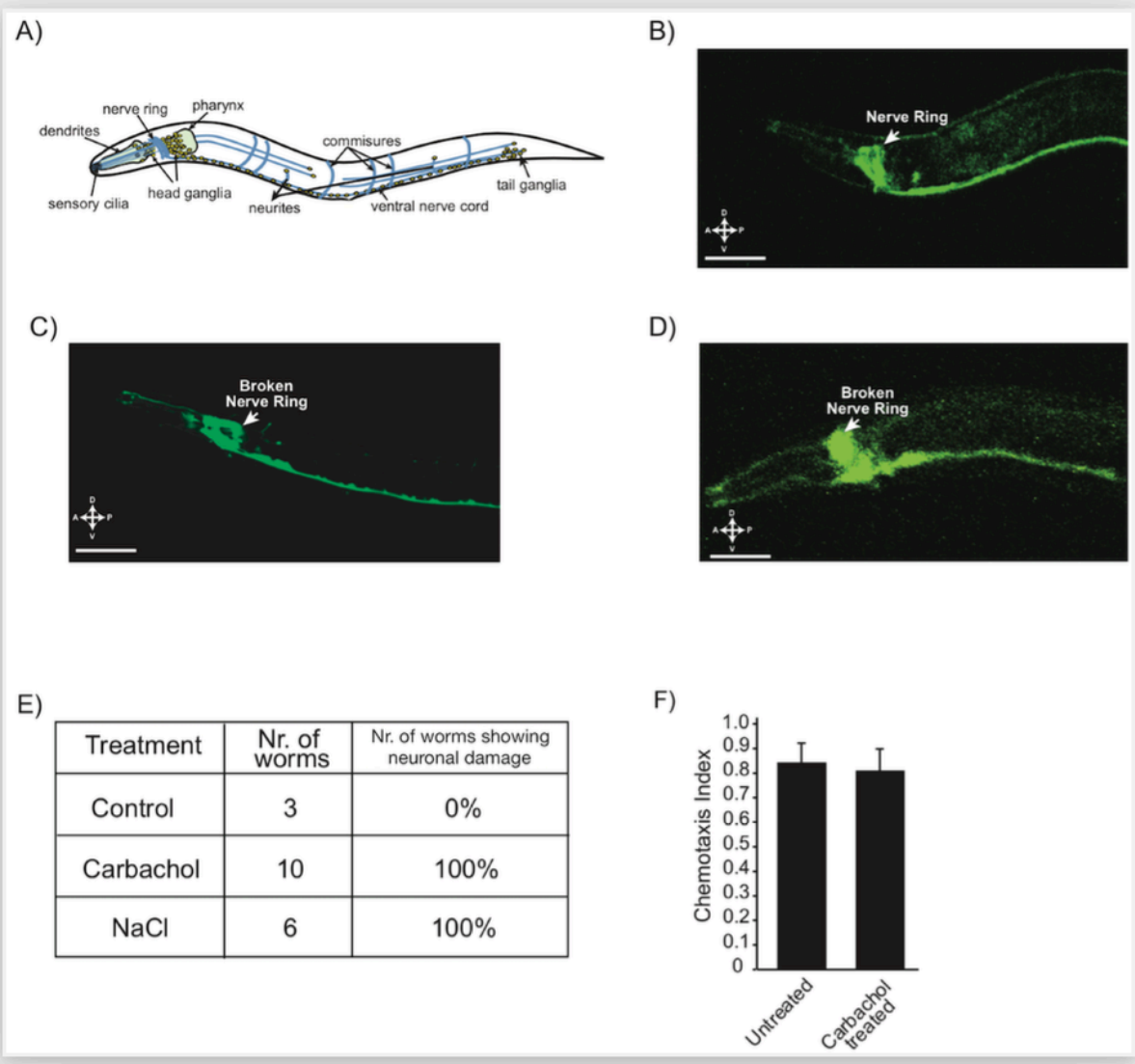

Treatment	Nr. of worms	Nr. of worms showing neuronal damage
Control	3	0%
Carbachol	10	100%
NaCl	6	100%

Figure II- 6. *Neurite retraction induced by membrane tension is seen in the neural network of C.elegans*

A) *General schematic of the nervous system of C. elegans.* ***B)*** *Untreated C. elegans that expresses GFP G-CAMP through the nerve ring and ventral nerve.* ***C)*** *A representative worm with 1mM carbachol for 30 minutes showing a broken nerve ring and pilling ventral nerve.* ***D)*** *A representative worm subjected to hyper-osmotic stress showing a broken nerve ring.* ***E)*** *Table showing the compiled results of each experimental condition and the number of resulting nerve rings that were broken.* ***F)*** *Results of a chemotaxis assay testing movement of C. elegans with and without lmM carbachol treatment.*

DISCUSSION:

In order for an organism to learn, neurons must break and reform connections with neighboring neurons and disruptions in these processes underlie learning-based neurological diseases and neurodegeneration. Despite the importance of synapse severing and formation, the mechanisms that underlie neural plasticity are not well understood (II-1). Previous studies of neural plasticity have mainly focused on contributors to neurogenesis in hippocampal neurons and cultured drosophila neurons, such as neuronal stem cells (II-49). Here, we have defined the synaptic breakage and neurite rupture in neural plasticity in terms of membrane tension and calcium-induced retraction that will allow for predictable actin remodeling.

Calcium is a crucial component for the growth, differentiation, and survival of neurons (II-12). Calcium helps to regulate the differentiation of specific neuronal types as well as their migration through the body, and calcium levels are directly liked to neurodegenerative diseases such as Alzheimer' s (II-49). We followed neuronal cell response to extended calcium signals that may mimic dysfunctional states. Unexpectedly, we find that extended calcium levels resulted in complete neurite retraction, and this retraction can be seen by following the plasma membrane, by a GPCR coupled to Gαq, and by $PI(4,5)P_2$. These data show that the Gαq signaling pathways are intimately involved with the mechanical properties of the cell.

The connection between calcium signals from GPCR/Gαq and cell mechanics was supported using fluorescent-tagged actin and by measuring retraction when overexpressing cofilin, an actin depolymerizing protein, or drebrin, an actin monomer recruitment protein. Overexpressing cofilin at a level 6x higher than endogenous levels allows for much faster velocities of neurite retraction initiated by GPCR-Gαq/Ca^{2+} after an initial lag period. These observations correlate well with cofilin's ability to depolymerize actin, but shows that activation of the Gαq/$PI(4,5)P_2$/Ca^{2+} pathway is a necessary prerequisite. In contrast, cells

overexpressing drebrin show a similar retraction rate as endogenous which correlates to its ability to stabilize actin monomers (II-39). This observation indicates that the behavior we are viewing is solely due to actin depolymerization without contributions of the polymerization events. Thus, while Ca^{2+} signals drive retraction, actin plays a passive role.

There are other physiological events that might play a role in neurite retraction. PLCβ is the primary effector of Gαq, but we also note Gαq activates proteins that impact RhoA (see (Sanchez-Fernandez et al., 2014)) potentially contributing to the mechanical changes associated with retraction. However, this contribution will only be operative for retraction that occurs in response to carbachol and not osmotic stress. Additionally, the loss of neurites during retraction shifts its associated plasma membrane population to the cytosol in the cell body. This net increase in the cytosolic PLCβ population will promote PLCβ's cytosolic roles in directing translation of specific mRNAs (*see* (II-52, II-52) which are typically not operative during Gαq stimulation. The net effect of cytosolic PLCβ would be shifting protein populations during longer times not probed in this study.

The coupling between calcium signaling and mechanical forces has been observed in cell motility and in dendritic spines during long-term potentiation, astrocyte calcium signaling, and during neurite protrusion and formation (II-53). Based on these studies, we postulated that neurite retraction results from changes in cortical tension brought about by receptor endocytosis, $PI(4,5)P_2$ hydrolysis and IP_3 generation, and an increase in intracellular calcium, and formulated a mechanochemical pathway to test this idea. We found that indeed, a force balance between cortical tension and actin-mediated forces, both of which are mediated by intracellular calcium levels, is sufficient to capture the dynamics of neurite retraction. This idea was explicitly tested by measuring changes in membrane stiffness with osmotic strength and by altering the effects of different actin remodeling proteins. We also

found that the effects of actin and cortical tension could be uncoupled to a certain extent, pointing towards multiple mechanical pathways that could exquisitely regulate neurite retraction. We acknowledge that the proposed model is phenomenological, and while it captures the key physics of the processes underlying neurite retraction, future studies will focus on elaborating on some of the phenomenological relationships proposed here.

Our results show that acetylcholine-induced calcium signals may have a dramatic impact on neuronal morphology and synaptic connections, and this idea was demonstrated in *C. elegans*. Neurite formation and extension is essential to transition from neuroblast to mature neuron and *C. elegans* are an excellent model system to understand neurite formation and retraction. The site of nascent neurite outgrowth is determined by cell intrinsic factors that orchestrate the localized regulation of actin and microtubules and in developing neurons, these factors are polarized at sites of neurite outgrowth in response to extracellular cues (II-54). Our finding that the neural network of this organism can be modified by Gαq activation or increased mechanical tension, may form a basis for studies that better describe neural rewiring paradigms.

In summary, our studies indicate the role of acetylcholine in facilitating neurite retraction. Further research on how this pathway interacts with other pathways to coordinate remodeling with such spatio-temporal precision will provide insights into understanding the molecular basis of neurodegeneration.

MATERIALS AND METHODS

Cell Culture, transfection and differentiation

PC12 cells, which are derived from rat pheochromocytoma (ATCC CRL-1721), were cultured in 35mm or 100mm poly-d-lysine coated petri dishes using Dulbecco's Modified Eagle's Medium (DMEM) (Gibco) with 10% heat-inactivated horse serum (Gibco), 5% fetal bovine serum (Atlanta Biologicals), and **1**% penicillin/streptomycin. The dishes were incubated with 5% CO_2 at 37°C. Cells were transfected using different amounts of plasmid based on the concentration tested using a NanoDrop. Cells were transfected using Lipofectamine 3000 (Invitrogen) following the protocol of the manufacturer. The media used in transfection was the same DMEM culture media with the exception of antibiotics, to increase transfection efficiency and the media was changed back to normal culture media after 24 hours. Cells were differentiated using media that contained DMEM, 1% heat-inactivated horse serum and 1% penicillin/streptomycin. Added to this would be a 1 to 1000 ratio of l00ng /µl nerve growth factor (NGF) (Novoprotein). This media is added to the cells for at least 48 hours and up to 96 hours to achieve long neurites.

Plasmids and Maxi/Mini prep

Fluorescent-tagged plasmids were obtained and maxi/min prepped using Qiagen kit and following the manufactures guidelines. The plasmids were obtained from Addgene. Actin #54967 derived by Michael Davidson at Harvard Medical School, Drebrin #40359 derived by Phillip Gordon-Weeks at King's College of London, Cofilin #51279 derived by James Bamburg at Colorado State University, Pleckstrin homology (PH)-domain of PLC8 # 21179 derived by Tobias Meyer at Stanford University, and the bradykinin type 2 receptor was modified from the construct provided by Porf. Leed-Lundber, Univ Texas San Antonio.

Calcium Green Staining

Prior to imaging, cells are washed with HBSS and then a 1/200 mixture of HBSS and Calcium Green (Thermofisher) is added and allowed to incubate for **1** hour before imaging.

Preparation of Carbachol

Carbachol in powdered form was obtained from Sigma Aldrich. It was dissolved in water to a final concentration of l mM at a volume of l0 mL and aliquoted into 500µL portions to be used for each experiment. The solutions were kept at -20°C.

Fluorescent Microscopy/ Stimulation of Cells

Fluorescent imaging was done using a Zeiss LSM510 inverted confocal microscope. Imaging was carried out at least 48 hours post transfection and differentiation. The cells were grown and imaged in a MAT-Tek 8 chamber glass bottom plates or a MAT-Tek 35mm glass bottom dish. Once a single cell was found visually that expressed the plasmid or stain, the microscope would be switched to the correct wavelength and laser intensity. A time series image was then started and stopped after 10 frames, the cells would then be manually stimulated by adding carbachol to the dish to achieve the desired final molarity, and the time series video was then started immediately after adding carbachol. Retraction velocities were determined by the software, *Re-Track*, see **Chapter 2 section 2** for full description.

Osmotic Stress and EDTA studies

Osmotic stress studies were done using calcium free isotonic media for imaging with the

addition of KCl at different concentrations to achieve osmotic stress. Studies that include EDTA, (J.T. Baker) cells were osmotically stressed and EDTA was added to the dish to give a final concentration of 0.5 for partial neurite retraction and 1μM for full neurite retraction.

Plasmid-specific studies

Calcium green and enhanced green fluorescent protein (eGFP) studies were imaged using an argon laser at 488nm. Red fluorescent protein (RFP) and mCherry were imaged using argon ion and HeNe lasers at 543nm. YFP and CFP were imaged using argon ion and HeNe lasers at a wavelength of 545nm. Multi-track imaging can also be done combining each of these set ups. Images were taken by alternating between probes when data for more than one are being monitored, and these images are subsequently merged.

Atomic Force Microscopy Stiffness Measurements

Live cells were probed utilizing an MFP-3D-BIO atomic force microscope (Asylum Research) and a DNP cantilever (Bruker) with nominal spring constant 0.06 N/m[1]. The cantilever was calibrated before each measurement to ensure accuracy. Cells were seeded on 60 mm poly-d-lysine coated petri dishes using Dulbecco's Modified Eagle's Medium (DMEM) (Gibco) with 10% heat-inactivated horse serum (Gibco), 5% fetal bovine serum (Atlanta Biologicals), and 1% penicillin/streptomycin. After 24 hours of recovery cells were differentiated using media containing DMEM, 1% heat-inactivated horse serum and 1% penicillin/streptomycin. Added to this would be a 1 to 1000 ratio of lO0ng/μl nerve growth factor (NGF) (Novoprotein). This would be added to the cells a minimum of 24 hours before measurements are taken.

Cells were viewed two days after plating and one day after treatment with nerve

growth factor (NGF). Cells with minimal cell-cell contact were selected to reduce the mechanical impacts of cell communication. Three force curves in separate perinuclear regions with cantilever velocity of 2μm/s and trigger point lnN were taken for each selected cell. Measurements were taken within 30 minutes of removal from the incubator to facilitate cell viability.

The stiffness of the measured cells ***E*** was determined from the force curve data utilizing the Hertz model for conical cantilever tip geometry:

$$\boldsymbol{E} = \mathrm{Kddrr}(1\text{-}v^2)/\ 2\mathrm{Ll}^2 \tan\ c/J$$

where ***k*** is the cantilever spring constant, dis the cantilever deflection, vis the poison's ratio (0.5 used for an assumed incompressible material), ***A*** is the sample indentation depth, and **<*P*** is the half- angle of the conical cantilever tip (35°). The force curves were processed using a custom MATLAB code that fits the indentation curve over a 500nm range after manual selection of the initial contact point.

Fluorescent Imaging of C. elegans

Worms were transferred into a microcentrifuge tube containing l mM carbachol and were submerged in the tube for 30 minutes at room temperature or 100mM NaCl solution for 10 minutes. After 30 or 10 minutes respectively, the worms were removed from solution and placed on a glass slide with a thin layer of agar on it for the worms to lay on. Excess carbachol was wicked up from the pad and the worms were paralyzed using 25M levamisole that does not a affect our pathway of interest. The worms were then imaged on an inverted confocal microscope and were visually checked for neurite rupture and retraction.

Chemotaxis Assay of C. elegans

Worms were transferred to a new seeded plate 24 hours prior to the experiment. The day of the experiment an unseeded plate is marked with a dot in the center and two circles on either ends of the plate with the “C” for control of DI water and “D” for diacetyl which is the attractant**.** Using approximately 1mL of s. basel the worms are washed into a microcentrifuge tube and allowed to pellet for 5-10 minutes. Once pelleted, the worms are washed with s. basel two more times and finally with water. 10μL of the suspended worms are transferred to the experimental plate previously made and the excess water is removed by wicking. The plate is then incubated for 45 minutes at 20^{o}C, and after, the number of worms that have moved either to the attracted or control is counted.

ACKNOWLEDGEMENTS

This work was supported by NIH GM116187 (SS) and AFOSR MURI FA9550-18-1-0051 (PR). We thank various members of the Rangamani and Scarlata labs for valuable discussion and manuscript review. We would like to thank the UCSD Interfaces Graduate Training Program and the San Diego Fellowship for funding and support for MB. MB was also supported by AFOSR MURI grant number FA9550-18-1-0051 to PR and a grant from the National Institutes of Health, USA (NIH Grant T32EB009380).

CHAPTER II SECTION 2: Re-track: Software to analyze the retraction and protrusion velocities of neurites, filopodia and other structures

Authors and manuscript breakdown: Manuscript was contributed to equally by Iman Mousavi and Katherine Pearce. The experiments were done by Katherine and the software creation was done by Iman.

ABSTRACT

We have developed new software, Re-track, that will quantify the rates of retraction and protrusion of structures emanating from the central core of a cell, such as neurites or filopodia. Re-Track, uses time-lapse images of cells in TIFF format and calculates the velocity of retraction or protrusion of a selected structure. The software uses a flexible moving boundary and has the ability to correct this boundary throughout analysis. Re-Track is fast, platform independent, and user friendly, and it can be used to follow biological events such as changes in neuronal connections, tip-growing cells such as moss, adaptive migration of cells, and similar behavior in non-biological systems.

INTRODUCTION

Many biological events involve the formation of processes and protrusions that emerge from a central structure, such as the cell body. Some of these structures allow for cell movement whereas others allow for the attachment of cells onto surfaces for adhesion, which are critical for events

such as immune responses and tissue development (II-55). Filopodia associated with migration play a critical role in the spread of cancer (II-56). Additionally, many cells naturally grow and retract structures that sample the environment and probe for presence of neighboring cells or nutrients (II-57). Retraction and protrusion events also play a major role in the development and restructuring of neuronal networks that are vital for learning and development (e.g. II-58).

Here, we describe the software, Re-track, that allows us to quantify the velocity of retraction and protrusion of structures independent of their size, using only a high-resolution time-lapse video of any magnification. As described below, Re-track fills a void in current software needed to analyze growth and morphology of neurons but is also general enough to be applicable to all natural and synthetic systems. The information gleaned from Re-track can help delineate environmental and cellular factors that contribute to the rates of these events.

MATERIALS AND METHODS - SOFTWARE

Demonstration of the software can be found in the linked videos.

Description of software

Re-track was developed to track tip growth/contraction in Java 1.7 or higher in the following operating systems: Windows (7), Mac OS X (10.9 or newer), or Linux (Ubuntu 10.04, RHEL 5.4 or newer)

The general procedure is the initial input of time-lapse images into the software in the TIFF format that contains continuous frames of a captured video, as detailed below. After opening the file, the user can see the video in the viewport. Changes in the length of a specific structure with time are calculated by selecting the structure of interest. A smaller viewport on the right side shows

the output of the algorithm based on the input parameters. After finding the optimal parameters for a frame, it can be used for the whole movie. It is also possible to use the parameters for other videos with a similar microscopic setup. The application is opened by double clicking on the JAR file or by using the following command:

```
cd path/to/separationtracker
java -jar separationtracker.jar
```

Definitions of buttons and settings:

Understanding how a software works is critical for proper use. Each of the sliders and parameters have distinct uses for analyzing videos in *Re-Track* and any combination of them could be used to properly analyze a video. The input file is imported into the software using **Open Stack.** This will open a single TIFF file or multiple images as a stack. The spatial position of the structure of interest can be located by clicking on its base and tip. After doing this, a red-line will appear on top of the main viewport. This line act as a guide to crop and rotate the original image. By re-adjusting this line at the different frames, *Re-Track* automatically interpolates its length, location, and direction for the intermediate frames. **Width** is the parameter that refers to the width of the cropped box around the red-line. After determining the line that connects the two manually clicked points, *Re-Track* will rotate and crop the images based on the line and apply the edge detection algorithm on the cropped image. After locating the structure, the threshold for the detection must be adjusted to optimize edge detection using the **Threshold** slider. This value may vary from one experiment to another. It's possible that some regions the structure seem to be edgeless or blended with the background of the image (due to low contrast imaging or noise or etc). In such cases, Re-Track might consider one structure as two. Depending on the specific video or stack file **Merge Dist** can

be adjusted to account for the discontinuity. This is important for videos where **Breaking** will be used. **Breaking** is utilized (checked) when cell structures (such as a synapse) are joined then snap during the video. If this option is unchecked, the first manually added point should be on the soma of the cell with the line extending past the structure (i.e. Neurite), see **video Re-Track breaking**. **Clear** determines the strength of erosion morphology. In the *Edge detector* viewport the background will be red and the blue pixels represent the structure of interest. For example, if the structure of interest is a neurite, the blue pixels in the *Edge detector* view should correspond to the same shape and size of the neurite in the file viewport. To reduce the noise of the input image, we apply a moving average with a window size determined by **Smooth**. This value can adjusted as necessary to account for varying amounts of noise. **Jump** will be used if the structure (i.e. neurite) makes large movements through the frames and cannot be followed properly. If the speed of a pixel movement is greater than the jump value, it would be consider a jump and be discard from the output data set. **Edge Detection View** displays the result of edge detection. The width is determined by *Width* and the height is the length of the red-line. After obtaining a satisfactory result, **From/To** adds a time interval of the original file to the output file. **Relative** refers to the positions and velocities relative to endpoints of the line. **Linear interpolation,** when checked, dictates the software to linearly interpolate the value for the Y position in the data when there is a discarded frame between two detected frames. When it is unchecked, the "Y" coordinate of any discarded frame is assigned to "-1". This will be helpful, for plotting the position data and/or calculating the velocity of the tip(s). **Progress Bar** corresponds to the percentage of the frames processed. **X** cancels the current task. **Positions** will save the positions of the tip in a text file. The output file consists of five columns (time, x1, y1, x2, y2).

The positions are based on the edge detection coordinates. If the application cannot determine the position of a tip, it gives -1,-1 as the x and y coordinate pair.

Method to detect the position of the tip.

Re-track uses a TIFF file of the high resolution video as the input and displays it in the viewport. As retraction/protrusion may happen in a portion of the movie, a time slider is located at the bottom of the viewport to determine the time interval of the process. The spatial region of the structure of interest can be determined by manually clicking the corresponding beginning and end of the structure in a way that the whole structure remains inside the region (box) at all times. To reduce the computational cost, Re-Track uses the initial and endpoint to rotate and crop the image. The height of the cropped images is equal to Euclidean distance between the two points and its width can be adjusted by the Width parameter. There is a secondary viewport on the right side of the main viewport, Edge Detection View, which presents the output of the applied algorithm on the cropped image.

With the cropped image, Re-track applies a moving average on the image to reduce the noise. The size of the filter is determined by the "Smooth" parameter. Then it applies a Laplace filter to find the edges. The result will turn to a red and blue image by applying a threshold. False detection can be reduced by applying an erosion morphology. The "Clear" parameters adjust the size of the erosion. Once the edges are properly detected, Re-track follows them from the tip(s) toward the end(s). To find the tip, Re-Track turns the secondary viewport to a h×w matrix of zeros(red pixels) and ones(blue pixel), where h is the height of the image and w is its width. Then it generates the h×w submatrixes, Ai, where n is adjusted by "Merg Dist" each of them is consists of i to i+n, i=1, ..., h-n rows of the main matrix. After generating each submatrix, Re-

Track calculates the summation of all of the components. If the result of the summation is equal to zero, that point is considered as the tip of the structure. Noise and moving particles near the tip can induce false detections. These false detections can be discarded using the "Jump" parameter. This parameter puts a maximum threshold for the tip displacement for every two adjacent frames. If the displacement of the tip passes this value between the ith frame and i+1, Re-Track discards the (i+1) frame and compares the displacement of the tip between ith and (i+2)th frames. It will continue this procedure until it finds a frame where the tip is within the determined range. Re-Track may lose the position of the tip during this procedure. In this case, it is necessary to readjust the parameters for a better result. A flowchart of the procedure is shown in Fig. 1. Upon opening the software, the following window will appear as in Fig. 2.

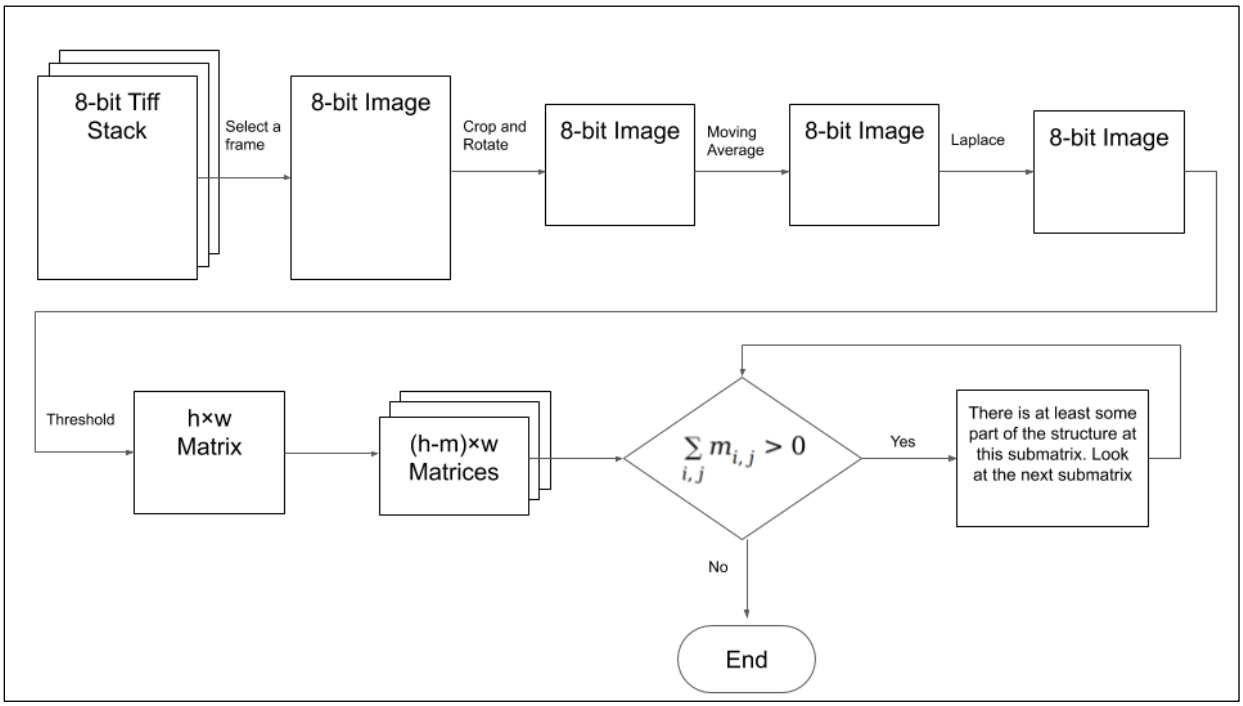

Figure II-II- 1.. *A flowchart of the tip detection algorithm*

Figure II-II- 2. *Screenshot of the initial Re-track program window. See video Re-Track_PC12.*

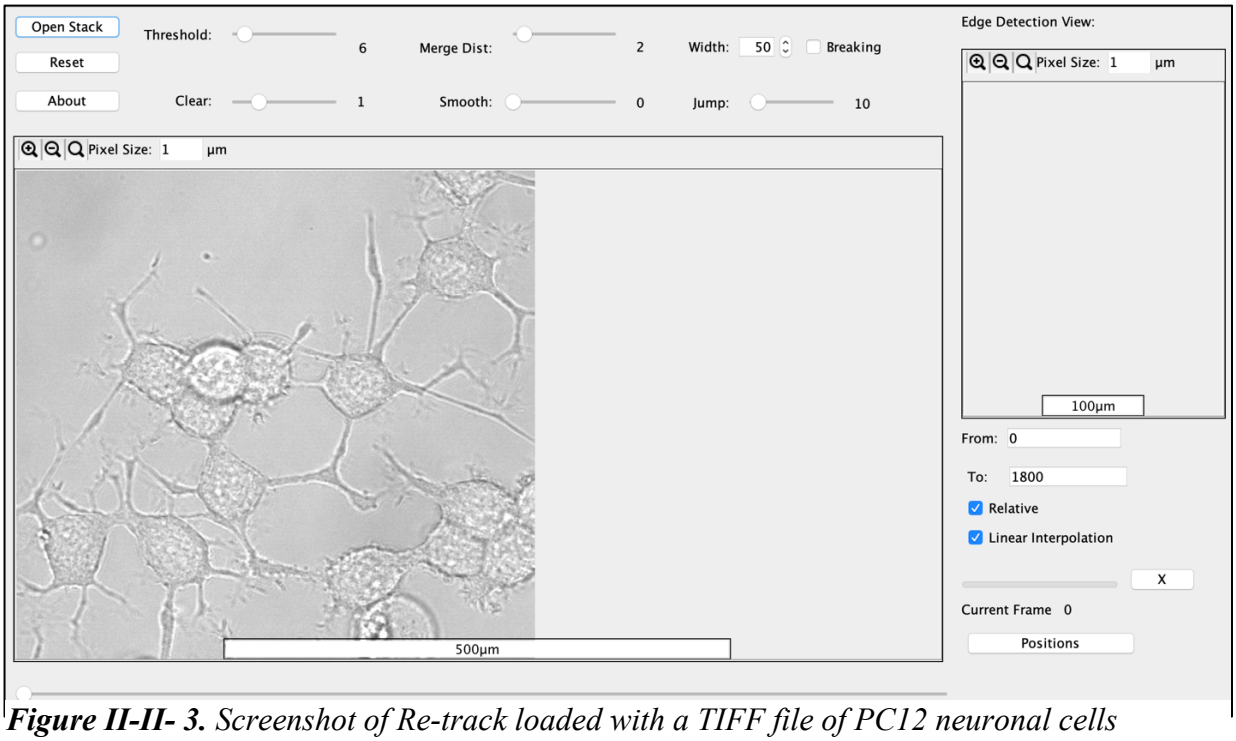

Figure II-II- 3. *Screenshot of Re-track loaded with a TIFF file of PC12 neuronal cells*

From this screen, individual neurites or comparable structures can be selected one at a time and then reset using the Reset button on the top left. See video Re-Track_PC12

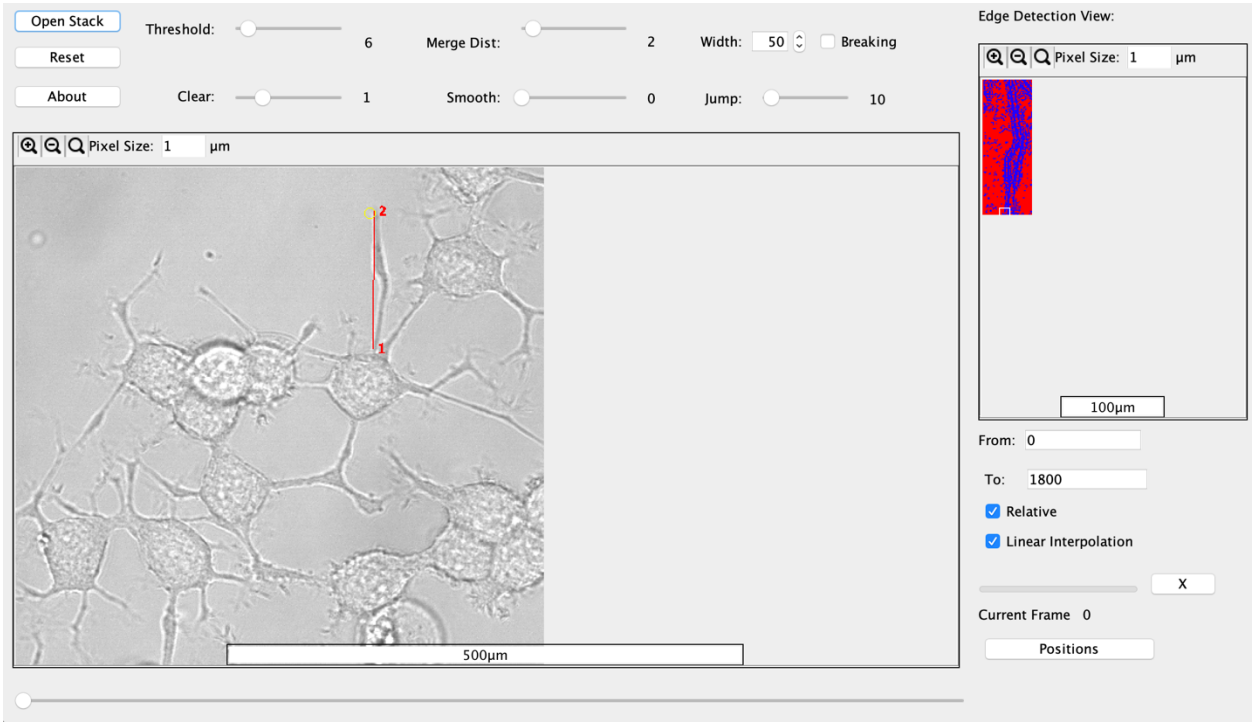

Figure II-II- 4. *Screenshot of a Re-track window*

Follows the retraction of a neurite where the red numbers (1 and 2) refer to the start and end points, respectively, and the line connecting them is in red which appears after selecting the time frame. To the right, you will see an edge detection view once the red line is drawn. The blue shows the region that the software identifies as the neurite and the background in red. If this detection view does not match your image, then a new line should be drawn. This neurite does not have two tips so the Breaking box located above Jump is unchecked.

Upon opening the software, the stack of images can be imputed using the Open Stack button. The images can be a single TIFF or separate files. It may take a few minutes to load the images depending on their size. After loading the input file, you should see the open images in the main window viewport similar to the one shown in Fig 3.

Re-track follows changes in specific structures with time. In some systems, the protrusion structures (i.e. neurites) are linked together but then separate during the retraction event. In these cases, the time parameter can be accessed by the Time slider to get closer to the separation time. For these circumstances, the Breaking checkbox can be checked. You can then determine the line that connects two cells by clicking one base of the structure on the main view. After the first click, the Time slider will be disabled until the user determines the other end point by clicking again.

Following the time period selection, click on the selected structure again. You should see a red line on the screen (see Fig 4). By doing this, you will have a Key Frame for the line following the neurite. You can change the length of the line by clicking again on the Key Frame. As you go through frames, you can re-draw the red line to more closely fit the neurite, if desired. This procedure allows for intermediate frames (Inbetweens) between two key frames. Re-Track will animate the line using linear interpolation. The line will not appear before the earliest key frame.

The two white boxes in the Edge Detection View determine the position of tips. When you are happy with the result, (i.e. how the line follows the retracting structure over time), you can click the Positions button and save the output as a text file and analyze further using software such as MATLAB or Microsoft Excel.

RESULTS

Analysis of neurite retraction in PC12 cells using Re-track.

We have used Re-track to analyze the retraction of neurites in PC12 cells under different experimental conditions. Use of the software for different samples are presented in the videos (see Supplemental material).

Using Re-track, we determined the retraction velocities of cultured mammalian PC12 cells induced by carbachol stimulation or hyper-osmotic stress (II-62). First, we created a graph that shows the average positions of neurite retraction of PC12 cells under different conditions where each point on the specific curve was calculated using the software (Figure 5). Conditions that induce rapid retraction is easily quantified. For example, cofilin is a protein that binds to actin filaments and assists in depolymerization resulting in a faster rate of depolymerization (II-63). We find that PC12 cells over-expressing cofilin show the fastest retraction velocity correlating well with cofilin function [8]. Another example is the change in the rate of neurite retraction with osmotic stress. Increasing the osmotic strength of the media increases osmotic stress causing neurites to retract into the soma of PC12 cells (II-62). This behavior is seen in Fig. 5 when we raise the the osmolarity from 300 to 600 mOsm. In contrast, no retraction occurs when cells are subjected to hypo-osmotic stress (i.e. 300 to 150 mOsm) since this condition creates an outward force on the plasma membrane (see Figure 5).

Re-track analyzes each trace as the Euclidean distance from the tip to the base. The traces analyzed in Fig. 5 used brightfield images, in Fig. 6 we show results from the analysis of fluorescence images as well as brightfield images. This comparison illustrates how Re-track can analyze any type of image since the user has to initiate the location of the original line to inform the software of the type of pixels it will be following. In this case, the software allows us to rapidly

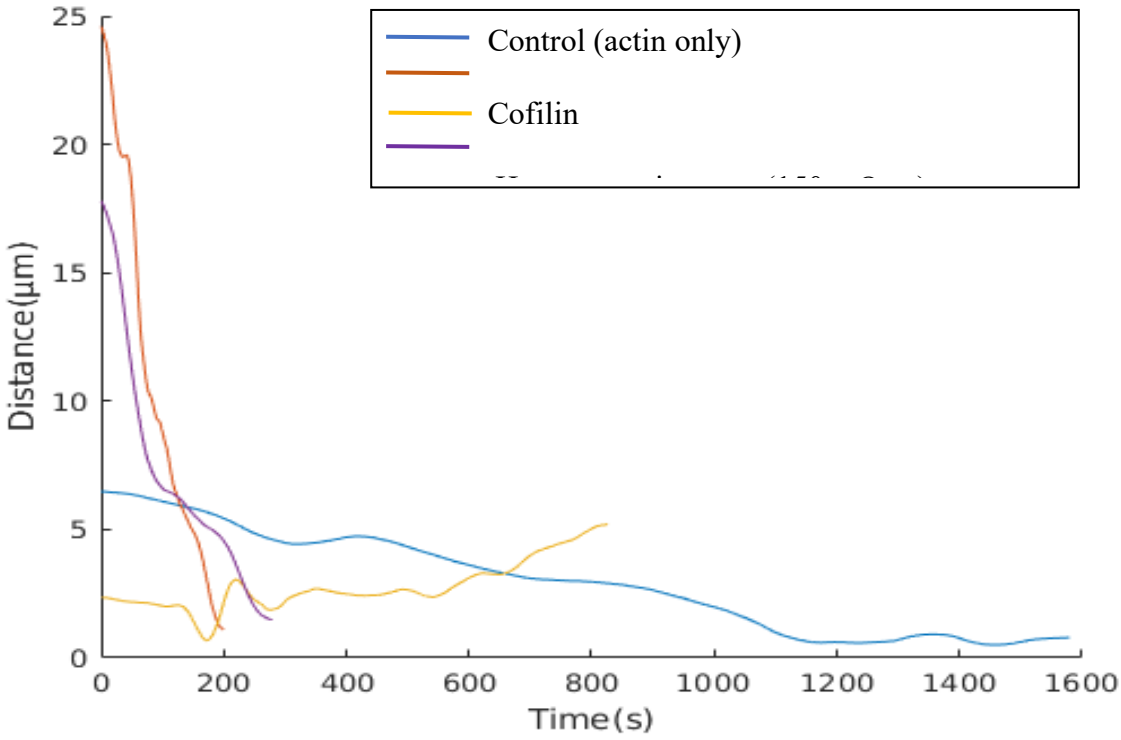

Figure II-II- 5. *Individual traces of four different conditions of PC12 cells over expressing mCherry-actin and co-transfected with cofilin which promotes disassembly of the cytoskeleton (), or subjecting cells to hyper-osmotic stress (600 mOsm) to promote neurite retraction. No retraction occurs in cells under hypo-osmotic stress (150 mOsm). Using the text file outputted by the Re-track software, the position vs time for each of the different conditions can be visualized by any plotting program. In this plot, individual traces show the wide range of velocities as the neurites retract while still highlighting the behavior for each condition.*

view the effect of different agents that impact actin assembly and membrane tension. Quantification of the retraction velocities by Re-Track permits an easy comparison between different experimental conditions during the time of the experiment even though the cell sizes, neurite lengths and other physical parameters may differ between the samples.

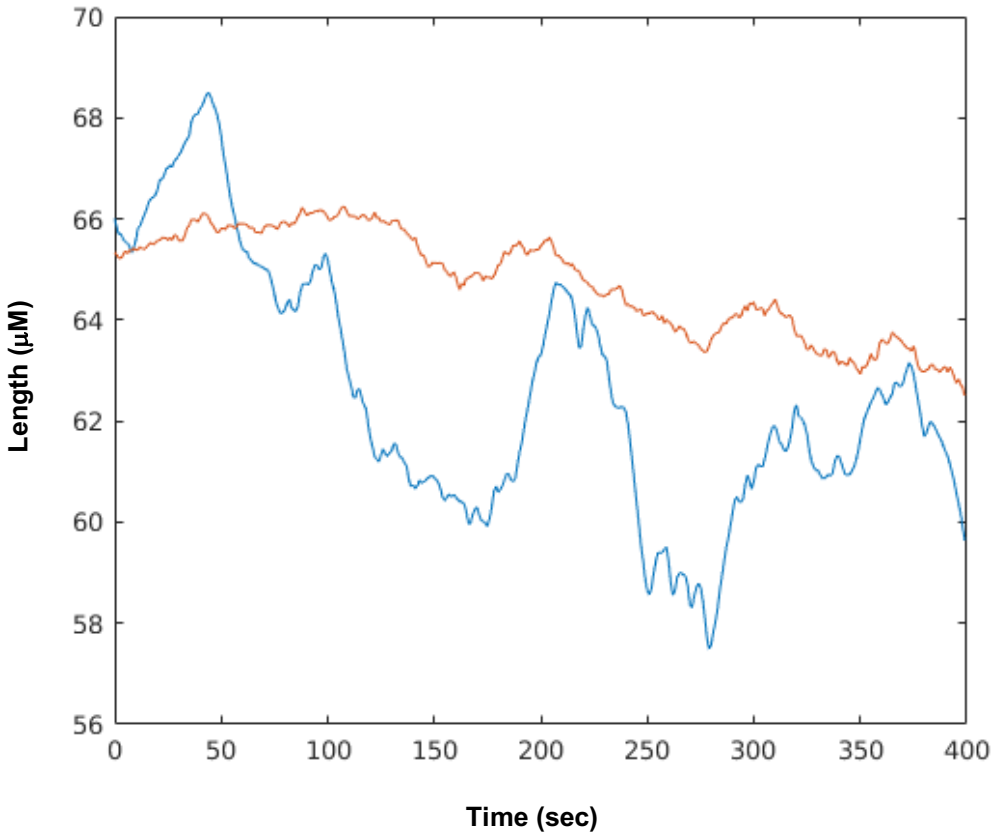

Figure II-II- 6. *Graph showing different retraction velocities of neurites in PC12 cells transfected with a fluorescent G protein coupled receptor (bradykinin type 2, B2R) upon the addition of bradykinin. While the membrane surrounding the neurite (orange) moves at a slower rate compared to B2R (blue), the data were at a lower resolution and show a time-averaged behavior.*

As mentioned above, Fig. 7 follows the retraction of a PC12 neurite in two separate channels, the brightfield and the fluorescence channel which detects the movement of a fluorescent-tagged GPCR (I.e. the bradykinin receptor type 2 (B2R)). While these channels were monitored at different resolutions, the same analysis is used for both (see Re-Track_fluorescent movie). In Fig. 6, we find that B2R moves from the neurite into the soma before the plasma membrane during retraction. Comparing these two velocities allows for an increased understanding of receptor movement and dynamics within the cell.

Determining the growth of moss protrusions using Re-track.

Re-track was used to analyze the growth behavior of a well-characterized system, moss. For this experiment, Physcomitrella patens tissue was imaged over 25 minutes (see Methods) to visualize the distance from the tip to the base. The resulting video was then analyzed using Re-Track to follow to tip growth over time. While previous work did not quantify the growth rates of the tip (II-64), we were able accurately follow the tip growth and obtain values in accord of these previous estimates.

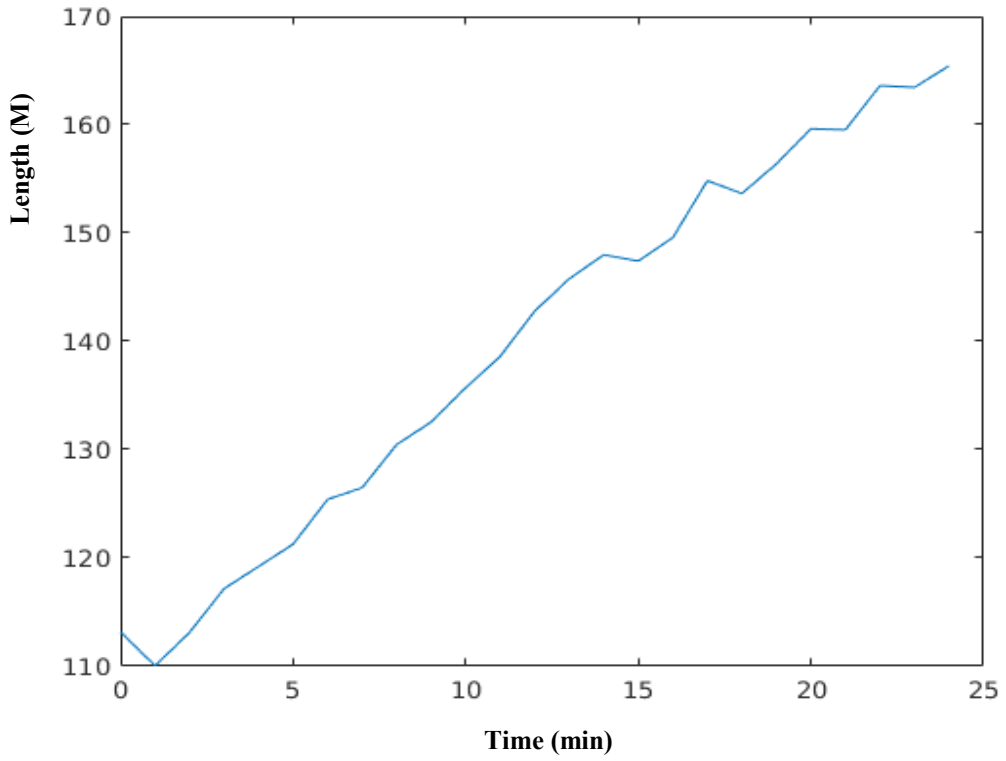

Figure II-II- 7. *Growth of moss as analyzed by Re-track software.*

DISCUSSION

In this study, we describe software that allows the calculation of the retraction velocity for protrusion and retraction of a growth that emanates from a central body. While the examples given here are for biological samples, this software can be applied to non-biological systems such as solar flares, stream flow from lakes, etc. The only requirement is a time series of equal intervals, and images at a resolution that allows protrusion to be identified. It is important to note that a minimum number of 300 frames is required for proper analysis and this requirement will depend on the variation in the retraction / protrusion behavior. The software is optimized for

videos of retraction only or protrusion only as the combination of retraction followed by protrusion will lead to the protrusion positions being disregarded by the software.

Re-track fills a void in software presently available and has been designed for use by the general public. Re-track complements presently available software packages that analyze assembly of cytoskeletal proteins in filopodia protrusions, such as Filopodyan (II-65), the number and lengths of filopodia, such as FiloDetect (II-66) dynamic changes in cell shape, including protrusions, such as CellGeo (II-67), changes in the distribution of fluorophores in cells, such as QuimP (II-68) and cell migration, such as ADAPT (II-69). Re-track is designed to be generally applicable to time series of any type of images that were measured individually or simultaneously in different channels for a given sample in a user friendly-format that, in most cases, can be carried out during the time of the experiment. Re-track can be coupled with other available software to fully view changes in morphology and differentiation of cells. The only comparable software, TrackMate (II-70) uses simple tracking that defines movements of a particle with time. Trackmate, as well as Simple neurite tracer software, which are both available open source through ImageJ cannot properly follow the dynamic movement of a retracting neurite, and they lack a simple user interface that can be used to easily plot change in position over time and calculate velocities (see Table 1). ImageJ also offers a kymograph feature that can be used to plot each slice of a time series to generate the speed of growth of a line over time as previously used in the same moss system studied here (II-64). Our methodology surpasses the ease of quantification and, unlike kymographs, has the ability to analyze multi-directional videos. This function plots speed versus time whereas Re-track plots changes in position with time giving us the flexibility to analyze

positional changes in either direction (i.e. growth vs. retraction). It is notable that Re-track gives identical results as those previously derived for moss using this latter procedure.

Re-Track gives the user the speed and ease of processing that allows quantification of data for real time adjustments to the specific experiments. The accuracy of Re-track can be seen in a comparison of neurite retraction data analyzed by Re-track versus images analyzed by hand (supplemental). This software has been optimized for fluorescent and brightfield image analysis (see videos, supplemental) but can be used to analyze images from any high-quality video. This range in ability comes from the first step of manually locating the retraction/protrusion tip which allows the software to properly orient within a given video, and gives the software the ability to re-locate the tip during the analysis. These combined features give the software a broad range of applications.

EXPERIMENTAL METHODS

Cell Culture, transfection and differentiation.

PC12 cells, which are derived from rat pheochromocytoma, were cultured in 35mm poly-d-lysine coated petri dishes using Dulbecco's Modified Eagle's Medium (DMEM) with 10% heat-inactivated horse serum, 5% fetal bovine serum, and 1% penicillin/streptomycin. Dishes were maintained in an incubator under 5% CO2 at 37□C. Cells were transfected using different amounts of plasmid (see details below) based on the concentration. Cells were transfected using Lipofectamine 3000 (Invitrogen, Inc.) following the manufacturer's protocol. . The media used in

transfection was the same as culture media with the exception that antibiotics were eliminated to increase transfection efficiency. The media was then returned to culture media in 24 hours.

Cells were differentiated using media that contained DMEM, 1% heat-inactivated horse serum and 1% penicillin/streptomycin. Differentiation was then induced by adding a 1 to 1000 ratio of nerve growth factor (NGF). Cells were then incubated for at least 48 hours and up to 96 hours to achieve full differentiation as seen by neurites whose lengths are greater than three time the diameter of the cell body (see (II-59, II-60).

Fluorescence microscopy studies

Fluorescence imaging was done using a Zeiss LSM inverted confocal microscope. Imaging occurred at least 48 hours post transfection and differentiation. The cells were imaged in MAT-Tek 8-chamber glass bottom dishes or MAT-Tek 35mm glass bottom dishes. Single cells expressing the plasmid or fluorophore of interest were first identified visually before switching to the desired wavelength and laser intensity. In the studies described in the Results, time series videos were initiated, stopped after 10 frames (100 frames per second), and treated with carbachol to induce retraction. The time series was then resumed.

Carbachol Preparation

Solid carbachol was obtained from Sigma Aldrich. It was dissolved in water to a final concentration of 1mM at a volume of 10mL and aliquoted into 500□L portions to be used for each experiment. The solutions were kept at -20°C.

Cellular fluorescence imaging

Calcium Green (Invitrogen) and enhanced green fluorescent protein (eGFP) studies were imaged using an argon laser at 488nm. Red fluorescent protein (RFP) and mCherry were imaged using the argon and HeNe lasers at 543nm. Enhanced yellow fluorescent protein (eYFP) was imaged using argon and HeNe lasers at a wavelength of 545nm. Multi-track imaging was carried out by combining the individual scanned images.

Experimental conditions for moss studies.

Physcomitrella patens tissue was cultured using standard methods according to (II-61). For imaging, a one week old moss plant was transferred in a 35 mm glass bottom petri dish (Matsunami) filled with agar. The petri dishes were prepared as follows: a 1 ml pipette tip was placed on the glass bottom of the petri dish followed by 4 ml of moss medium with agar. Once the agar solidified, the pipette tip was extracted, leaving a well. The well was then filled with 70 µl of the moss medium followed by placement of a plant after solidification. The thin layer of agar in the well allows for visualization of the moss sample on the microscope, while the outer thick layer of agar keeps the chamber moisturized. All imaging of moss was done in a glass bottom dish following the same procedure found above in fluorescent microscopy/ stimulation of cells.

Software	Re-Track	Track-Mate	Simple Neurite Tracer	By Hand
Pros of software	Analyzes growth and retraction very rapidly. Allows for analysis of multiple, simultaneous events. Simple and initiative to use for students and general scientists and engineers.	Analyzes growth and retraction	Available open source though ImageJ. Follows multiple neurites through slices of TIFF files Could be used in conjunction with other software to both trace and show velocity over time.	Analyzes growth and retraction.
Cons of software	Requires manual location of neurite tip.	Complicated for those without experience in coding or a background in computer science.	Does not properly follow the dynamic movement of neurite retraction. Seems to work only	Time consuming: Requires visual identification of points in each frame of the movie,

			with growth and not retraction.	and subsequent calculations.

Table 1. *Comparison of Re-Track to the two other methods of retraction analyses.*

ACKNOWLEDGEMENTS

The authors would like to thank Luis Vidali and Giulia Galotto for their help with the moss experiments. This work was supported by NIH GM116187.

Authors contributions. SS and KMP initiated and conceptualized the project. SIM wrote the software. KMP carried out all of the experimental work. SS wrote the paper and response letter. ET helped develop and improve the software.

CHAPTER III – Extended Gαq stress in *C. elegans* leads to age-dependent changes in neuronal morphology and increased mitochondrial stress

ABSTRACT

The neural system of *C.elegans* is a model for human disease since it shares many common features with mammalian neurons, such as signaling through the Gαq/PLCβ/calcium pathway. This pathway mediates calcium signals in response to hormones and neurotransmitters. Here, we have studied the response of one of the *C.elegans* touch neurons, PVM, expressing a GFP neuronal tag to repeated Gαq stimulation in young, middle-aged, and old worms. In unstimulated worms, aging is associated with the appearance of beads and waves along the PMV extensions in accord with previous work. We find that Gαq stimulation increases the presence of these morphologies, and this effect is more pronounced with longer durations of stimulation and with the age of the worm. Recovery of morphology was also age-dependent with older worms showing a reduced ability to return to normal morphology. Studies using a worm strain with a mitochondrial marker are consistent with the idea that beads contain mitochondria, and we find that the number of neuronal beads can be directly correlated to mitochondria health. Taken together, these studies suggest that extended Gαq stimulation results in characteristics associated with reduced longevity.

INTRODUCTION

Understanding the complexity of aging and cellular stresses that increase the likelihood of an aged neuronal morphology is essential to understanding why some humans retrain normal brain function with age while other suffer from neurological decline (1). Here we use *Caenorhabditis elegans* to investigate how extended Gαq stimulation increases cellular stress leading to an overall

aged morphology in *C. elegans* touch neurons. Similar to humans *C. elegans* show a loss in neuronal function with age accompanied by changes to the overall neuronal structure and decrease in synaptic vesicles. (1,2). Previous studies using a transgenic strain with fluorescently labeled touch neurons (pMec-4GFP) have shown there to be specific age related morphologies such as beading, misshapen soma and neurite branching (2,3,4) in aging *C. elegans* touch neurons. Mitochondria have also been found in the axon swelling sites accompanied with these aged morphologies and microtubule disorganization (4,5,6).

The Gαq / phospholipase Cβ signaling system is a conserved pathway whose activation leads to the hydrolysis of phosphoinositol 4,5 bisphosphate (PIP_2) which in turn leads to a series of events that result in increased intracellular calcium and changes in the activity of a host of calcium-dependent pathways (7, 8). Natural stimulants of this pathway include acetylcholine, serotonin, histamine, endothelin II and others. Binding of these small molecules to their specific G protein coupled receptor (GPCR), causes the release of calcium from ER stores and the mitochondria and influx of extracellular calcium, which occur in the first ~30s after their addition. Down-regulation of this signal involves internalization of the GPCR, reduced PIP~~2~~ on the membrane, and deactivation of Gαq. The return to basal calcium levels takes several minutes.

In previous studies, we followed calcium levels in a cultured neuronal cell line (PC12) after the addition of carbachol, a stable form of acetylcholine (9). Following cells for extended times, i.e. 10-20 minutes, showed that in the initial stages of recovery, cell neurites retracted into the soma resulting in spherical cells. This retraction was postulated to be caused by changes in the tension of the plasma membrane due to hydrolysis of PIP_2, calcium flux, and internalization of GPCRs. Once initiated, retraction continues until complete. These studies were extended to the model organism *C. elegans* whose 302 neurons in the hermaphrodite express the Gαq/ PLCβ

signaling system (7). Carbachol activation of *C.elegans* neurons tagged with a fluorescent neuronal marker showed that Gαq stimulation resulted in synaptic breakage of the neural ring, which is analogous to the brain, as well as beading and waving, along the ventral nerve, which is analogous roles to the spinal cord (see Figure 1).

Because the effects of short and long-term extended stimulation of the Gαq pathway in *C. elegans* as well as in mammalian systems are unknown, we studied alterations in the neurological function of *C. elegans* subjected to extended Gαq stimulation. Here, we have imaged changes in the PVM touch neurons in *C. elegans* of different ages when the Gαq /PLCβ / calcium pathway is stimulated, and their ability to recover. Our studies support the idea that beading and waving of the PMV axon positively correlates to the age of the worm and the duration of Gαq stimulation, while recovery is negatively correlated with age and duration. These age-related morphologies can also be induced by reducing worm stiffness osmotically and are associated with the loss of mitochondria function, giving insight into how extended calcium signals impact neuronal aging (5,10).

This study aims to understand the connection between mitochondria and age-related neuronal morphologies as well as investigate the effect of membrane tension change brough on as a result of Gαq stimulation. Extended stimulation presents an aged morphology in *C. elegans* touch neurons, similar to what was found in cells. Both a decline in mitochondrial health and a decrease cellular tension are hallmarks of aging. Understanding how Gαq stimulation exacerbates these normal aging mechanisms with could give insight into how cellular stress effects neuronal structure in disease.

RESULTS

Gαq stimulation enhances the age-associated neuronal phenotype in *C.elegans* PVM neurons.

We imaged a strain of *C.elegans* strain that expresses a GFP tag in the PVM neurons at three different ages, young (day 1), middle aged (day 5) and old (day 8) (**Fig.1A**). As previously reported, PVM neurons show beading and waving as they age.

Our previous studies found that stimulation of Gαq with a neurotransmitter such as carbachol, reduces membrane tension in cultured cells and causes transient contraction of *C.elegans* neurons resulting in breakage of contacts in the neural ring and spine that recover after several minutes. When focusing only on PVM neurons, we find that Gαq stimulation increases the number of worms whose PVM display beads and waves (**Fig. 1**). These results suggest that stimulation of Gαq may induce the same morphological features that occur naturally with age.

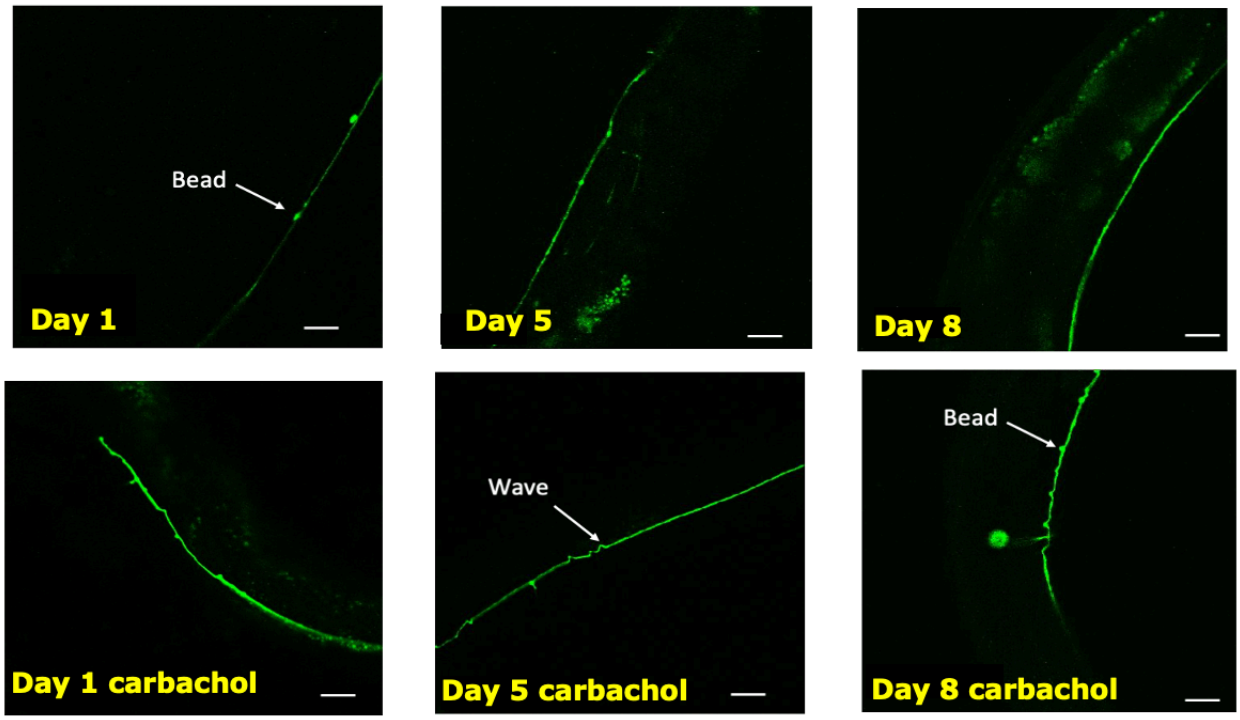

Figure III- 1. *Description of morphological changes in C. elegans axons a representative image of a day 1 worm axon. This axon is showing the beading morphology that can naturally occur. (b) an image of a day 1 stimulated axon where slight beading can be seen along the length of the axon (c) a representative day 5 axon. (d) a day 5 stimulated axon that is showing the waving morphology as indicated by the white arrow. This morphology only occurs in one section of axon but can occur throughout. (e) a representative day 8 axon. (f) a day 8 axon that shows the soma of the neuron as well as the beading morphology throughout the length of the axon. All scale bars are 20μM.*

To better characterize morphological changes, we first focused on changes in beading after Gαq stimulation, noting that beading and waving should similar behavior (see below). **Fig. 2A** shows the increase in beading along a PVM with age and immediately after Gαq stimulation. We first note that the number of beads along a neurite are lowest in young worms, but show similar

values in middle-aged and older worms. Young worms showed a small increase with stimulation while a larger increase appears to occur for middle-aged and older worms. We quantified the spacing between beads and waves in PVM neurons that occur with age and with carbachol stimulation (**Fig. 2C-D**), and found little change with the exception of Day 8 which showed a slight increase with stimulation.

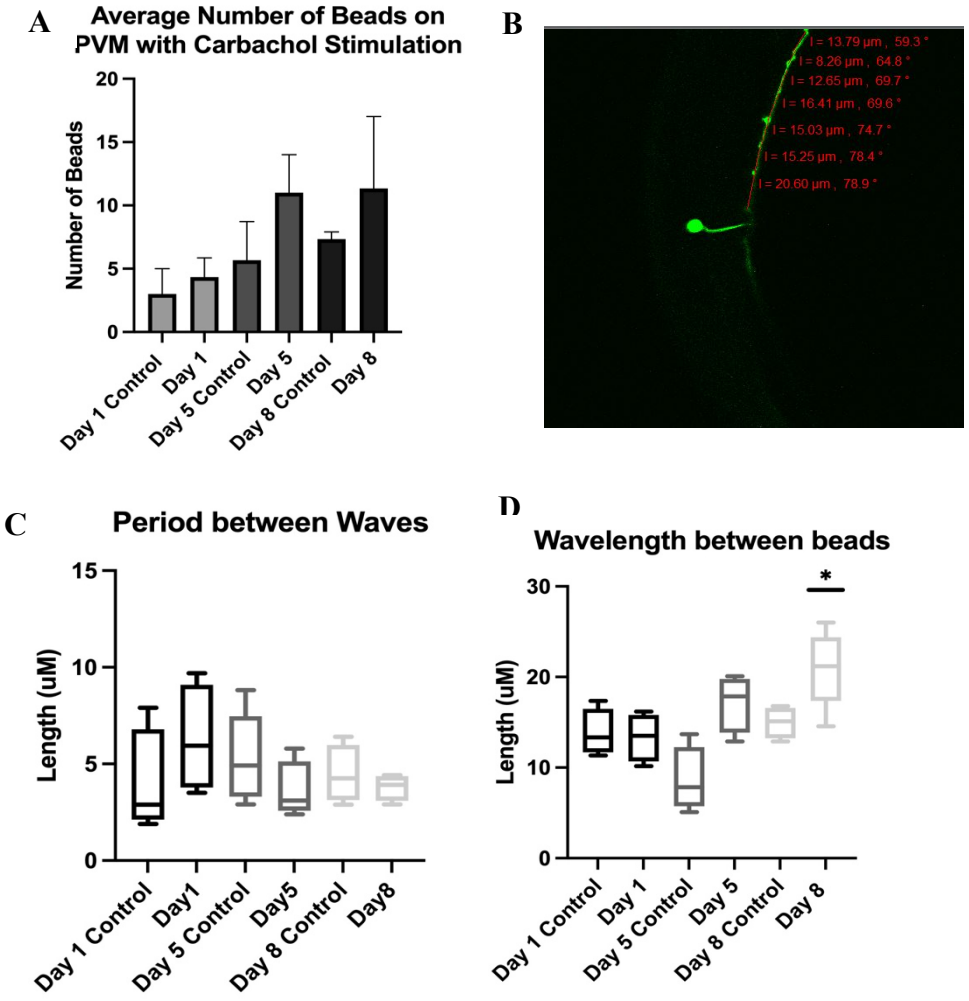

Figure III- 2*. Further analysis of beading and waving throughout age (a) graph showing the average number of beads that are found along the PVM throughout the ages of the worms. Each group has an n number of at least 5 and a t test was done to compare each group to respective*

control (i.e. compare day 1 to day 1 control). (b) representative photo of wavelength between beads using Zeiss LSM software. (c) box plot of the wavelength between beads found on the PVM. Each group has an n number of at least 5 and a t test was used to compare each group to its respective control. Day 8 was statistically significant $p<0.05$. (c) Period between waves was measured and is shown here in a boxplot. No statistical significance was found.

In **Fig. 3A** we present compiled results of the number of worms showing beading and waving and no morphology as worms were imaged 30 minutes after carbachol stimulation. We note that each neuron displays multiple beads and waves but a PVM displaying multiple morphologies is counted only once. The results show a dramatic increase in worms with no morphology from ~30% for unstimulated Day 1 worms to ~100% for stimulated Day 8 worms. Altogether, the data clearly show that Gαq stimulation promotes age-related morphologies.

PVM morphology may be related to tension.

It has been found that the tension of worms decreases with age (2), and it is possible the enhanced appearance of waves and beads with age could be due softening of the worms associated with to reduced tension. To determine whether this is the case, we directly changed membrane tension osmotically through the addition of salt. We subjected worms to enhanced salt for multiple time periods and found that more than 10 minutes of stimulation resulted in morbidity. In **Fig. 3B** we show that salt produces a very similar increase in beading and waving as Gαq stimulation. Because Gαq stimulation has been shown to impact membrane tension, these results are consistent with the idea that changes in morphology are brought about by reduced tension (see Discussion).

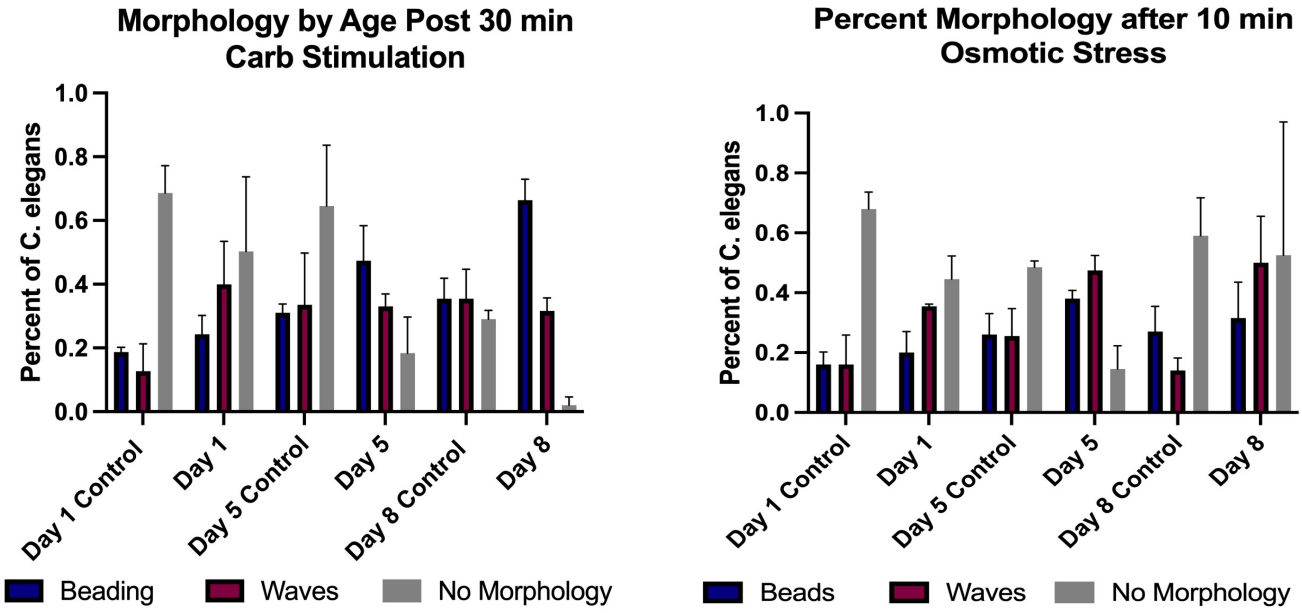

Figure III- 3. *Morphological differences with stimulation of carbachol vs osmotic stress (a) Morphology with age was characterized after stimulation of carbachol for 30 minutes and imaged immediately. Each group has an n number of at least 15. (b) Morphology with age after osmotic stress. Worms were stimulated for 10 minutes and immediately.*

Extended Gαq stimulation impacts PMV morphology

Gαq signals are regulated by aggregation of the ligand-bound receptors on the plasma membrane, subsequent internalization and then recycling to return to the basal state. We determined whether extended Gαq stimulation, which may produce multiple rounds of Gαq stimulation and receptor internalization and recycling, would cause beading and waving to continue to form. This idea was tested by subjecting worms at the three different ages to continuous Gαq stimulation from 30 min to 48 hrs and observing their morphologies after 30 min and 24 hours recovery. Results are shown in (**Fig. 4A-F**). The trends for beads and waves are noisy, but 'no morphology' at both 30 min and 24 hours recovery show that he duration of stimulation with increased age and time of stimulation reduced this population. These results show that PVM morphology does not fully recover regardless of the time of Gαq stimulation.

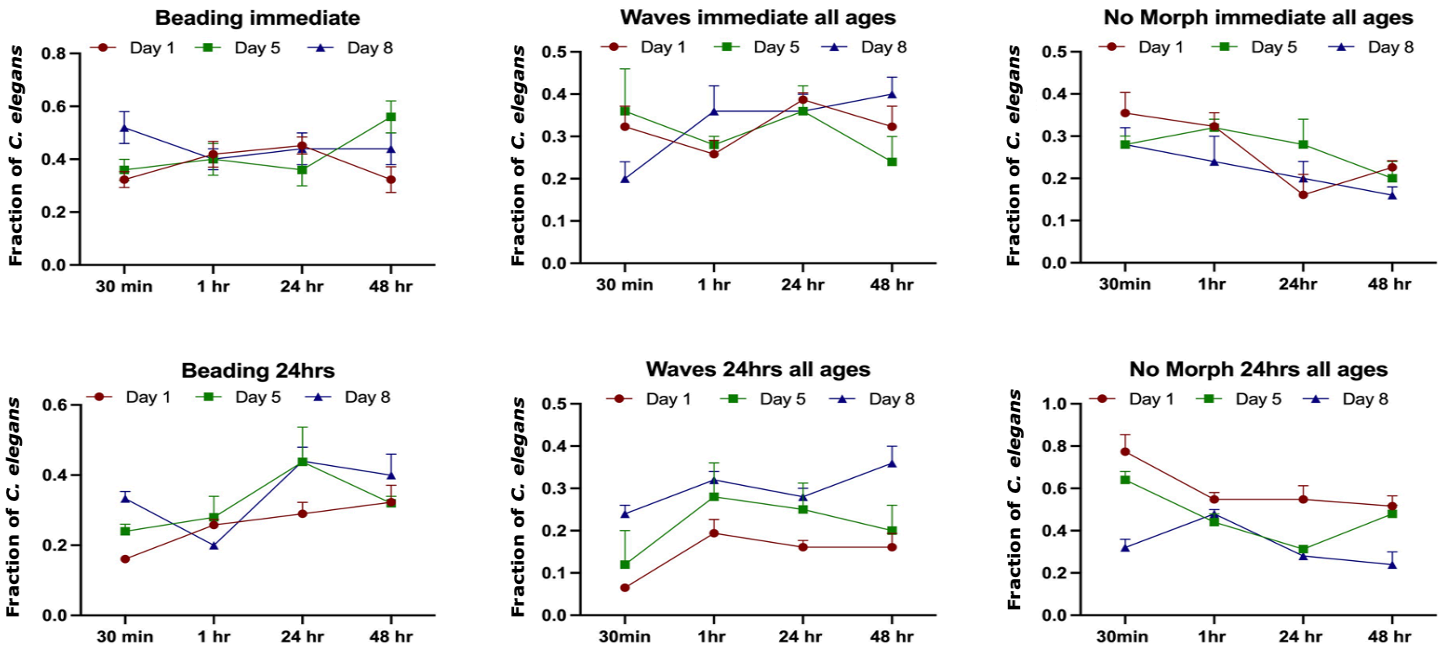

Figure III- 4. *Trend of morphological changes that occur with age and time of stimulation. Worms were stimulated for four different times 30 minutes, 1 hour, 24 hours and 48 hours. Each worm was imaged immediately following stimulation and then 24 hours later after being washed and left to recover on a seeded plate. (a) beading immediately after stimulation with carbachol. (b) beading 24 hours later of the same worms that have recovered. (c) waving immediately after stimulation with carbachol. (d) waving 24 hours after recovery. (d) no morphology immediately after stimulation. (e) no morphology 24 hours after recovery of the same worms.*

Morphology changes with Gαq stimulation are accompanied by reduced mitochondria function

The data above indicate that Gαq stimulation promotes an aged phenotype in PVM neurons. Several studies have shown a direct connection between mitochondria health and aging (11, 12). However, the effect of Gαq stimulation on promoting mitochondria degradation is unknown. Using a worm strain CLP215 that tags mitochondria with fluorescent mCherry in the six soft touch neurons, we tested the idea that repeated Gαq stimulation will promote the formation of mitochondria aggregates of Day 1 worms. In comparing **Fig. 5** to **Fig. 1B**, we find that control worms show mitochondrial beads spaced approximately twice the length as PVM beads. Upon stimulation, we see a shift from uniform wavelengths between mitochondrial aggregates to sporadically spaced whose mean becomes shorter with repeated stimulation. After stimulating several times, the spacing between the beads becomes identical the Gαq and age-related beads in PVM neurons.

a)

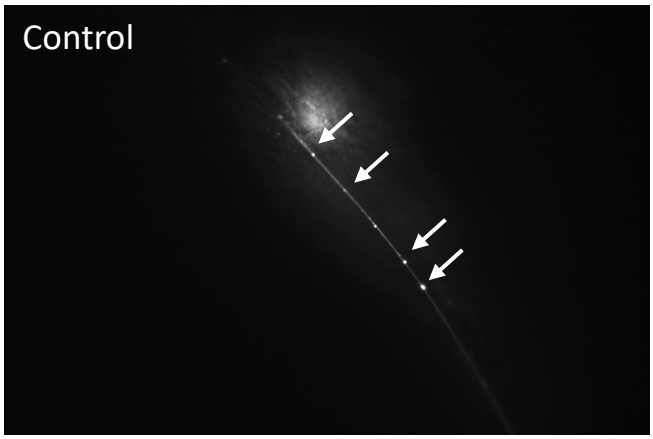

b)

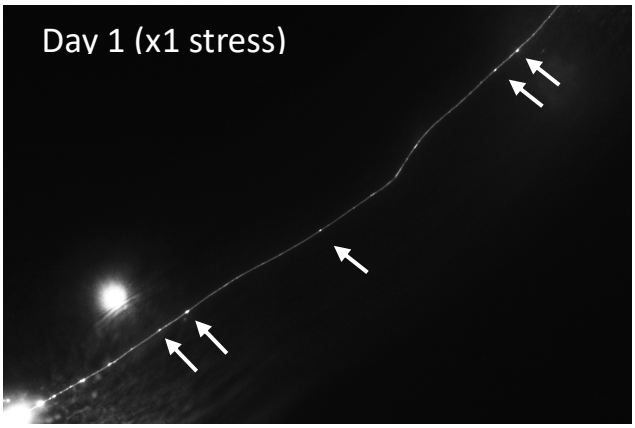

c)

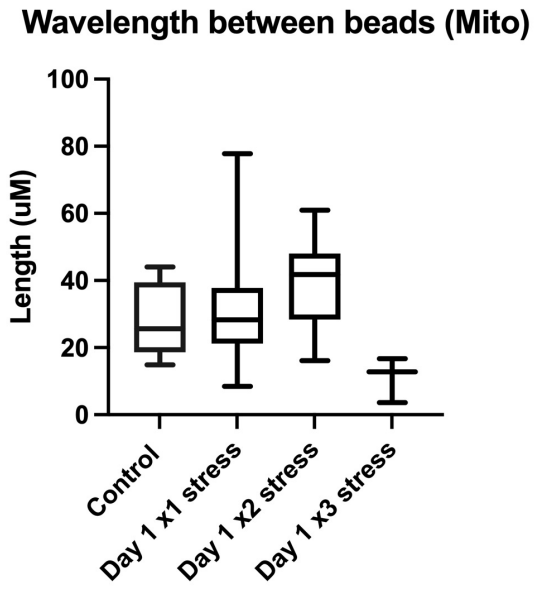

Figure III- 5. *Mitochondria show similar morphological changes with stimulation (a) representative image of day 1 control worm that has not been stimulated. (b) image of stimulated day 1 worm showing change in mitochondria location along the axon. (c) Wavelength between mitochondria/beads. No statistical differences were seen with multiple stresses of carbachol.*

DISCUSSION

In this study, we find that Gαq stimulation promotes morphologies associated with aging PVM touch neurons. This aging morphology appears to be related to tension change, which has been shown to be impacted by the Gαq /PLCβ /calcium pathway (7-9). The appearance of beading and waving morphology increases with age and stimulation and is not completely reversible. Additionally, Gαq stimulation promotes changes in mitochondrial morphology that accompanies aging and dysfunction.

Gαq is one of the four G protein families that allow cells to respond to signals from both distant and neighboring cells and transduces calcium signals from extracellular agents such as acetylcholine (13). While initiation of Gαq signals are very rapid, down-regulation and recovery processes can be much slower depending on the cell components. Previous studies in our lab have shown that extended Gαq stimulation of PC12 cells leads to retraction of neurites into the cell soma, and a general contraction of the cell due to changes in membrane tension caused by receptor internalization, calcium flux and PIP_2 hydrolysis (9). Additional studies using a *C.elegans* strain expressing fluorescent GCaMP in neurons to follow calcium levels upon Gαq stimulation showed breaking within the nerve ring and along the ventral nerve consistent with neurite retraction and cell contraction of the organism. Functional studies showed that Gαq stimulation initially causes the worms to cease moving and take on a 'C' shape due to muscle contraction, but after ~30 minutes, the worms return to their basal state and can swim towards an attractant.

Here, we have used a worm strain fluorescently tagged pMec-4GFP in the six soft touch receptors, which show bright somas and long extending axons (14). The six soft touch neurons are found along the cuticle with three anterior facing neurons (AVM, AMLM, ALMR) as well as three posteriorly faced neurons (PVM, PLML, PLMR). We have specifically focused on the PVM

due to its close proximity to the cuticle and uterus that aid in fluorescent visualization and axon identification. The two axonal morphologies studied here, beads and waves, have been shown to occur naturally in the PVM and their appearance increases at a linear rate with age (14). However, these previous studies only quantified the total number of these morphologies found along the axon. Here, we also find that the wavelength between beads increases as worms age and take on a less stiff and more swollen morphology.

By focusing on PMV, we were able to better characterize morphological changes with extended Gαq stimulation using fluorescence imaging. We measured the recovery of PVM morphologies in different aged worms immediately following 30 min, 1 hour, 24 hours and 48 hours after Gαq stimulation and find that even young worms do not completely recover, thereby maintaining the 'aged' morphology. Functionally, when we view the ability of worms to swim during and after recovery, we find that worms recover their ability to swim within 30-60 minutes showing that muscle extension again occurs even when the stimulant is still present.

As worms age, they naturally lose cellular tension due to an inability to retain water similar to humans (15). Changes in membrane tension can lead to a variety of morphological changes within the cell and to widespread dysfunction if the salt content is not regulated properly. While cells regulate the number of ions by expelling or uptaking water from the surrounding area, with age this regulation decreases, which may be exasperated by disease. Our data here correlate with the idea that tension plays a role in axonal health either by exhibiting a beading morphology surrounded by a thinning axon. Decreased tension additionally promotes waves and small protrusion from neurites (15). The PVM specifically is located very close to the cuticle layer and underlying muscle. Activation of Gαq changes neuronal morphology and contract the muscles that flank the axon. This contraction increases the number of waves in addition to promoting

beading due to excess membrane due to reduced tension, and as we show, are partially reversible. Alternately, changing membrane tension osmotically ultimately leads to death after 10 min.

It has been proposed that beading in C. *elegans* protects mitochondria from external stress and age-related degradation (5,6), and our results indicate that age-related degradation can be promoted by extended Gαq stimulation. Using a worm strain with fluorescently tagged mitochondria in the soft touch neurons, we find a correlation between the mitochondrial aggregates (16), as seen in the form of beads, and the axonal beads upon Gαq stimulation. While the physical state of the beads are unclear, our results show that Gαq stimulation, and repeated stimulation, promotes mitochondrial aggregation.

Whether beading is a mechanism for mitochondrial health is not fully understood, it does offer new questions on how extended Gq stimulation as well as osmotic stress affect longevity. Waving can be partially explained by contractions of underlaying muscles that flank each axon but the mechanism behind beading is unknown. The increase in calcium caused by Gq stress could lead to a direct feedback loop causing a much higher concentration of calcium than normally found in the cell. An increase in cellular calcium is found in many neurodegenerative diseases such as Alzheimer's and Multiple Sclerosis and Autism (17). While there are many different models (18), here we have described evidence that shows that the beads formed under Gq stimulation and hyper-osmotic stress have a striking resemblance to degrading mitochondria and therefore may act as a shield to delay degradation form the extended stress.

MATERIAL AND MATHODS

C. elegans culture. Standard culture methods were used to maintain C. *elegans* on nematode growth media (NGM) agar seeded with OP50 Escherichia coli (E. coli). The strains were maintained at 20°C.

C. elegans strains. ZB154 zdIs5[pmec-4::gfp] graciously given to the lab by the Driscoll Lab (Rutgers), CLP215 twnEx8 (mec-7p::tomm20::mCherry + myo-2p::GFP) which was obtained from C. elegans Genetics Center.

Synchronization. Synchronized worms were collected two ways. Gravid worms were collected in a tube, washed with S. Basel then lysed with bleach to release the eggs. The tube was then spun down, and the eggs were collected and plates for use. Or the eggs were individually picked and passed onto a new seeded plate for use after they became the proper age.

Preparation for Fluorescent Microscopy. Fluorescent worms were picked and moved onto an unseeded plate for stimulation, either 1mM carbachol or 100mM sodium chloride and stimulated for various amount of time. Generally, each stimulation would consist of 5-10 worms. Once stimulated they were washed with S. basel and placed onto an agar pad on a cover slip for viewing. The agar pad allowed the worms to stay hydrated during imaging. If multiple stimulations were to be done the worms were taken off the agar pad and placed back on an unseeded plate for more stimulation. Otherwise, they were removed and placed on a seeded plate for recovery.

Fluorescent Microscopy. Worms of various ages and stimulations were imaged on Zeiss LSM inverted confocal microscope using the 40x objective for stimulation of ZB154 studies. CLP215

of various ages and stimulation times were imaged on Nikon Eclipse Ti-U inverted confocal microscope using the 63x objective.

ACHKNOWLEDMENTS

This work was funded by NIH (SS). We thank the many members of the Srinivasan Lab (WPI) for countless hours of help with maintenance, plate making, general questions and microscope training.

CHAPTER IV – Osmotic stress induces novel cell retraction behavior

Author and manuscript contributions: This manuscript was contributed equally by Katherine M Pearce and Dionna Defazio. Retraction, hyper-osmotic stress, and AFM studies were completed by KMP. AFM was done in collaboration with Jiazhang Chem (Wu Lab). Morphology, squiggle analysis, and Laurdan studies were completed by DD. Contributions to this manuscript for modeling done by Duncan Wright (S. Olsen lab).

ABSTRACT

Membrane tension underlies many cellular events such as endo- and exocytosis as well as morphology. Here, we have studied the effects of membrane tension using a cultured cell line that differentiates into a neuronal morphology, PC12, which typically displays 3-4 neural outgrowths from a large soma. We have previously found that stimulation of the Gαq/PLCβ/Ca^{2+} signaling pathway by neurotransmitters results in retraction of PC12 neurites into the soma. Here, we show that changing membrane tension by subjecting the cells to hyper-osmotic stress through the addition of salt similarly results in neurite retraction. Once started, retraction was irreversible and continued over several minutes until complete. Osmotically induced retraction is only seen when KCl is used and not $MgCl_2$ or glycerol suggesting a contribution of monovalent ion exchangers. Monitoring cellular calcium levels indicate that retraction is not linked to the extent of internal calcium or spatial inhomogeneities. Surprisingly, while neurotransmitter stimulation always causes linear retraction of neurites, retraction initiated osmotically often caused the neurites to form waves or 'squiggles' as they retract into the soma. Increasing the amount of added salt did not affect the retraction rate but changed the percent of neurites that retract, and the percent that

squiggle during retraction. Varying the amount of salt used to induce retraction shows a non-linear dependence where the percent of neurites that did not respond peaks at 40% salt, which is also the concentration where squiggling is lowest and where induced calcium changes are highest. Taken together, these studies report that changing in membrane tension by added salt induces unexpected changes in cell properties that may impact cells such as those in the kidney.

INTRODUCTION

Membrane tension has been proposed to regulate cell shape and processes such as fusion and motility (for review IV-1). Membrane tension serves as a sensor to alert cells to engage in processes that reset membrane composition when needed by synthesizing lipids or promoting lipid processing. Membrane tension helps optimize hydrophobic interactions of the lipid chains and polar interactions on the surface that maintain bilayer structure.

Our laboratory studies the Gαq / phospholipase Cβ / PIP_2 signaling system. This pathway is triggered by the binding of an extracellular hormone or neurotransmitter to its specific G protein coupled receptor (GPCR), which in turn activates Gαq and then PLCβ. Activated PLCβ catalyzes the removal of the large phosphoinositide head group of PIP2 leaving the lipid portion, diacylglycerol in the membrane. The ligand bound GPCR aggregates on the membrane surface where it is subsequently endocytosed and eventually recycled back to the plasma membrane (IV-2).

Recently, we found that activation of the Gαq/PLCβ/$PI(4,5)P_2$ pathway causes retraction of the neurites of differentiated PC12 cells into the soma. This retraction began after the initial calcium spike and continues over a period of 5-20 minutes until the neurite is fully retracted into the soma. Experimental and theoretical results support the idea that retraction is due changes in

membrane tension brought about by a combination of PIP_2 hydrolysis, which reduces the area of the inner leaflet, GPCR internalization, which causes a loss in membrane, and calcium flux which changes the membrane potential. The resulting retracted cells, which are more deformable than un-retracted, are healthy and survive for as long as the culture is kept (IV-3). In carrying out those studies, we noted a significant population of the neurites (~30%) were unaffected by Gαq stimulation and remained extended throughout the experiment.

In this study, we sought to understand the relationship between the degree of membrane tension and the rate of retraction, and that reason that certain neurites are not susceptible to retraction. We again used PC12 cells, which in differentiated form typically display 3-4 neurite extensions around a circular body (IV-4). Using osmotic stress to induce membrane tension, we found that retraction initiated by salt is impacted by the distance between neurite tip and organelles involved in calcium. We also observe a non-linear retractive behavior not seen in Gαq stimulation that may result from the ability of the soma to accommodate excess lipid.

RESULTS

Hyperosmotic stress induces unique morphologies. PC12 cells were originally derived from adenocarcinoma, and when they are induced to differentiate by the addition of nerve growth factor (NGF), they take on two major morphologies; neurons with a spherical somas and long spindly neurites, or chromaffin cells which have more trapezoid bodies and thicker neurites with triangular bases (**Fig 1a-d**). These varied morphologies allowed us to determine whether the rate and morphological changes of retraction differ. We thus stimulated PC12 cells with carbachol to initiate the Gαq/PLCβ/PIP_2/Ca^{2+} signaling pathway and studied the retraction of cells in these two morphological groups. We found that cells in both groups showed a linear retraction of neurites

into the soma with similar overall rates retracted with a similar rates (0.08-0.025 uM/sec) (**Fig. 1e**). Because the length and thickness of these neurites were so variable, the similarity in their retraction behavior suggests that relative dimensions of the neurites and shape of the soma do not play a role in retraction.

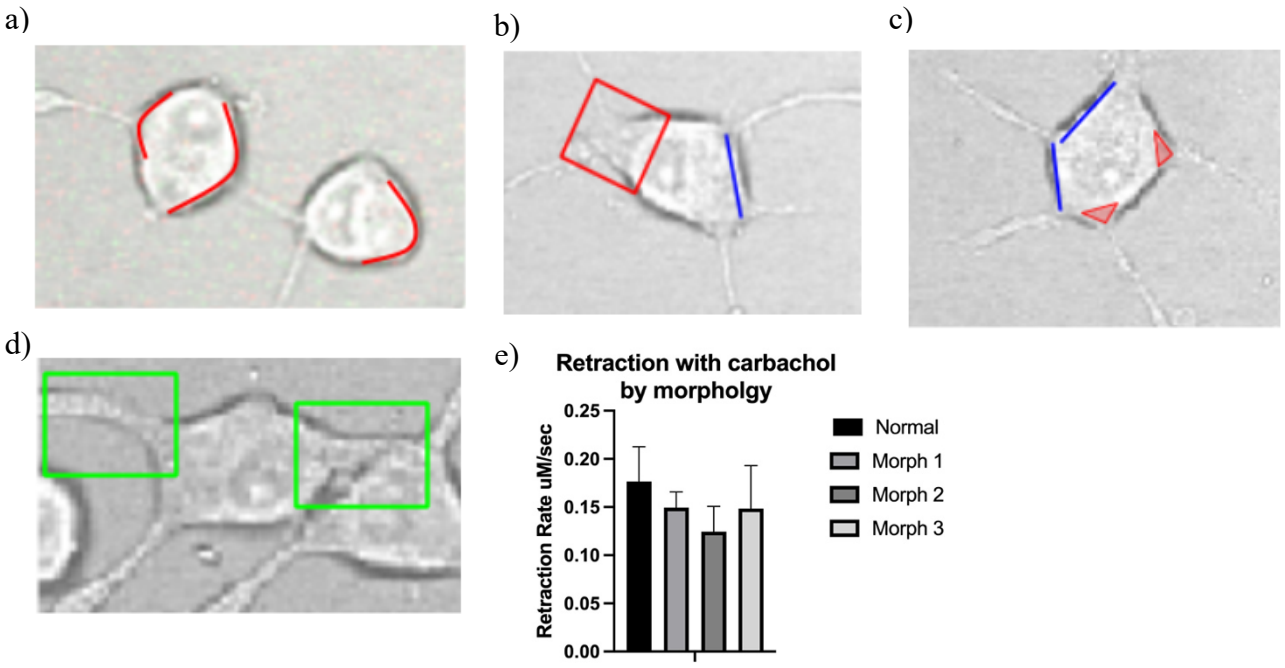

Figure IV- 1. *Morphological guideline for differentiated PC12 cells. (a) Normal cells that have a round shape (shown by the red line). They are generally round and have long thin neurites. (b) Morph 1 slightly more elongated or angular cell body, neurites are thicker at the base making them appear more like extensions of the cytoplasm. (c) Morph 2 cells are typically larger in size and very polygonal, angular and flat looking often with relatively straight sides. The bases of the neurites are pyramidal. (d) Cells are highly irregular in both body and neurite shape. Cell bodies are often large and angular with irregularly thick neurites. (e) retraction rates after 5uM carbachol.*

Assessment of membrane tension. In our previous studies, we initiated the Gαq/PLCβ/PIP_2/Ca^{2+} signaling pathway at different agonist concentrations and found similar rates of neurite retraction, although these studies were only expected to induce a limited range of membrane tension. To better understand how membrane tension influences retraction, we needed to expand the range of tension felt by the membrane. The simplest way to do this is by changing tension through osmotic stress, which can be easily varied by the addition of different amounts of salt.

We assessed membrane tension via cell stiffness measurements quantified by atomic force microscopy (AFM) at increasing amount of added KCl. This method measures the force needed for a probe to penetrate the cell surface, and thus yields information about the tension of plasma membrane as well as the underlying cytoplasm. In **Fig. 2A-B** we show changes in the viscoelasticity and cell stiffness at varying levels osmolarity. We find that adding small amounts of KCl reduce the viscoelasticity, as expected, but that these values are unchanged will large amounts of salt. The stiffness of the cell increase but only until 40% salt where a reduction was seen suggesting that this level of salt induces some type mechanism that reverses salt effects.

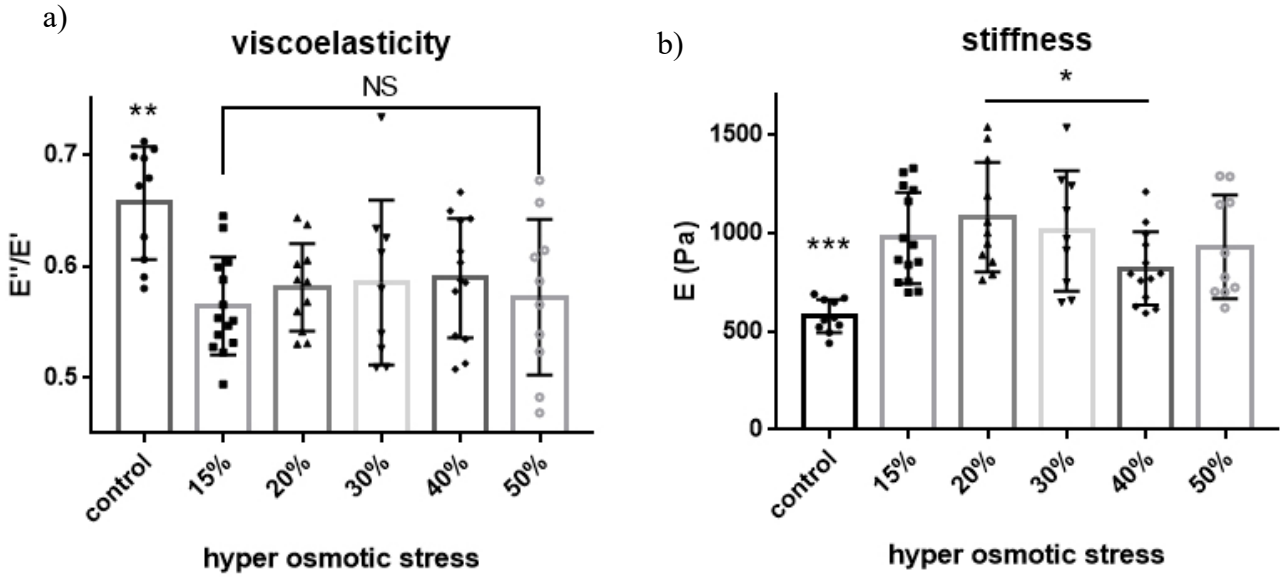

Figure IV- 2. *Change in membrane stiffness under different levels of hyper osmotic stress. (a) viscoelasticity of different osmotic strengths applied to differentiated PC12 cells. (b) stiffness after the addition of KCl Osmotic strengths by percent are as follows: control 300mOsm, 15% - 350mOsm, 20% - 400mOsm, 30% - 450mOsm, 40% - 500mosm, 50% - 550mOsm.*

Retraction behavior varies with osmotic stress. We measured neurite retraction at several osmotic strengths with the goal of developing relationships between external osmotic force, membrane tension and retraction. To this end, we measured the rates of retraction of neurites when we subjected cells to varying amounts of added salt to induce hyper-osmotic stress. We find that the percentage of cells that do not retract varies with osmotic strength but not in a systematic way (**Fig. 3A)**. Because cells that are connected generally do not retract, we only followed the behavior of isolated cells. Low osmotic stress >10% salt or mOsm failed to drive retraction, however, the highest percent of neurite retraction (~90%) occurred at 20% salt. This percentage decreased until 40% salt where only ~10% retraction was seen, and the trend reversed at 50% where a higher

amount retract. We note that even cells that did not retract showed a visible response to salt where by rippling and folding of the membrane was seen (**Fig. 3B**).

Retraction must involve breakdown of the actin filaments comprising the backbone of the neurites, and so we determined whether the amount of non-retractors would increase with actin over-expression. To this end, we found that actin resulted in a small increase in the amount of non-retractors from 2 to 6% suggesting that actin is not playing a major role in retraction (**Fig.3A**). This study was supported by experiments in which we overexpressed the actin-severing protein, cofilin, which increases the rate of neurite retraction. Unexpectedly, we found that cofilin significantly increases the number of non-retractors to 20% suggesting that breakage of the cytoskeleton better allows for osmotic flow out of neurites (see Discussion).

a)

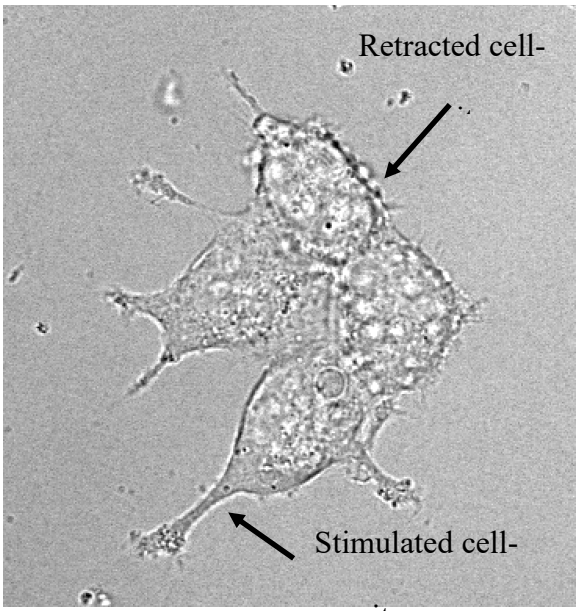

b)

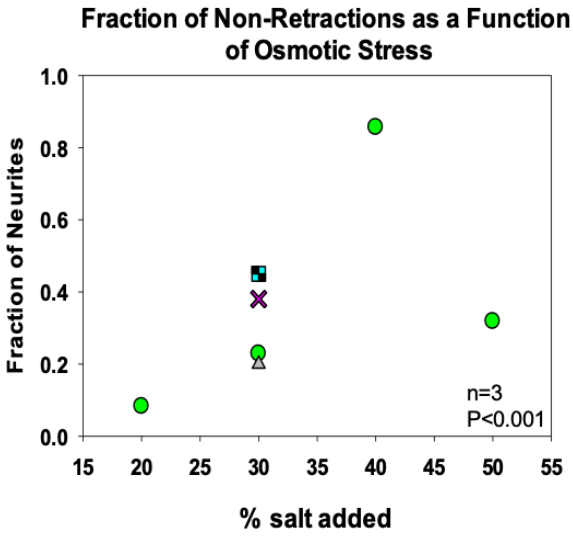

Figure IV- 3. *Non retraction as a function of hyper osmotic stress.*

(a) representative cells that show a stimulated group of cells some of which have retracted neurites and blebbed somas and the bottom cells that do not have retracted neurites. (b) non-retractors as a function of osmotic stress. The green dots corresponds to percent of osmotic stress (20, 30, 40, 50), black/blue box is EGFR, purple x is cofilin and the grey triangle is actin.

Retraction occurs through differences in cellular calcium in the recovery phase. The calcium increase that occurs upon Gαq activation reaches a maximum in ~20-30s. This increase, which initially involves PIP_2 hydrolysis and release of Ca^{2+} from the ER, can also triggers calcium release from the mitochondria and the opening of calcium activated calcium channels. After, recovery mechanisms are initiated that include pumping Ca^{2+} out of the cell and into stores in the ER and mitochondria. It is in the recovery period that receptors internalize, and neurite retraction occurs.

Here, we tested the idea that ion channels, such as Na+/K+ /Ca2+ or calcium-activated calcium channels or other ion channels contribute to retraction. We first attempted to induce differentiation by the addition of glycerol to a concentration that osmotically matches 30% salt. Under these conditions, no retraction is observed suggesting that retraction is driven by ionic forces. We then repeated the study substituting $MgCl_2$ for KCl at a concentration that osmotically matches 30% KCl. Again, no retraction is observed suggesting that Na+/K+ channels in some way contribute to retraction.

We have previously found that upon Gαq stimulation, calcium levels in the recovery period differ in the neurites versus the soma most likely due to the presence of ER and mitochondria uptake in the cell body. Thus, it is possible that differences in the concentration of calcium in the neurites versus soma might underlie the collapse of the neurite into the soma. We tested this idea by measuring the levels of calcium in the bodies and neurites of cells at several salt concentrations (**Fig. 4**).

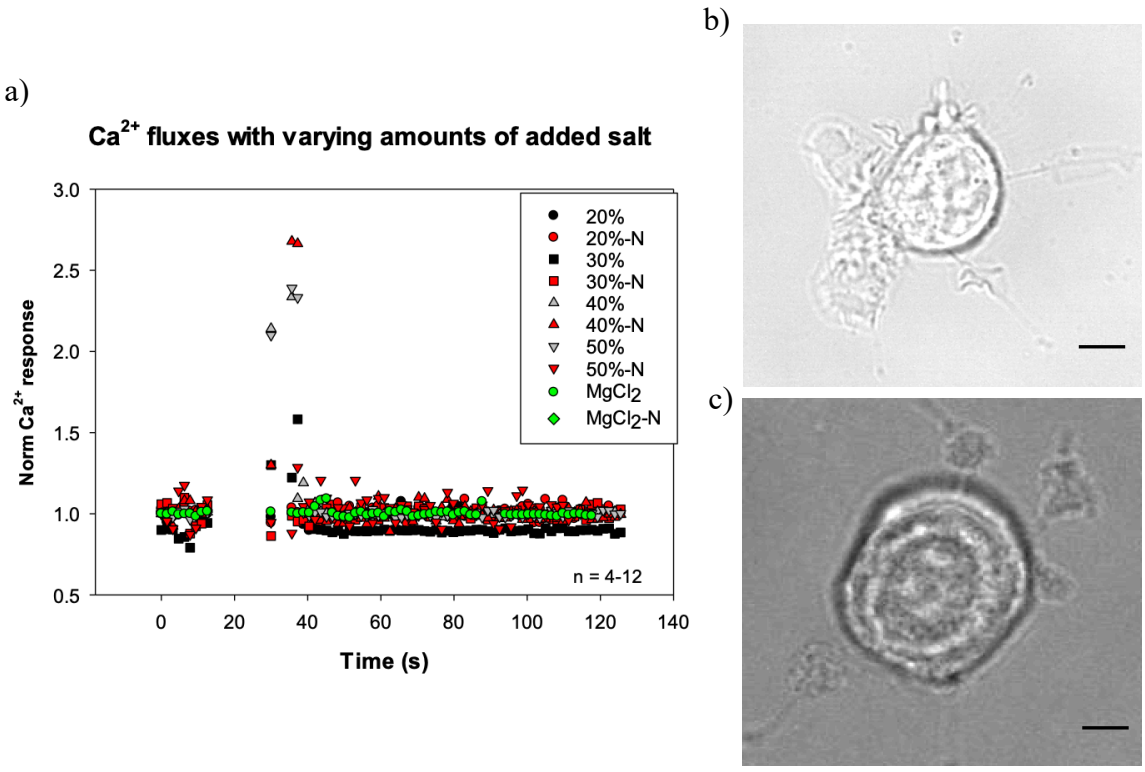

Figure IV- 4. *Calcium efflux and intensity change in soma compared to neurites.*

(a) Normalized intensity graph showing the change in calcium efflux depending on the salt concentration added. Note the change in neurite intensity at 40% (500mOsm). (b) image showing the calcium response in the soma as 30% (450mOsm) KCl is added. (c) image showing the calcium response as 30% $MgCl_2$ is added.

We first note that the addition of salt only changes the initial levels of calcium that recover instantly. This contrasts with the extended duration of calcium seen in Gαq signaling, and the several minutes that retraction occurs. The addition 20% salt does not produce calcium increases, or produces a change so short, it was not in our detection window. This lack of change was surprising since we see the highest percentage of retractors at this concentration. 30% salt showed a small response, but 40% salt shows a substantial response, similar to neurotransmitter activation of Gαq, both in the cell bodies and neurites. The response was lower in the 50% samples. Note

that all responses return to basal conditions within 10-12s. Taken together, these studies argue against the idea that retraction is promoted by spatial differences in calcium concentration but do show that 40% KCl induces a specific change in cell properties that reduces cell stiffness, reduces retraction, and allows for short bursts of calcium. When comparing all the neurites in **Fig. 4B** we see that only 40% neurites show an increase in calcium intensity. This could be due to an imbalance of osmotic pressure between the soma and neurite of the cell. This could also account for the high rate of non-retractors that is also seen at 40% osmotic stress.

Neurites display two types of retractive behavior. Neurite retraction resulting from Gαq/PLCβ/Ca^{2+} stimulation occurs in a linear and symmetric collapse of neurites into the soma. However, we found that when we induce retraction using salt, retraction occurred in waves or squiggles (**Fig. 5A**). We define squiggles as neurites that adopt irregularly spaced alternating inward and outward bends during retraction into the soma. The periodicity of squiggling is quite variable.

Like the number of retractors, the percentage of neurites that display squiggling varies with the amount of salt used to induce retraction as shown in **Fig. 5B**. In this figure, only the number of squiggles is calculated only over the population that retracts (i.e. non-retractors are not considered). Interestingly, the percent of neurites showing squiggles paralleled the number of retractors (i.e, the higher the propensity to retract, the more probable squiggling during retraction will occur) suggesting that the underlying physical basis for both behaviors might be linked. Using phalloidin to follow actin, we find that actin filaments are uniformly spaced in and along the squiggles.

a)

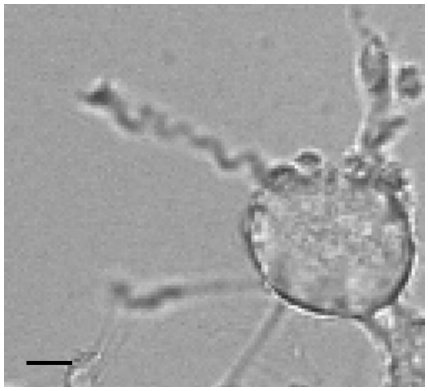

b)

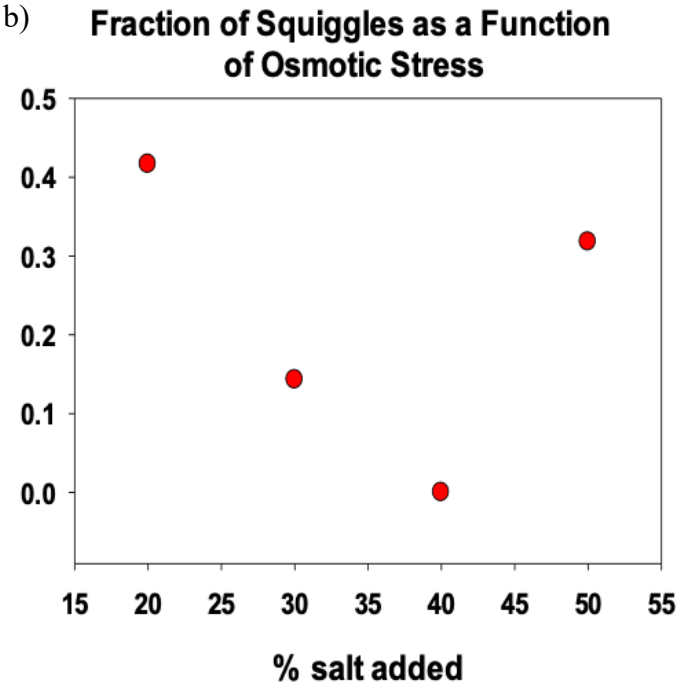

Figure IV- 5*. Squiggles as a function of osmotic stress. (a) representative image showing a squiggle mid-retraction toward the soma. (b) fraction of squiggles with osmotic strength using KCl. We see that at 20% there is a high present of squiggles followed by a steep drop off at 30 and 40% then another increase at 50%.*

Incorporating integral proteins into the plasma membrane alters retraction. We tested whether the ability to retract and the nature of the retraction reflects the properties of the plasma membrane. These studies were carried out by transfecting PC12 cells with two types of proteins that would be expected to impact retraction behavior.

The first is caveolin-1/-3, which is not endogenous to PC12 cells. Cav-1 and Cav-3 are the structural components of large caveolae domain found on the plasma membrane of cells that undergo stretch and deformation, such as muscle, endothelial and vascular cells. Caveolins adopt a horseshoe-like structure that penetrates the inner leaflet of the membrane. PC12 cells do

not endogenously express Cav and we first determined the impact of Cav expression in these cells. The expansion of the inner leaflet produced by the incorporation of caveolin is expected to increase membrane tension.

We introduced caveolin proteins into PC12 cells by lentiviral transfection. Confocal imaging suggests the proteins are mainly plasma membrane localized (**Fig.6a-c**). In accord with previous work (IV-7, IV-8), the presence of Cav-1 substantially enhances Gαq-induced calcium release while Cav-3 shows a smaller increase (**Fig.6a-c**). Since Gαq appears to be exclusively localized on the plasma membrane [5], these results support the plasma membrane localization of the transfected proteins. Studies in the lab using number and brightness to look at higher order oligomerization have shown that Cav1 and Cav3 do not form caveolae in PC12 cells most likely due to poor expression. However, we do see slightly increased levels of aggregations of Cav3 compared to Cav1. This could possibly explain why cells transfected with Cav3 have a higher retraction rate compared to Cav1 and control. The aggregations of Cav3 could be more disruptive the inner leaflet of the membrane compared to Cav1.

Caveolin molecules aggregate to form caveolae domains which appear as 50-100 nm invaginations on the plasma membrane. These invaginations flatten and deform upon stretch. Our previous studies have shown that introducing caveolae into Fischer rat thyroid cells prevents cell rupture when hypo-osmotic stress increases from 20% to 90%. Thus, if transfected Cav molecules aggregated into domains, we will expect the cells to be more resistant to rupture upon the addition of water. If the transfected caveolins formed caveolae domains, then cells should be able to withstand swelling from hypo-osmotic stress (IV-9). In **Fig. 6d** we find that the opposite is true – both constructs caused the cells to be less resistant to rupture; transfection with Cav-1 or Cav-3 made cells more susceptible to rupture. Additionally, we find that while the caveolins had

only minor effects on overall cell stiffness as measured by AFM. We find that Laurdan measurements indicated a large change in membrane tension with Cav-1 transfection suggesting that this protein is alternating membrane structure. Taken together, these results indicate that caveolin molecules are largely dispersed in the plasma membrane.

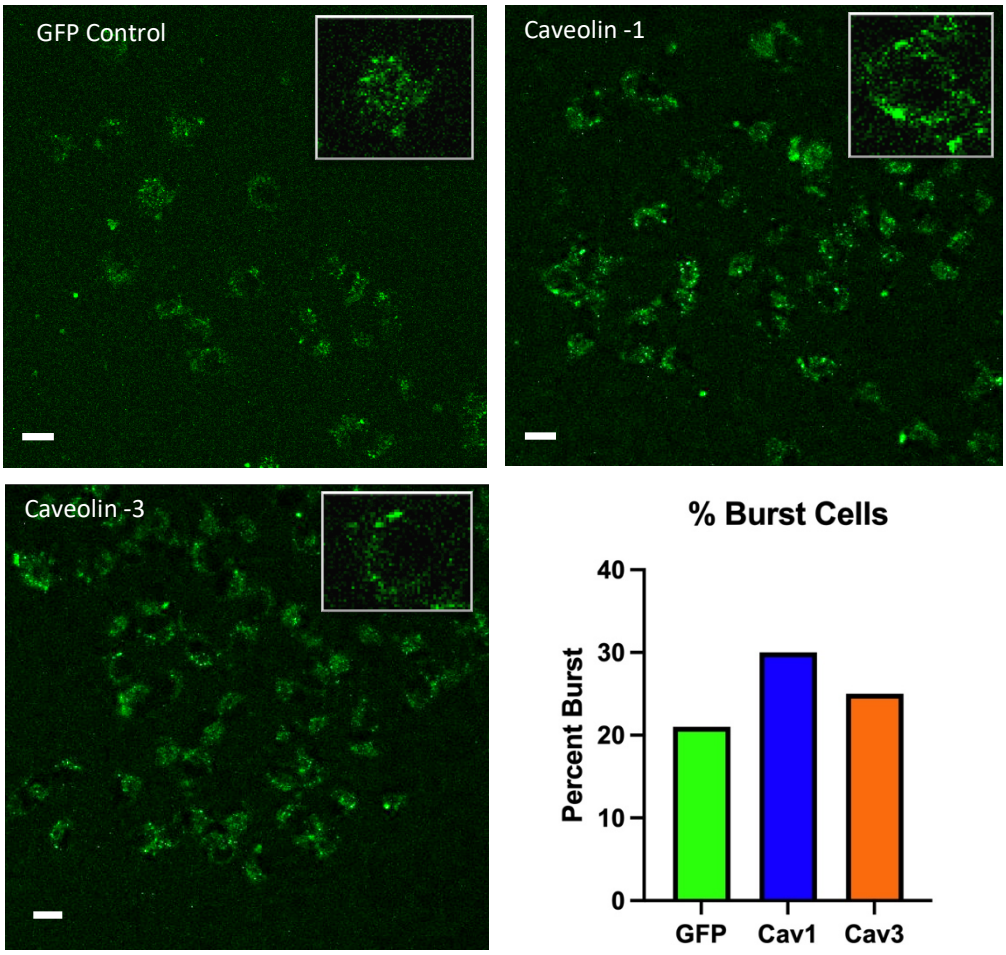

Figure IV- 6. Localization of Caveolin and the effect on osmotic pressure.

(a) localization of lentiviral eGFP control vector in differentiated PC12 cells. (b) localization of lentiviral caveolin-1 eGFP showing increased expression around the membrane but can also be

seen throughout the cell. (c) localization of lentiviral caveolin-3 eGFP showing more punctate expression along the membrane. (d) percent of cell that burst with addition of water to the media.

We determined whether changes in Cav affect tension as assessed by both AFM and Laurdan intensity ratios (**Fig. 7A**). As expected the same trends were seen using both methods supporting the use Laurdan to assess membrane tension (IV-10). We find that both Cav3 and control are significantly different ($p=0.0006$) but the difference with Cav1 is not as significant ($p=0.035$). Interestingly, the values of the two Cavs are very different reflecting differences in the properties of the two proteins.

We determined whether the presence of Cav proteins altered the rate of retraction. For this analysis, we accounted for linear as well as squiggling retraction. We find no significant differences between control and either Cav proteins (**Fig. 7b**). Additionally, the presence of Cav proteins did not affect the percent of neurites squiggling. However, when transfected with Cav3, all neurites retracted (**Fig. 7b**).

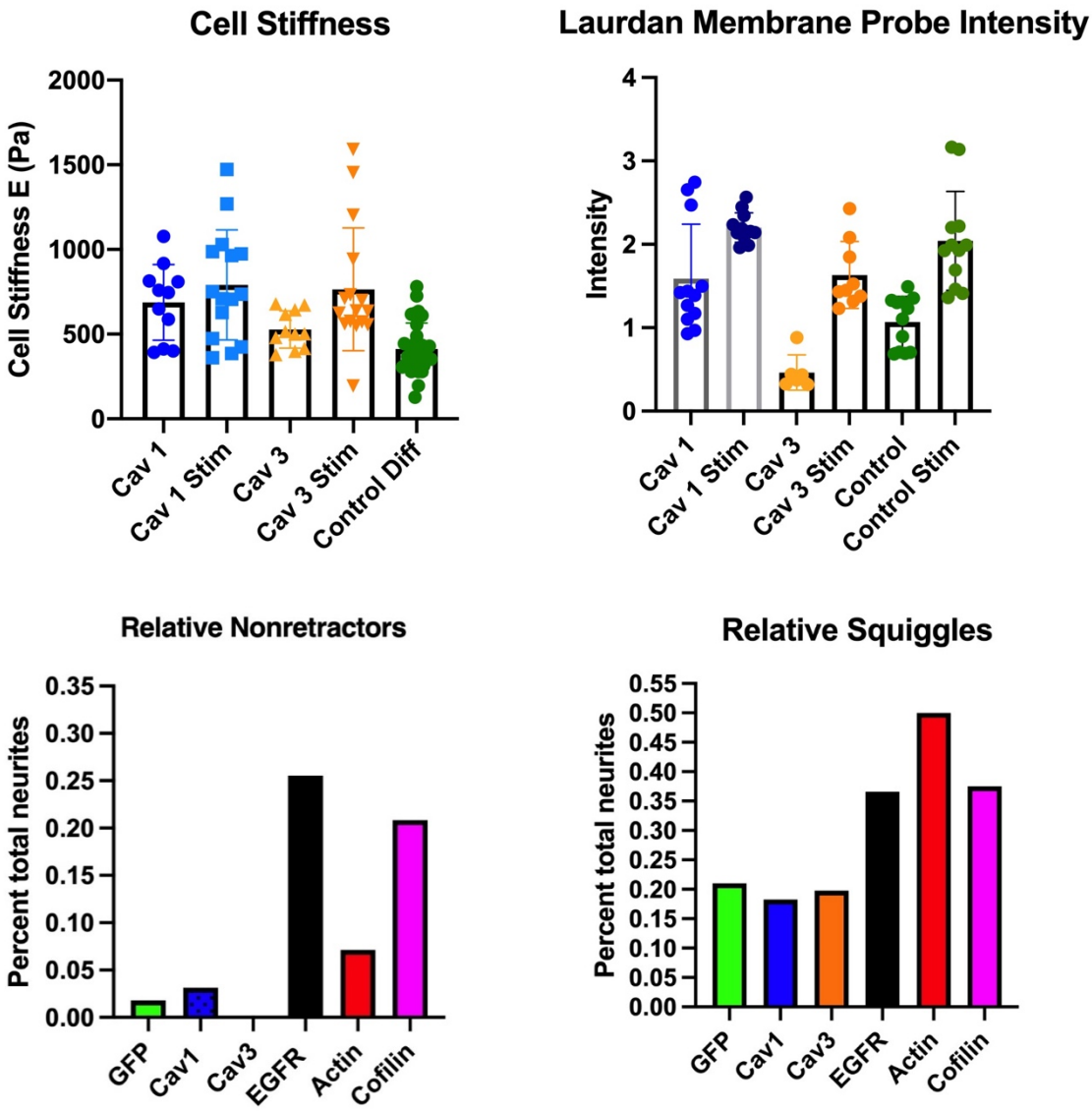

Figure IV- 7. Changes in membrane tension tested by AFM and Laurdan tension probe.

a) AFM data showing a slight increase in stiffness after stimulation with KCl. (b) membrane tension data using LAURDAN probe. (c) Percent of total non-retractors comparing the addition of different modifying proteins. (d) Following the same modifying proteins looking at the precent of cells where a neurite that squiggled was shown.

We compared the impact of Cav-1/3 on membrane properties using EGFR. EGFR is a transmembrane protein has large intra- and extracellular domains with a single transmembrane domain and is expected to expand membrane area without greatly affecting lipid content. Over-expression of EGFP will increase the protein context of the neurite similar to Cav-1/3 but will reinforce the cylindrical shape of the local area. Similar to the caveolin proteins, EGFR did not impact PC12 morphology but did increase the number of non-retractors and the number of squiggles (**Fig. 7c-d**). We find that the presence of EGFR greatly increased the number of non-retractors as well as increased the percent squiggling.

DISCUSSION

The morphology of neuronal cells are dynamic and the synaptic connections formed by neurites change during learning, development and memory formation (IV-11). Our recent studies found that the elevated intracellular calcium that results from acetylcholine stimulation, causes neurite retraction. Our studies suggested that retraction stemmed from a combination of membrane tension, GPCR endocytosis and PIP_2 hydrolysis, and we found that we could induce retraction simply by applying osmotic stress. In this study, we better characterized the effects of membrane tension on PC12 cell properties and found interesting results. In doing so, we have uncovered mechanisms that mediate the retraction process, as well as the novel behaviors of the retraction process.

After stimulation of the Gαq pathway, there is a calcium efflux into the cytosol from the ER. This increase in calcium can start a chain reaction in the cell and change the calcium homeostasis that is so tightly regulated (IV-12). Under stimulated conditions we see a large spike in cellular calcium followed by a slow decrease and return to basal levels. In previous work. we

have shown that an extended stimulation of receptor-gated calcium release led to retraction of neurites. Receptor-gated calcium release such as the Gαq stimulation is one of the leading ways calcium ions are released from intracellular stores in the ER (IV-2). Using calcium green (Thermo) we followed the spike of calcium in the cell under different conditions and found that with both acetylcholine stimulation and hyper-osmotic stress we see a spike in calcium levels. We found that there was a difference in calcium intensity between the soma of cells neurites regardless of stimulation. We found unsurprisingly that the soma of the cell has a higher calcium intensity increase after stimulation compared to the neurites. This is most likely due to small volume in neurites which does not allow for full ER extension therefore less calcium release directly into the neurites

The small volume in neurites also plays a role in the recovery of calcium homeostasis after change in osmotic pressure. With the addition of salt to induce hyper-osmotic stress water is expelled from the cell in a uniform fashion from pores throughout the membrane (IV-13). As the cell begins to recover after retraction the soma of the cell has gained membrane and now houses the majority of ion channels and pores. The resulting model that was built from this is that after osmotic stress water and ions are expelled from the cell in both soma and neurites. However, the recovery process including re-uptake of water and ions is done primarily in the soma of the cell.

The basic physical properties of the plasma membrane surrounding cells, such as membrane tension, may underlie these changes in shape (IV-14). Membrane tension has been well characterized in model membranes and the basic concepts learned from these studies appear to be operative in natural cells. Reduced tension promotes results in excess membrane causing the formation of protrusions and invaginations, while increased tension has the opposite effect promoting retraction of protrusions and contraction of the cell. Membrane tension has been

proposed to regulate cell shape and cellular processes such as fusion and motility (for rev see IV-1). Membrane tension serves as a sensor to alert cells to engage in processes that reset tension when needed by synthesizing lipids or promoting lipid processing. Because membrane tension can arise from non-uniformities in the membrane, we introduced Cav1, Cav3, and EGFR that would perturb membrane properties. We saw that upon Gαq Cav1 and Cav3 disrupted membrane tension leading to a faster retraction rate compared to control but did not change the chances of squiggling. This disruption was most likely due to their inability to form caveolae. However, with the addition of a large transmembrane protein like EGFR we saw an increase in non-retractors and squiggles adding the point that caveolae domains were most likely not formed because thus effect was not shown.

We tested that squiggles result from differences in the flow of integral membrane proteins versus the lipid molecules, and can be understood in terms of two-dimensional particle-laden flow (i.e. two-phase flow where one of the phases is continuously connected and the other phase is made up of small, immiscible, and dilute particles, such as proteins). We speculated that the basis for squiggles is the large difference in compressibility between the protein and the lipid content of the membrane (IV-15). Because proteins are essentially incompressible, the more compressible membrane lipids can diffuse more easily into the soma leaving protein to aggregate and form an incompressible region creating a kink.

The studies here used mammalian neuron based cells that are unlikely to experience natural fluctuations in osmolarity. However, it is possible that podocytes in the kidney, which have many long foot-like processes and filter proteins, salt and small molecules may show retraction.

MATERIALS AND METHODS.

PC12 cell culture and differentiation – PC12 cells (ATCC) are cultured at 37°C with 5% CO2. Cells are cultured in Dulbecco's Modified Eagle Medium (DMEM) supplemented with 10% Heat-Inactivated horse serum (Gibco), 5% Fetal Bovine Serum (Atlanta Biological) and 1% penicillin/streptomycin (Gibco). Media is changed every two days. Differentiation media contains DMEM, 1% heat-inactivated horse serum and 1% penicillin/streptomycin. Cells were differentiated using nerve growth factor 1/1000 in media of 100ng/uL (novoprotien). Cells were transfected using Lipofectamine 3000 (Invitrogen) following the manufacturers protocol. Different amounts of plasmid were used based on concentration tested by nanodrop.

Plasmids– Lentiviruses for eGFP, eGFP-Cav-1 and eGFP-Cav-3 were a gift from Dr. Hemal Patel (UCSD).

Fluorescence imaging – Fluorescence imaging was carried out on an ISS K2 FLIM/FLC instrument equipped with a Nikon Eclipse Ti-U inverted confocal microscope
confocal microscope for Laurdan studies.

Retraction rates - The retraction rates were measured two different ways; using Re-Track which a software that calculates retraction rates over time to yield retraction velocity of any high quality image stack [3], as well as done by hand using ImageJ. In this latter process, at least 3 different neurite lengths are taken over time and the data are plotted to find the retraction rate over time. The combination of these two methods corroborates the retraction software and is used as a control.

Tension- Laurdan (Thermofisher) was reconstituted in ethanol and added to differentiated cells transfected with lentiviruses to express either eGFP, eGFP-Cav1 or eGFP-Cav3 (see above).

Briefly, Laurdan was dissolve in ethanol to an ~1 mM solution. Volume of Laurdan stock was added to the ~1mL media. Cells were immediately imaged using a MaiTai multiphoton laser set at 800nm excitation using a blue (specs) and green (specs) emission filter.

AFM Stiffness and Viscoelasticity Assay - Live cells were probed using an MFP-3D-BIO atomic force microscope (Asylum Research, Santa Barbara, CA, USA) and a DNP cantilever (Bruker, Camarillo, CA, USA) with nominal spring constant 0.06 N/m. Cantilevers were calibrated for spring constant (k) through thermal tuning, and for inverse optical lever sensitivity (InvOLS) through linear force curve fitting on glass in liquid, in order to ensure accuracy. Differentiated PC12 cells were measured 48 h after differentiation on the 60 mm Petri dishes in DMEM The confluency was controlled at 5 ~ 10 %, and only isolated cells were chosen to make measurements to reduce the effect of contact between cells. To align the cantilever tip with the region of interest on the cells, the phase contrast microscopy in the MFP-3D-BIO was utilized. All the cells were taken optical images before they were touched by the probe. For each cell measured, three different locations were chosen in the perinuclear region to take individual force curves, in order to avoid local stiffness bias and ensure the thickness of the measurement location was significantly greater than the indenting depth. Each force curve was taken at approaching and retracting velocities of 2 μm/s and to a trigger point of 0.5 nN, with force distance of 6 μm. 10–16 cells were measured per dish and the measurement time was limited less than 30 min after the dish was taken out from the incubator to minimize the effect from temperature change.

The force curve contains the deflection-indentation curve. Stiffness values (E) were determined from the deflection-indentation curve of the approaching branch. Using a custom MATLAB code that automatically or manually select the initial contact point and fit the force curve over a 200 nm indentation range, the curves fits with the Hertz model of a conical tip:

$$E = \frac{kd\pi\left(1-\nu^2\right)}{2\Delta^2 \tan\phi}$$

where k is the cantilever spring constant, d is the deflection of the cantilever, ν is the Poisson's ratio (assumed as an incompressible material $\nu = 0.5$), Δ is the indentation depth of the sample, and ϕ is the half angle of the conical cantilever tip (17.5° for DNP-10) (IV-5) (IV-6)

The cell fluidity was simultaneously measured with the stiffness. We used a custom function to drive the probe to apply a sinusoidal oscillation on the cell surface, 25 nm in amplitude, 10 Hz in frequency for 1.5 s when it reaches the trigger point of indentation. The fluidity of the cell plasma and cytoskeleton is represented by the phase lag between cell deformation and driving signal.

ACKNOWLEDGMENTS

This study was funded by NIH (SS). We would like to thank all the members of the Scarlata lab for valuable discussion and manuscript review.

CHAPTER V – GENERAL DISCUSSION AND FUTURE DIRECTIONS

The Gαq/calcium signaling pathway is a crucial first step for important neurological events such as development and learning (V-1) Activation of this pathway by neurotransmitters such as acetylcholine followed by the hydrolysis of phosphatidylinositide 4,5 bisphosphate (PIP_2) leading to the binding of inositol trisphosphate (IP3) to receptors in the endoplasmic reticulum (ER) and subsequent release of calcium. Calcium then acts as a downstream effector

for many processes such as neuronal differentiation and plasticity (V-2). While this pathway has been studied for many years, the global effect of extended stimulation of the Gαq/calcium pathway is not fully understood. Using differentiated PC12 cells as a neuronal model, we found a phenomenological event occurred under extended stimulation by acetylcholine. The neurites of the cells retracted back toward the soma of the cell on a timescale of 10-45 minutes. In this thesis, efforts were made to explore the causes of retraction and understand effect that excess calcium caused has on the cell as well as the changes to actin cytoskeleton and change in membrane tension by use of fluorescent microscopy. This work was also translated into the small animal model C. *elegans* where we similar global effects with extended Gαq stimulation were seen by loss of fluorescence in the nerve ring and beading along the ventral nerve. We also used explored the morphological changes and recovery that occur under stress with age to compare the normal changes that accompany aging with those under extended stimulation.

Our initial aim was to understand the mechanism of retraction in PC12 cells. We wanted to understand the effect that extended stimulation has on calcium levels, membrane tension and actin forces within the cell. This aim is discussed in the second chapter of this thesis. Calcium-mediated retraction was followed in PC12 cells that had been stained with fluorescent calcium sensor. We found that with no other external factors, such as protein over expression, we see a calcium spike after stimulation followed by retraction of the neurites toward the soma of the cell.

At this point, we began a collaboration with Dr. Rangamini at University of California San Diego where we developed a general hypothesis that the mechanism of retraction was a combination of actin depolymerization forces and changes in membrane tension brought on by increase in cellular calcium. Our next step was to build a model of retraction. Miriam Bell in the Rangamani lab at, helped build a mechanical model that combined a special model of Gαq

dynamics with an ordinary differential equation model of neurites. To properly get phenomenological constraints for the model, cells that has been transfected with mCherry actin and a PIP_2 reporter PLCδ were used. This preliminary data worked as a starting point of the model that predicated retraction based on the force of actin pushing away from the soma compared to the membrane tension pulling back toward the soma. If these forces were equal, then there would not be retraction and neurite length would remain the same. However, if membrane tension changes due to PIP_2 hydrolysis and calcium release then the forces pulling back toward the soma would be greater than the actin forces pushing out and the neurite would retract.

To support this model, we carried out studies using- actin modifying proteins to better understand the role of actin in retraction. Cofilin, an actin depolymerization protein [V-3] and drebrin, an actin stabilizing protein (V-4) were transfected into PC12 cells and unsurprisingly with an up-regulation of cofilin into the cells (about 6x the endogenous levels) the rate of retraction increases due to the increased actin depolymerization following stimulation. It was thought that over-expression of drebrin would severely hinder retraction, but it was found that there was so significant decrease in retraction rate compared to control. We believe this result points towards actin taking a back seat in retraction overall. While actin is not the driving force leading retraction , we proposed that the force of membrane tension to play larger role.

To individually follow membrane tension we utilized hypo- and hyper- osmotic stress to mechanically change the tension of cells. Under hypo-osmotic stress, we saw no retraction as the cell swells with the addition of water fitting model that increasing the membrane tension forces pushing out away from soma in addition the actin forces would lead to no retraction. Under hyper-osmotic conditions where the osmolality was increased from 300mOsm to ~400mOsm, we saw retraction as the cell shriveled. When the cell expels water, the change in membrane tension

creates force towards the soma overpowering outward actin forces leading to retraction. With this experimental and modeling data we were able to compile the key factors underlying neurite retraction; changes in membrane tension, actin depolymerization, both being governed by calcium dynamics.

Initially, we analyzed the retraction rate by hand. Thus, we created a semi-automated software, Re-Track, in collaboration with the Tuzel lab at WPI. This software, described in chapter 2 section 2, follows the decrease in length of the neurite and distance travelled to compute the velocity of retraction. The resulting text file that could then be graphed to see trends. After importing a high-resolution TIFF stack into the software, the user would drop a pin at the tip of the neurite telling the software this is the point to follow. Depending on the image, the resulting line of retraction could be manually adjusting using the software to ensure that it matched the experimental retraction.

Our results have shown that calcium induced retraction may have a large impact on neuronal plasticity and signaling connections. To explore this further we tested our current model in *Caenorhabditis elegans.* C. *elegans* are a great neuronal model as they have a complete connectome and a short growth cycle from eggs to adult in 3 days (V-5, V-6) It was found that exposing C. *elegans* to prolonged acetylcholine exposure led to breaking in the nerve ring and beading along the ventral nerve. These morphological changes are consistent with our current model. In future studies, it would be interesting to follow calcium after extended stimulation to understand if the majority of calcium was being taken up into the ER after signaling or going to the mitochondria where it could set off the reactive oxygen species (ROS) pathway (V-7). This study would give further understanding to the role of calcium in neuronal degradation. Naturally re-uptake of calcium by the mitochondria and ER slowly decline the with age. This leaves more calcium to stimulate calcium-induced calcium release from the ER and the ROS pathway where increased

levels of cytosolic calcium can not only increase the number of ROS created in the cell, but delay the processes that bind ROS leaving them in the cytosol where they are damaging.

In the third chapter, we further explored the effect of Gαq stimulation on C. *elegans* soft touch neurons at different ages. As C. *elegans* age, they show increased morphological changes along their axons such as beading, and waving outlined in previous studies (V-8). Here, we see an increase in these morphologies with Gαq stimulation and with age and duration of stimulation in the Posterior Ventral Mechanosensory neuron (PVM). The PVM was chosen as the axon of focus due to its proximity to the cuticle and the uterus making it clearly visible for fluorescent studies. This increase in morphology was characterized two ways for beads; by the number of beads along the PVM and the wavelength between the beads. For waves, we characterized them by period between waves. We saw an increase in the number beads after stimulation compared to control as the worms aged. While these changes are expected, we did see an increase in morphologies in younger adults (Day 1) that only occurred by extended Gαq stimulation.

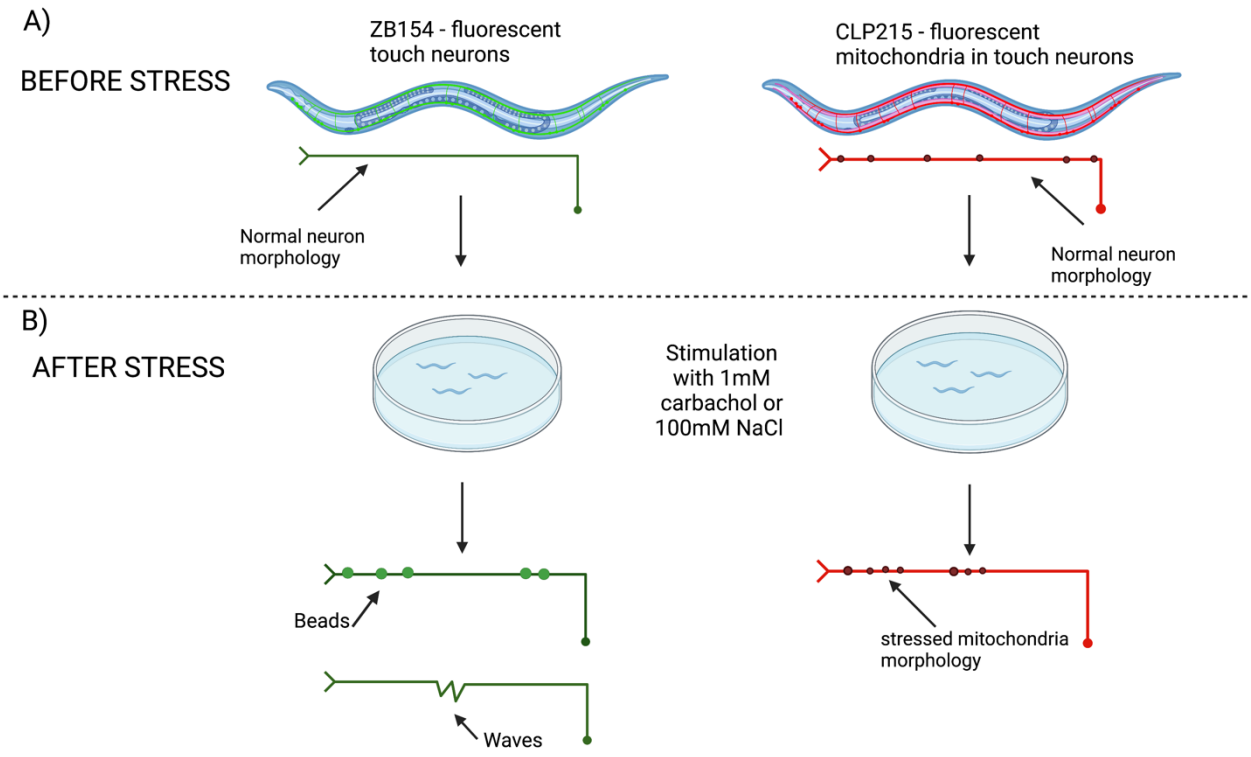

Figure V- 1. Model of morphology changes after Gαq stimulation of C.elegans neurons. *(a) ZB514 with GFP soft touch neurons (left) and CLP215 with red fluorescent mitochondria in soft touch neurons (right). Before stimulation, the vast majority of ZB154 axons are straight and show no morphology. Before stimulation, CLP215 neurons show mitochondria uniformly spaced along the axon with some grouping. (b) After stimulation of either 1mM carbachol or 100mM NaCl we see two morphologies appear for ZB154 (left) beading and waving. For CLP215we see large groups of mitochondria and increased size for some. Figure made using Biorender.com.*

Waving morphology is far less studied than beading but it is known to occur throughout the life cycle of C. *elegans and* has been linked to neurite outgrowths (V-9) in the ALM and PLM. However in the PVM this is not something that we saw but we did find an increased presence in development (L1-L4) compared to adults (V-10). Young worms were stimulated with the same

strength carbachol and salt as adults and that may contribute to the overall degradation and increased wavy morphology that we found. In our work, we saw a few different trends arise with waving. We found that overall, the number of waves was not impacted by age with only Day 8 showing a slight increase in the number of worms showing waving. We did not detect statistical differences in the period between waves that occurred naturally in control and after stimulation. However, we when compare all ages, we found that the period decreased with age, and that under hyper-osmotic stress, there was an overall increase in waves compared to beads across all ages. For waving, our data points to the contribution of other mechanisms that cause waving such as muscle contraction. The PVM sits very close to the muscle and with a change in osmotic pressure the muscle would contract resulting a wave in the axon. While this is just speculation further studies of the underlying muscle will be needed to corroborate the contraction with osmotic stress.

Under stressed conditions it has been shown that protein and organelles will aggregate until the stress is removed (V-11). In touch neurons the model that mitochondria will cluster together under stress has been studied but not fully understood. In an effort to understand the beading morphology with both age and stimulation we looked to use a fluorescent mitochondrial strain to see whether the distribution of mitochondria after stimulation of carbachol would match what we see as beading. While we did find a change in the distribution of mitochondria after stimulation to become more clustered and exhibit changes in size these do not exactly match the beading we have seen previously. However, we were able to display comparable aging morphologies usually seen in geriatric worms (Day 8 or later) in as young as Day 1 after carbachol stimulation. So while this data does not fully explain the beading morphology it does give insight into the importance of mitochondrial health with age and how extended Gαq stimulation leads to a decline in mitochondrial health even in young C. *elegans*.

Taking both morphologies into account, we asked how these morphologies effected the recovery of the axon and overall behavior. When stimulating at multiple time points (30min, 1hr, 24hrs, 48hrs) and tracking recovery we found that 30min and 24hrs showed the greatest increase in "no morphology" after 24hrs recovery meaning these stimulation times allowed for the greatest percent of worms to recover. This is an interesting finding showing that recovery is not completely linear with time stimulated but could point towards a cyclical recovery period in the worms and further studies of recovery kinetics will be needed to thoroughly test this idea.

In the fourth chapter, we took a closer look into the mechanism of retraction under hyper osmotic stress. With the addition of salt to a system, water is expelled rapidly from the cell and slowly recovers. During this time, there is a redistribution of ion channels that help re-equilibrate the cell. Using differentiated PC12 cells, we further investigated the mechanism of retraction and found that not only does the addition of salt at different concentrations cause retraction of neurites back toward the soma but also leads to a calcium spike of varying degrees. Various levels of hyper-osmotic stress were used to test the idea that membrane tension alone was enough to cause retraction. Starting with cells at 300mOsm as controls, we incrementally increased the salt until we were at an osmolarity of 550mOsm that simulated the strongest degree of osmotic stress found under diseased conditions such as inflammatory diseases (V-12). Throughout this study, we realized that two types of retraction were occurring under osmotic stress: a linear retraction similar to what we see with Gαq, and a squiggle-like retraction that is characterized by kinks forming as the neurite retracts toward the soma. This new retraction morphology was not seen under Gαq stimulation leading us to believe that it is caused by grouping of large membrane bound proteins that cannot be compressed like the lipids found in the membrane. When this happens, the large transmembrane proteins cluster together in an

accordion-style fashion as the neurite retracts. This it is an interesting phenomenon that will need further exploration to fully understand.

A different but equally important role in understanding the mechanism of retraction is to why not all neurites retract. Under acetylcholine addition, we believed it to be from a lack of Gαq stimulation. However, with hyper-osmotic stress that is not the case and we found that the percent of osmotic shock changes the percent neurites that retract. An interesting finding when analyzing non-retractors was that cells over-expressing EGFR had the highest number of non-retractors which tracks with our hypothesis that large transmembrane proteins are disrupting membrane tension changes that lead to retraction. Caveolin was also used to test the role of membrane tension in PC12 cells, and we found that expression of caveolin and 1 and 3 were not sufficient alone to form caveolin domains thus disrupted the inner leaflet of the membrane leading to faster retraction times. While this is not expected result it does advance our understand of how disruption of the plasma membrane enhances neurite retraction overall.

FUTURE DIRECTIONS

This project has given many insights into how extended Gαq stimulation effects neuronal health and structure there are still many questions left to be answered. Future directions of this project should include understanding the downstream effects of increased calcium in the cell. This can be done in cultured cells and C. *elegans* to understand the differences in both. Following where the calcium is going within the cell, whether it is binding to protein, going to mitochondria for re-uptake or to set off the ROS pathway or being re-taken back into the ER would give insight into how cells respond to calcium overflow in a diseased or aged state.

WORKS CITED PAGE

Chapter I

I-1. Sharma N, Classen J, Cohen LG. Neural plasticity and its contribution to functional recovery. *Handb Clin Neurol*. 2013;110:3-12. doi:10.1016/B978-0-444-52901-5.00001-0

I-2. Südhof TC. Neuroligins and neurexins link synaptic function to cognitive disease. Nature. 2008 Oct 16;455(7215):903-11. doi: 10.1038/nature07456. PMID: 18923512; PMCID: PMC2673233.

I-3. Algattas H, Huang JH. Traumatic Brain Injury pathophysiology and treatments: early, intermediate, and late phases post-injury. Int J Mol Sci. 2013 Dec 30;15(1):309-41. doi: 10.3390/ijms15010309. PMID: 24381049; PMCID: PMC3907812.

I-4. CHOI, D.W. (1994), Calcium and Excitotoxic Neuronal Injury. Annals of the New York Academy of Sciences, 747: 162-171. https://doi.org/10.1111/j.1749-6632.1994.tb44407.x

I-5. Erwin Neher, Takeshi Sakaba, Multiple Roles of Calcium Ions in the Regulation of Neurotransmitter Release, Neuron, Volume 59, Issue 6,2008,Pages 861-872,ISSN 0896-6273 https://doi.org/10.1016/j.neuron.2008.08.019.

I-6. Berridge MJ. Nuronal Calcium Signaling. Neuron Volume 2,1 Issue 1, Pages 13-26 https://doi.org/10.1016/S0896-6273(00)80510-3.

I-7. Nguyen RL, Medvedeva YV, Ayyagari TE, Schmunk G, Gargus JJ. Intracellular calcium dysregulation in autism spectrum disorder: An analysis of converging organelle

signaling pathways. Biochim Biophys Acta Mol Cell Res. 2018 Nov;1865(11 Pt B):1718-1732. doi: 10.1016/j.bbamcr.2018.08.003. Epub 2018 Aug 9. PMID: 30992134.

I-8. Bahar E, Kim H, Yoon H. ER Stress-Mediated Signaling: Action Potential and Ca(2+) as Key Players. *Int J Mol Sci*. 2016;17(9):1558. Published 2016 Sep 15. doi:10.3390/ijms17091558

I-9. Deniaud, A., Sharaf el dein, O., Maillier, E. *et al.* Endoplasmic reticulum stress induces calcium-dependent permeability transition, mitochondrial outer membrane permeabilization and apoptosis. *Oncogene* **27,** 285–299 (2008). https://doi.org/10.1038/sj.onc.1210638

I-10. Head BP, Hu Y, Finley JC, et al. Neuron-targeted caveolin-1 protein enhances signaling and promotes arborization of primary neurons. *J Biol Chem*. 2011;286(38):33310-33321. doi:10.1074/jbc.M111.255976

I-11. Hepler JR, Gilman AG. G-proteins. Trends Biochem Sci. 1992;17:383–387.

I-12. Jong YI, Harmon SK, O'Malley KL. Intracellular GPCRs play key roles in synaptic plasticity. ACS Chem Neurosci. 2018;9:2162–2172.

I-13. Devi LA. Heterodimerization of G-protein-coupled receptors: Pharmacology, signaling and trafficking. Trends Pharmacol Sci. 2001;22:532–537.

I-14. Runnels LW, Scarlata S. Determination of the affinities between heterotrimeric G protein subunits and their phospholipase C- b effectors. Biochemistry. 1999;38:1488–1496.

I-15. Penela P, Ribas C, Sánchez-Madrid F, Mayor F. G protein-coupled receptor kinase 2 (GRK2) as a multifunctional signaling hub. Cell Mol Life Sci. 2019;76:4423–4446.

I-16. Neves SR, Ram PT, Iyengar R. G protein pathways. Science. 2002;296:1636–1639.

I-17. Lee CH, Park D, Wu D, Rhee SG, Simon MI. Members of the Gq alpha subunit gene family activate phospholipase C beta isozymes. J Biol Chem. 1992;267:16044–16047.

I-18. Drin G, Scarlata S. Stimulation of phospholipase C[beta] by membrane interactions, interdomain movement, and G protein binding – how many ways can you activate an enzyme? Cell Signal. 2007;19:1383–1392.

I-19. Bittner MA, Holz RW. Phosphatidylinositol-4,5-bisphosphate: Actin dynamics and the regulation of ATP-dependent and -independent secretion. Mol Pharmacol. 2005;67:1089–1098.

I-20. Dickinson GD, Ellefsen KL, Dawson SP, Pearson JE, Parker I. Hindered cytoplasmic diffusion of inositol trisphosphate restricts its cellular range of action. Sci Signal. 2016;9:ra108.

I-21. Rosenberg SS, Spitzer NC. Calcium signaling in neuronal development. Cold Spring Harb Perspect Biol. 2011;3:a004259.

I-22. Stiber JA, Rosenberg PB. The role of store-operated calcium influx in skeletal muscle signaling. Cell Calcium. 2011;49:341–349.

I-23. Park D, Jhon D, Lee CW, Lee KH, Rhee SG. Activation of phospholipase C isozymes by G protein βγ subunits. J Biol Chem. 1993;268:4573–4576.

I-24. Runnels LW, Jenco J, Morris A, Scarlata S. Membrane binding of phospholipases C-b1 and C-b2 is independent of phosphatidylinositol 4,5-bisphosphate and the a and bg subunits of G proteins. Biochemistry. 1996;35:16824–16832.

I-25. Yang B, Pu M, Khan HM, et al. Quantifying transient interactions between bacillus phosphatidylinositol-specific phospholipase-C and phosphatidylcholine-rich vesicles. J Am Chem Soc. 2015;137:14–17.

I-26. Suzuki KGN, Fujiwara TK, Edidin M, Kusumi A. Dynamic recruitment of phospholipase C gamma at transiently immobilized GPI-anchored receptor clusters induces IP3-Ca2+ signaling: Single-molecule tracking study 2. J Cell Biol. 2007;177:731–742.

I-27. Lyon AM, Dutta S, Boguth CA, Skiniotis G, Tesmer JJ. Full-length Galpha(q)-phospholipase C-beta3 structure reveals interfaces of the C-terminal coiled-coil domain. Nat Struct Mol Biol. 2013;20:355–362.

I-28. Huang Y, Thathiah A. Regulation of neuronal communication by G protein-coupled receptors. FEBS Lett. 2015;589:1607–1619.

I-29. Rebecchi M, Pentylana S. Structure, function and control of phosphoinositide-specific phospholipase C. Physiol Rev. 2000;80:1291–1335.

I-30. Hill-Eubanks DC, Werner ME, Heppner TJ, Nelson MT. Calcium signaling in smooth muscle. Cold Spring Harb Perspect Biol. 2011;3:a004549.

I-31. Philip F, Kadamur G, Silos RG, Woodson J, Ross EM. Synergistic activation of phospholipase C-23 by G±q and G23 describes a simple two-state coincidence detector. Curr Biol. 2010;20:1327–1335.

I-32. Cabrera-Vera TM, Vanhauwe J, Thomas TO, et al. Insights into G protein structure, function, and regulation. Endocr Rev. 2003;24:765–781.

I-33. Desarmenien and Spitzer 1991 Desarmenien MG and Spitzer NC. Role of calcium and protein kinase C in development of the delayed rectifier potassium current in Xenopus spinal neurons. Neuron 7: 797–805, 1991.

I-34. Gu X, Spitzer NC. Distinct aspects of neuronal differentiation encoded by frequency of spontaneous Ca2+ transients. Nature. 1995 Jun 29;375(6534):784-7. doi: 10.1038/375784a0. PMID: 7596410.

I-35. Görlach A, Bertram K, Hudecova S, Krizanova O. Calcium and ROS: A mutual interplay. *Redox Biol*. 2015;6:260-271. doi:10.1016/j.redox.2015.08.010

I-36. A. Verkhratsky, A. Shmigol, Calcium-induced calcium release in neurones, Cell Calcium, Volume 19, Issue 1, 1996, Pages 1-14, ISSN 0143-4160, https://doi.org/10.1016/S0143-4160(96)90009-3.

I-37. Christine Grienberger, Arthur Konnerth, "Imaging Calcium in Neurons", Neuron, Volume 73, Issue 5,2012,Pages 862-885,ISSN 0896-6273

I-38. Radu V. Stan, Structure of caveolae, Biochimica et Biophysica Acta (BBA) - Molecular Cell Research, Volume 1746, Issue 3, 2005, Pages 334-348, ISSN 0167-4889, https://doi.org/10.1016/j.bbamcr.2005.08.008.

I-39. Bender F, Montoya M, Monardes V, Leyton L, Quest AF. Caveolae and caveolae-like membrane domains in cellular signaling and disease: identification of downstream targets for the tumor suppressor protein caveolin-1. Biol Res. 2002;35(2):151-67. doi: 10.4067/s0716-97602002000200006. PMID: 12415732.

I-40. U. Vogel, K. Sandvig, B. van Deurs; Expression of caveolin-1 and polarized formation of invaginated caveolae in Caco-2 and MDCK II cells. *J Cell Sci* 15 March 1998; 111 (6): 825–832. doi: https://doi.org/10.1242/jcs.111.6.825

I-41. Ann K. Corsi[1§], Bruce Wightman[2§], and Martin Chalfie[3§] *Introduction WormBook*, ed. The *C. elegans* Research Community, WormBook, doi/10.1895/wormbook.1.7.1, http://www.wormbook.org.

I-42. Brenner, S., 1988 *Foreword. The Nematode Caenorhabditis elegans,* edited by W. B. Wood, Cold Spring Harbor Laboratory Press, Cold Spring Harbor, NY.

I-43. Driscoll M, Chalfie M. The mec-4 gene is a member of a family of Caenorhabditis elegans genes that can mutate to induce neuronal degeneration. Nature. 1991 Feb 14;349(6310):588-93. doi: 10.1038/349588a0. PMID: 1672038.

Chapter II

II-1. Licht T, Goshen I, Avital A, Kreisel T, Zubedat S, Eavri R, Segal M, Yirmiya R, Keshet E (2011). Reversible modulations of neuronal plasticity by VEGF. Proc Natl Acad Sci USA 108, 5081–5086.

II-2. Stuchlik A (2014). Dynamic learning and memory, synaptic plasticity and neurogenesis: an update. Front Behav Neurosci 8, 106–106.

II-3. Takeuchi T, Duszkiewicz AJ, Morris RGM (2014). The synaptic plasticity and memory hypothesis: encoding, storage and persistence. Philos Trans R Soc Lond B Biol Sci 369, 20130288.

II-4. Clapham DE (2007). Calcium signaling. Cell 131, 1047–1058.

II-5. Brini M, Cali T, Ottolini D, Carafoli E (2014). Neuronal calcium signaling: function and dysfunction. Cell Mol Life Sci 71, 2787–2814.

II-6. Goldberg DJ, Grabham PW (1999). Braking news: calcium in the growth cone. Neuron 22, 423–425.

II-7. Gomez TM, Spitzer NC (1999). In vivo regulation of axon extension and pathfinding by growth-cone calcium transients. Nature 397, 350–355.

II-8. Mattson MP (2007). Calcium and neurodegeneration. **Aging Cell** *6*, 337–350.

II-9. McKay SE, Purcell AL, Carew TJ (1999). Regulation of synaptic function by neurotrophic factors in vertebrates and invertebrates: implications for development and learning. **Learn Mem** *6*, 193–215.

II-10. Gilbert J, Man H-Y (2017). Fundamental elements in autism: from neurogenesis and neurite growth to synaptic plasticity. **Front Cell Neurosci** *11*, 359–359.

II-11. King AE, Woodhouse A, Kirkcaldie MT, Vickers JC (2016). Excitotoxicity in ALS: overstimulation, or overreaction? **Exp Neurol** *275*(Pt 1), 162–171.

II-12. Rosenberg SS, Spitzer NC (2011). Calcium signaling in neuronal development. **Cold Spring Harb Perspect Biol** *3*, a004259.

II-13. Voglis G, Tavernarakis N (2006). The role of synaptic ion channels in synaptic plasticity. **EMBO Rep** *7*, 1104–1110.

II-14. West AE, Chen WG, Dalva MB, Dolmetsch RE, Kornhauser JM, Shaywitz AJ, Takasu MA, Tao X, Greenberg ME (2001). Calcium regulation of neuronal gene expression. **Proc Natl Acad Sci USA** *98*, 11024–11031.

II-15. Kadamur G, Ross EM (2013). Mammalian phospholipase C. **Annu Rev Physiol** *75*, 127–154.

II-16. Guo Y, Rebecchi M, Scarlata S (2005). Phospholipase Cbeta2 binds to and inhibits phospholipase Cdelta1. **J Biol Chem** *280*, 1438–1447.

II-17. Lohmann C, Wong RO (2005). Regulation of dendritic growth and plasticity by local and global calcium dynamics. **Cell Calcium** *37*, 403–409.

II-18. Freedman NJ, Lefkowitz RJ (1996). Desensitization of G protein-coupled receptors. **Recent Prog Horm Res** *51*, 319–351; discussion 352–313.

II-19. Berstein G, Blank JL, Jhon D-Y, Exton JH, Rhee SG, Ross EM (1992). Phospholipase C-β1 is a GTPase-activating protein for $G_{q/11}$, its physiologic regulator. **Cell** *70*, 411–418.

II-20. Dohlman HG, Thorner J (1997). RGS proteins and signaling by heterotrimeric G proteins. **J Biol Chem** *272*, 3871–3874.

II-21. Raucher D, Stauffer T, Chen W, Shen K, Guo S, York JD, Sheetz MP, Meyer T (2000). Phosphatidylinositol 4,5-bisphosphate functions as a second messenger that regulates cytoskeleton-plasma membrane adhesion. **Cell** *100*, 221–228.

II-22. Sheetz MP, Dai J (1996). Modulation of membrane dynamics and cell motility by membrane tension. **Trends Cell Biol** *6*, 85–89.

II-23. van Rheenen J, Jalink K (2002). Agonist-induced PIP(2) hydrolysis inhibits cortical actin dynamics: regulation at a global but not at a micrometer scale. **Mol Biol Cell** *13*, 3257–3267.

II-24. Bittner MA, Holz RW (2005). Phosphatidylinositol-4,5-bisphosphate: actin dynamics and the regulation of ATP-dependent and -independent secretion. **Mol Pharmacol** *67*, 1089–1098.

II-25. Diz-Munoz A, Fletcher DA, Weiner OD (2013). Use the force: membrane tension as an organizer of cell shape and motility. **Trends Cell Biol** *23*, 47–53.

II-26. Datar A, Ameeramja J, Bhat A, Srivastava R, Bernal R, Prost J, Callan-Jones A, Pullarkat PA (2019). The roles of microtubules and membrane tension in axonal beading, retraction, and atrophy. **Biophys J** *117*, 880–891.

II-27. Logan MR, Mandato CA (2006). Regulation of the actin cytoskeleton by PIP2 in cytokinesis. **Biol Cell** *98*, 377–388.

II-28. Rangamani P, Fardin MA, Xiong Y, Lipshtat A, Rossier O, Sheetz MP, Iyengar R (2011). Signaling network triggers and membrane physical properties control the actin cytoskeleton-driven isotropic phase of cell spreading. **Biophys J** *100*, 845–857.

II-29. Franze K, Gerdelmann J, Weick M, Betz T, Pawlizak S, Lakadamyali M, Bayer J, Rillich K, Gogler M, Lu YB, *et al*. (2009). Neurite branch retraction is caused by a threshold-dependent mechanical impact. **Biophys J** *97*, 1883–1890.

II-30. Kerstein PC, Nichol RI, Gomez TM (2015). Mechanochemical regulation of growth cone motility. **Front Cell Neurosci** *9*, 244.

II-31. Sengupta P, Samuel ADT (2009). *Caenorhabditis elegans*: a model system for systems neuroscience. **Curr Opin Neurobiol** *19*, 637–643.

II-32. Greene LA, Tischler AS (1976). Establishment of a noradrenergic clonal line of rat adrenal pheochromocytoma cells which respond to nerve growth factor. **Proc Natl Acad Sci USA** *73*, 2424–2428.

II-33. Drubin DG, Feinstein SC, Shooter EM, Kirschner MW (1985). Nerve growth factor-induced neurite outgrowth in PC12 cells involves the coordinate induction of microtubule assembly and assembly-promoting factors. **J Cell Biol** *101*, 1799–1807.

II-34. Hassinger JE, Oster G, Drubin DG, Rangamani P (2017). Design principles for robust vesiculation in clathrin-mediated endocytosis. **Proc Natl Acad Sci USA** *114*, E1118–E1127.

II-35. Getz M, Swanson L, Sahoo D, Ghosh P, Rangamani P (2019). A predictive computational model reveals that GIV/girdin serves as a tunable valve for EGFR-stimulated cyclic AMP signals. **Mol Biol Cell** *30*, 1621–1633.

II-36. Simunovic M, Manneville JB, Renard HF, Evergren E, Raghunathan K, Bhatia D, Kenworthy AK, Voth GA, Prost J, McMahon HT, *et al*. (2017). Friction mediates scission of tubular membranes scaffolded by BAR proteins. **Cell** *170*, 172–184.e111.

II-37. Bornschlogl T, Romero S, Vestergaard CL, Joanny JF, Van Nhieu GT, Bassereau P (2013). Filopodial retraction force is generated by cortical actin dynamics and controlled by reversible tethering at the tip. **Proc Natl Acad Sci USA** *110*, 18928–18933.

II-38. McCullough BR, Blanchoin L, Martiel JL, De la Cruz EM (2008). Cofilin increases the bending flexibility of actin filaments: implications for severing and cell mechanics. **J Mol Biol** *381*, 550–558.

II-39. Mikati MA, Grintsevich EE, Reisler E (2013). Drebrin-induced stabilization of actin filaments. **J Biol Chem** *288*, 19926–19938.

II-40. Calabrese B, Saffin JM, Halpain S (2014). Activity-dependent dendritic spine shrinkage and growth involve downregulation of cofilin via distinct mechanisms. **PLoS One** *9*, e94787.

II-41. Grintsevich EE, Reisler E (2014). Drebrin inhibits cofilin-induced severing of F-actin. **Cytoskeleton (Hoboken)** *71*, 472–483.

II-42. Pavlov D, Muhlrad A, Cooper J, Wear M, Reisler E (2007). Actin filament severing by cofilin. **J Mol Biol** *365*, 1350–1358.

II-43. Sharma S, Grintsevich EE, Phillips ML, Reisler E, Gimzewski JK (2011). Atomic force microscopy reveals drebrin induced remodeling of f-actin with subnanometer resolution. **Nano Lett** *11*, 825–827.

II-44. Mikati MA, Grintsevich EE, Reisler E (2013). Drebrin-induced stabilization of actin filaments. **J Biol Chem** *288*, 19926–19938.

II-45. Nair RR, Patil S, Tiron A, Kanhema T, Panja D, Schiro L, Parobczak K, Wilczynski G, Bramham CR (2017). Dynamic arc SUMOylation and selective interaction with F-actin-binding protein drebrin A in LTP consolidation in vivo. **Front Synaptic Neurosci** *9*, 8.

II-46. Hartzell CA, Jankowska KI, Burkhardt JK, Lewis RS (2016). Calcium influx through CRAC channels controls actin organization and dynamics at the immune synapse. **Elife** *5*, e14850.

II-47. Nourse JL, Pathak MM (2017). How cells channel their stress: interplay between Piezo1 and the cytoskeleton. **Semin Cell Dev Biol** *71*, 3–12.

II-48. He L, Tao J, Maity D, Si F, Wu Y, Wu T, Prasath V, Wirtz D, Sun SX (2018). Role of membrane-tension gated Ca(2+) flux in cell mechanosensation. **J Cell Sci** *131*, jcs208470.

II-49. LaFerla FM (2002). Calcium dyshomeostasis and intracellular signalling in Alzheimer's disease. **Nat Rev Neurosci** *3*, 862–872.

II-50. Sanchez-Fernandez G, Cabezudo S, Garcia-Hoz C, Beninca C, Aragay AM, Mayor F Jr, Ribas C (2014). Galphaq signalling: the new and the old. **Cell Signal** *26*, 833–848.

II-51. Scarlata S, Singla A, Garwain O (2018). Phospholipase Cβ interacts with cytosolic partners to regulate cell proliferation. **Adv Biol Regul** *67*, 7–12.

II-52. Scarlata S (2019). The role of phospholipase Cβ on the plasma membrane and in the cytosol: How modular domains enable novel functions. **Adv Biol Regul** *73*, 100636.

II-53. Mutalik SP, Joseph J, Pullarkat PA, Ghose A (2018). Cytoskeletal mechanisms of axonal contractility. **Biophys J** *115*, 713–724.

II-54. Randlett O, Poggi L, Zolessi FR, Harris WA (2011). The oriented emergence of axons from retinal ganglion cells is directed by laminin contact **in vivo. Neuron** *70*, 266–280.

II-55. J.H. Schwartz, Eric R. Kandel, Thomas M. Jessell, Steven A. Siegelbaum, A.J. Hudspeth, Principles of Neural Science, fifth ed., McGraw Hill Professional, 2012.

II-56. G. Jacquemet, H. Hamidi, J. Ivaska, Filopodia in cell adhesion, 3D migration and cancer cell invasion, Curr. Opin. Cell Biol. 36 (2015) 23–31.

II-57. P.K. Mattila, P. Lappalainen, Filopodia: molecular architecture and cellular functions, Nat. Rev. Mol. Cell Biol. 9 (2008) 446.

II-58. T. Takeuchi, A.J. Duszkiewicz, R.G.M. Morris, The synaptic plasticity and memory hypothesis: encoding, storage and persistence, Philos. Trans. R. Soc. Lond. B Biol. Sci., 369 20130288-20130288.

II-59. O. Garwain, S. Scarlata, Phospholipase Cβ-TRAX association is required for PC12 cell differentiation, J. Biol. Chem. 291 (2016) 22970–22976.

II-60. L.A. Greene, A.S. Tischler, Establishment of a noradrenergic clonal line of rat adrenal pheochromocytoma cells which respond to nerve growth factor, Proc. Natl. Acad. Sci. U. S. A 73 (1976) 2424–2428.

II-61. F. Furt, Y.C. Liu, J.P. Bibeau, E. Tüzel, L. Vidali, Apical myosin XI anticipates F-actin during polarized growth of Physcomitrella patens cells, Plant J. 73 (2013) 417–428.

II-62. K.M. Pearce, M. Bell, W.H. Linthicum, Q. Wen, J. Srinivasan, P. Rangamani, S. Scarlata, Galphaq-mediated calcium dynamics and membrane tension modulate neurite plasticity, Mol. Biol. Cell (2019) mbcE19090536.

II-63. D. Pavlov, A. Muhlrad, J. Cooper, M. Wear, E. Reisler, Actin filament severing by cofilin, J. Mol. Biol. 365 (2007) 1350–1358.

II-64. X. Ding, L.M. Pervere, C. Bascom Jr., J.P. Bibeau, S. Khurana, A.M. Butt, R.G. Orr, P.J. Flaherty, M. Bezanilla, L. Vidali, Conditional genetic screen in Physcomitrella patens reveals a novel microtubule depolymerizing-end-tracking protein, PLoS Genet. 14 (2018) e1007221.

II-65. V. Urbančič, R. Butler, B. Richier, M. Peter, J. Mason, F.J. Livesey, C.E. Holt, J.L. Gallop, Filopodyan, An open-source pipeline for the analysis of filopodia, J. Cell Biol. 216 (2017) 3405.

II-66. S. Nilufar, A.A. Morrow, J.M. Lee, T.J. Perkins, FiloDetect: automatic detection of filopodia from fluorescence microscopy images, BMC Syst. Biol. 7 (2013) 66.

II-67. D. Tsygankov, C.G. Bilancia, E.A. Vitriol, K.M. Hahn, M. Peifer, T.C. Elston, CellGeo, A computational platform for the analysis of shape changes in cells with complex geometries, J. Cell Biol. 204 (2014) 443–460.

II-68. L. Bosgraaf, P.J. van Haastert, T. Bretschneider, Analysis of cell movement by simultaneous quantification of local membrane displacement and fluorescent intensities using Quimp2, Cell Motil Cytoskeleton 66 (2009) 156–165.

II-69. D. Barry, C. Durkin, J. Abella, M. Way, Open source software for quantification of cell migration, protrusions, and fluorescence intensities, J. Cell Biol. (2015) 209.

II-70. J.-Y. Tinevez, N. Perry, J. Schindelin, G.M. Hoopes, G.D. Reynolds, E. Laplantine, S.Y. Bednarek, S.L. Shorte, K.W. Eliceiri, TrackMate: an open and extensible platform for single-particle tracking, Methods 115 (2017) 80–90.

Chapter III

III-1. Jackson, L, Qifti, A, Pearce, KM, Scarlata, S. Regulation of bifunctional proteins in cells: Lessons from the phospholipase Cβ/G protein pathway. Protein Science. 2020; 29: 1258– 1268. https://doi.org/10.1002/pro.3809

III-2. Kankanamge D, Ubeysinghe S, Tennakoon M, et al. Dissociation of the G protein βγ from the Gq-PLCβ complex partially attenuates PIP2 hydrolysis. J Biol Chem. 2021;296:100702. doi:10.1016/j.jbc.2021.100702

III-1. Pearce K.M, Bell M., Linthicum W.H., Q. Wen, J. Srinivasan, P. Rangamani, S. Scarlata, Galphaq-mediated calcium dynamics and membrane tension modulate neurite plasticity, Mol. Biol. Cell (2019) mbcE19090536.

III-2. Frooninckx Lotte, Van Rompay Liesbeth, Temmerman Liesbet, Van Sinay Elien, Beets Isabel, Janssen Tom, Husson Steven, Schoofs Liliane. Neuropeptide GPCRs in C.

elegans. Frontiers in Endocrinology. Vol 3. 2012. 167. 0.3389/fendo.2012.00167. ISSN. 1664-2392

III-3. Pan CL, Peng CY, Chen CH, McIntire S. Genetic analysis of age-dependent defects of the Caenorhabditis elegans touch receptor neurons. *Proc Natl Acad Sci U S A*. 2011;108(22):9274-9279. doi:10.1073/pnas.1011711108

III-4. Herndon, L. A., Wolkow, C. A., Driscoll, M., & Hall, D. H. (2017). effects of ageing on the basic biology and anatomy of C. elegans. In A. Olsen, & M. S. Gill (Eds.), Ageing: Lessons from C. elegans (pp. 9–39). Cham, Switzerland: Springer International Publishing.

III-5. Hahm JH, Kim S, DiLoreto R, Shi C, Lee SJ, Murphy CT, Nam HG. C. elegans maximum velocity correlates with healthspan and is maintained in worms with an insulin receptor mutation. Nat Commun. 2015 Nov 20;6:8919. doi: 10.1038/ncomms9919. PMID: 26586186; PMCID: PMC4656132.

III-6. Toth, ML et al. Neurite Sprouting and synapse deterioration in the aging Caenorhabditis elegans. J Neurosci. **32** 8778-8790 (2012).

III-7. Driscoll M, Chalfie M. The mec-4 gene is a member of a family of Caenorhabditis elegans genes that can mutate to induce neuronal degeneration. Nature. 1991 Feb 14;349(6310):588-93. doi: 10.1038/349588a0. PMID: 1672038.

III-8. Berstein G, Blank JL, Jhon D-Y, Exton JH, Rhee SG, Ross EM (1992). Phospholipase C-β1 is a GTPase-activating protein for $G_{q/11}$, its physiologic regulator. **Cell** *70*, 411–418.

III-9. Tissenbaum Heidi A, Genetics, Life Span, Health Span, and the Aging Process in *Caenorhabditis elegans*, *The Journals of Gerontology: Series A*, Volume 67A, Issue 5, May 2012, Pages 503–510, https://doi.org/10.1093/gerona/gls088

III-10. Goodman Miriam B and Piali Sengupta GENETICS *May 1, 2019 vol. 212 no. 1 25 51; https://doi.org/10.1534/genetics.118.300241*

III-11. Maglioni S, Mello DF, Schiavi A, Meyer JN, Ventura N. Mitochondrial bioenergetic changes during development as an indicator of *C. elegans* health-span. *Aging (Albany NY)*. 2019;11(16):6535-6554. doi:10.18632/aging.102208

III-12. Lin MT, Beal MF. Mitochondrial dysfunction and oxidative stress in neurodegenerative diseases. Nature. 2006 Oct 19;443(7113):787-95. doi: 10.1038/nature05292. PMID: 17051205.

III-13. Rossignol DA, Frye RE. Evidence linking oxidative stress, mitochondrial dysfunction, and inflammation in the brain of individuals with autism. Front Physiol. 2014 Apr 22;5:150. doi: 10.3389/fphys.2014.00150. PMID: 24795645; PMCID: PMC4001006.

III-14. Patten DA, Germain M, Kelly MA, Slack RS. Reactive oxygen species: stuck in the middle of neurodegeneration. J Alzheimers Dis. 2010;20 Suppl 2:S357-67. doi: 10.3233/JAD-2010-100498. PMID: 20421690.

III-15. Caldwell Kim A., Willicott Corey W., Caldwell Guy A; Modeling neurodegeneration in *Caenorhabditis elegans*. *Dis Model Mech* 1 October 2020; 13 (10): dmm046110. doi: https://doi.org/10.1242/dmm.046110

III-16. Datar A, Ameeramja J, Bhat A, Srivastava R, Bernal R, Prost J, Callan-Jones A, Pullarkat PA (2019). The roles of microtubules and membrane tension in axonal beading, retraction, and atrophy. **Biophys J** *117*, 880–891.

Chapter IV

IV-1. Diz-Munoz A, Fletcher DA, Weiner OD (2013). Use the force: membrane tension as an organizer of cell shape and motility. **Trends Cell Biol** *23*, 47–53.

IV-2. Pearce K.M, Bell M., Linthicum W.H., Q. Wen, J. Srinivasan, P. Rangamani, S. Scarlata, Galphaq-mediated calcium dynamics and membrane tension modulate neurite plasticity, Mol. Biol. Cell (2019) mbcE19090536.

IV-3. Garwain O, Pearce KM, Jackson L, Carley S, Rosati B, Scarlata S. Stimulation of the Gαq/phospholipase Cβ1 signaling pathway returns differentiated cells to a stem-like state. FASEB J. 2020 Sep;34(9):12663-12676. doi: 10.1096/fj.201902668R. Epub 2020 Aug 6. PMID: 32761888.

IV-4. Das Kaberi P, Freudenrich Theresa M, Mundy William R, Assessment of PC12 cell differentiation and neurite growth: a comparison of morphological and neurochemical measures, Neurotoxicology and Teratology, Volume 26, Issue 3, 2004, Pages 397-406, ISSN 0892-0362, https://doi.org/10.1016/j.ntt.2004.02.006.

IV-5. Thomas, G.; Burnham, N. A.; Camesano, T. A.; Wen, Q. Measuring the Mechanical Properties of Living Cells Using Atomic Force Microscopy. J. Visualized Exp. 2013, No. 76, e50497.

IV-6. Hertz, H. Ueber die Berührung fester elastischer Körper. Journal für die reine und angewandte Mathematik (Crelle's Journal) 1882, 1882, 156.

IV-7. Guo Y, Yang L, Haught K, Scarlata S. Osmotic Stress Reduces Ca2+ Signals through Deformation of Caveolae. J Biol Chem. 2015 Jul 3;290(27):16698-707. doi: 10.1074/jbc.M115.655126. Epub 2015 May 8. PMID: 25957403; PMCID: PMC4505420.

IV-8. Sengupta P, Philip F, Scarlata S. Caveolin-1 alters Ca(2+) signal duration through specific interaction with the G alpha q family of G proteins. *J Cell Sci*. 2008;121(Pt 9):1363-1372. doi:10.1242/jcs.020081

IV-9. Sinha B, Köster D, Ruez R, et al. Cells respond to mechanical stress by rapid disassembly of caveolae. *Cell*. 2011;144(3):402-413. doi:10.1016/j.cell.2010.12.031

IV-10. Gunther, G.; Malacrida, L.; Jameson, D. M.; Gratton, E.; Sánchez, S. A., LAURDAN since Weber: The Quest for Visualizing Membrane Heterogeneity. *Accounts of Chemical Research* **2021,** *54* (4), 976-987

IV-11. Zucker RS, Calcium- and activity-dependent synaptic plasticity, Current Opinion in Neurobiology, Volume 9, Issue 3, 1999, Pages 305-313, ISSN 0959-4388, https://doi.org/10.1016/S0959-4388(99)80045-2.

IV-12. Budde, T., Meuth, S. & Pape, HC. Calcium-dependent inactivation of neuronal calcium channels. *Nat Rev Neurosci* **3,** 873–883 (2002). https://doi.org/10.1038/nrn959

IV-13. Brocker C, Thompson DC, Vasiliou V. The role of hyperosmotic stress in inflammation and disease. *Biomol Concepts*. 2012;3(4):345-364. doi:10.1515/bmc-2012-0001

IV-14. Sitarska Ewa, Diz-Muñoz Alba, Pay attention to membrane tension: Mechanobiology of the cell surface, Current Opinion in Cell Biology, Volume 66, 2020, Pages 11-18, ISSN 0955-0674, https://doi.org/10.1016/j.ceb.2020.04.001.

IV-15. Fowler PW, Hélie J, Duncan A, Chavent M, Koldsø H, Sansom MS. Membrane stiffness is modified by integral membrane proteins. *Soft Matter*. 2016;12(37):7792-7803. doi:10.1039/c6sm01186a

Chapter V

V-1. Rosenberg SS, Spitzer NC. Calcium signaling in neuronal development. *Cold Spring Harb Perspect Biol*. 2011;3(10):a004259. Published 2011 Oct 1. doi:10.1101/cshperspect.a004259

V-2. Blankenship AG, Feller MB. Mechanisms underlying spontaneous patterned activity in developing neural circuits. *Nat Rev Neurosci*. 2010;11(1):18-29. doi:10.1038/nrn2759

V-3. Tanaka, K., Takeda, S., Mitsuoka, K. *et al.* Structural basis for cofilin binding and actin filament disassembly. *Nat Commun* **9,** 1860 (2018). https://doi.org/10.1038/s41467-018-04290-w

V-4. Yufei Shan, Stephen Matthew Farmer, Susan Wray. Drebrin regulates cytoskeleton dynamics in migrating neurons through interaction with CXCR4. Proceedings of the National Academy of Sciences Jan 2021, 118 (3) e2009493118; DOI: 10.1073/pnas.2009493118

V-5. White JG, Southgate E, Thomson JN, Brenner S. The structure of the nervous system of the nematode Caenorhabditis elegans. Philos Trans R Soc Lond B Biol Sci. 1986 Nov 12;314(1165):1-340. doi: 10.1098/rstb.1986.0056. PMID: 22462104.

V-6. Sengupta P, Samuel AD. Caenorhabditis elegans: a model system for systems neuroscience. *Curr Opin Neurobiol*. 2009;19(6):637-643. doi:10.1016/j.conb.2009.09.009

V-7. Görlach A, Bertram K, Hudecova S, Krizanova O. Calcium and ROS: A mutual interplay. *Redox Biol*. 2015;6:260-271. doi:10.1016/j.redox.2015.08.010

V-8. Toth, ML et al. Neurite Sprouting and synapse deterioration in the aging Caenorhabditis elegans. J Neurosci. **32** 8778-8790 (2012).

V-9. Pan CL, Peng CY, Chen CH, McIntire S. Genetic analysis of age-dependent defects of the Caenorhabditis elegans touch receptor neurons. *Proc Natl Acad Sci U S A*. 2011;108(22):9274-9279. doi:10.1073/pnas.1011711108

V-10. Deleaneys MQP

V-11. Rodriguez M, Snoek LB, De Bono M, Kammenga JE. Worms under stress: C. elegans stress response and its relevance to complex human disease and aging. Trends Genet. 2013 Jun;29(6):367-74. doi: 10.1016/j.tig.2013.01.010. Epub 2013 Feb 18. PMID: 23428113.

V-12. Brocker C, Thompson DC, Vasiliou V. The role of hyperosmotic stress in inflammation and disease. *Biomol Concepts*. 2012;3(4):345-364. doi:10.1515/bmc-2012-0001